Nonsmooth Methods for Process Integration

by

Caroline J. Nielsen

Submitted to the Department of Chemical Engineering
in partial fulfillment of the requirements for the degree of

Doctor of Philosophy in Chemical Engineering

at the

MASSACHUSETTS INSTITUTE OF TECHNOLOGY

May 2022

Author .....
Department of Chemical Engineering
April 5, 2022

Certified by .....
Paul I. Barton
Lammot du Pont Professor of Chemical Engineering
Thesis Supervisor

Accepted by .....
Patrick S. Doyle
Graduate Officer, Chemical Engineering

Nonsmooth Methods for Process Integration

by

Caroline J. Nielsen

Submitted to the Department of Chemical Engineering
on April 5, 2022, in partial fulfillment of the
requirements for the degree of
Doctor of Philosophy in Chemical Engineering

Abstract

Process integration is a promising method to improve sustainability and reduce waste in chemical processes by recovering excess resources such as heat, water, or other materials. However, calculating the maximum amount of resource that can be reused is challenging because resource sinks can only take in resource if it is of high enough quality. As a result, most current integration methods are either limited and heuristic or use large superstructure formulations that must assess all possible matches between the resource sources and sinks.

Therefore, this thesis presents new computational methods for maximizing resource recovery that use nonsmooth functions to compactly describe the resource that is available at different qualities. This work can be divided into three main contributions that improve process integration for systems with different resources and assumptions:

1. A generalized approach to process integration that uses a system of two nonsmooth equations to describe optimal reuse for a wide variety of resources, including multiple resources simultaneously,

2. An extension of this general approach to more complex mass and water systems with multiple contaminants that can limit their reuse,

3. A nonsmooth optimization formulation that applies our integration approach to design variable-temperature cogeneration systems that convert process waste heat into electricity.

By utilizing nonsmooth equations, each of these contributions exhibits improved scaling compared to other integration methods and have numbers of equations or constraints that remain the same regardless of the size and complexity of the system. In addition, unlike other methods, our approaches have the flexibility to either determine resource requirements or the process variables that achieve a given target.

This thesis describes the formulation and implementation of each of these nonsmooth approaches and applies them to a wide of range of example applications.

These applications include carbon-constrained energy planning, hydrogen conservation networks, water recovery from petroleum refining with multiple contaminants, and designing improved cogeneration systems for sulfuric acid and cement production processes. The results from these examples show the flexibility and scalability of our approaches and the breadth of improvements they can provide. Together, our contributions increase the applicability of computationally efficient process integration methods to improve the sustainability of a wide range of chemical processes.

Thesis Supervisor: Paul I. Barton
Title: Lammot du Pont Professor of Chemical Engineering

Acknowledgments

I am grateful to the OCP Group for providing financial support for this research and to the Université Mohammed VI Polytechnique - MIT Research Program for supporting and facilitating this collaboration. But I am particularly appreciative to have been a part of a wonderful community at MIT. When I first visited, I was drawn in by the friendly and engaging people, and they have lived up to my expectations.

I want to acknowledge my committee for the taking the time to facilitate my Ph.D. I especially want to thank Professor Green for his flexibility and being willing to jump on as a committee member partway through my Ph.D. I also was honored to have had Professor Swan as a part of my committee. He was my first choice as a committee member because of the kindness and care with which he treated his students. Most of all, I appreciate having found Paul as an advisor. He has supported me in following my research interests and taking ownership of my thesis work. He has also pushed me to think rigorously and taken the time to both teach me fundamentals and make complex topics accessible.

Outside of my research, my experience as a member of the ChemE Communication Lab has been an important part of my time at MIT. Caitlin has been such an encouraging mentor who has worked with me to support my interests and growth as a communicator. With her guidance, I have been able to build skills that I know will add value to whatever I do next.

I am also so happy to have been a part of the 2016 entering class of ChemE graduate students. I could not have asked for classmates who were more accepting, supportive, excited to share their insights and expertise, and deliberate about balancing course work and research with plenty of fun. I want to thank the friends who made MIT feel like home during my first year, including Mark, Matt, Sharon, and AJ. I am glad to have had people to go on skiing and camping adventures, play games with, and search for my phone in the snow. I am grateful to Suzane for navigating math and the Barton lab with me. She has helped me keep my worries in perspective when I get in my head and inspired with her independence and confidence. I am

also thankful to have Kevin as a friend, especially towards the end of my Ph.D. I am honored to be someone he asks for feedback on his brilliant ideas, and I will sorely miss having him nearby always ready for an adventure or chat.

Last, and probably most, thank you to my wonderful family. I am so lucky to have Kindle in my life, who has become family over the past five years. She has made every moment of my graduate experience better, whether good or bad. I appreciate her unconditional acceptance and how she inspires me to take things in stride and enjoy the moment. I am also grateful to have a sister like Sophia who constantly makes laugh and always has my back, maybe even when I don't deserve it. Finally, I want to thank my darling Momsie and Popsie. I appreciate them holding back their worries and letting me make my own decisions, including tackling a Ph.D, and I am grateful for their unwavering support along the way. I am so glad to have a family who are my best friends and who I have so much fun with, and I am looking forward to having you with me as I start my next adventure.

Contents

List of Figures

List of Tables

Chapter 1

Introduction

As demand for chemcial production and manufacturing grows, its environmental impacts become more clear, and as resource scarcity, costs, and regulations increase, there are significant incentives to reduce resource use in chemical processes. One promising approach for reducing resource requirements and waste is process integration. Process integration identifies opportunities for reusing a resource throughout the system. By capturing and recovering excess heat, water, or other materials, process integration decreases both the amount that is wasted and the total required.

This approach to process design is important because it focuses on making a system as efficient and sustainable as possible. Thus, it can be used both to assess the full potential of new designs and to improve existing processes. Process integration is a particularly important tool for improving existing processess because it does not require any changes to be made to the process. Thus, it can be applied when new processes are not yet available or have too high a cost and has the potential to improve many well-established processes that were designed without a focus on sustainability.

Given these benefits, methods for performing process integration have been widely proposed and utilized for a variety of resources. These computational methods calculate the optimal resource reuse for a chemical process by assessing feasible connections between resource sources and sinks in the system. As a result, they provide minimum fresh and waste resource requirements to screen and design processes to improve their sustainability.

1.1 Types of Integration Problems

Process integration was first introduced for heat integration problems, which determine how best to use heat from process streams that decrease in temperature to warm cold streams that require increases in temperature. In these problems, heat reuse between streams is limited by their temperatures as heat can only be transfered from high to low temperature streams. The idea of process integration was then extended to recovering material from rich streams that need to decrease in the concentration of a component using lean streams that need to increase in concentration in a mass exchange network. Here, instead of temperature, mass transfer is limited by the material concentrations in the rich and lean streams. These mass integration problems were also modified to consider the direct reuse of water flows in a system based on the concentrations of contaminants present. Seminal works in these fields include Hohman and Linnhoff et al. for heat integration [48, 61], El-Halwagi and Manousiouthakis for mass integration [31], and Wang and Smith and Dhole et al. for water allocation [91, 26].

More recently, integration methods have also been applied beyond these traditional areas to new resources such as hydrogen [7], oxygen [99], carbon dioxide [82], electrical power [67], and even time in inventory and scheduling problems [19]. Additionally, to further decrease resource use, integration is being considered for increasingly large systems, including resource sharing between plants co-located in eco-industrial parks [14].

However, to have a significant impact on sustainability, this increasing application and scope of process integration requires integration methods that are generalizable to these new applications and scale well with the size of the system. As a result, the goal of this thesis is to develop new flexible and scalable approaches for process integration that can efficiently assess the potential for resource recovery across proposed designs.

1.2 Traditional Approaches to Process Integration

Process integration problems are challenging because the resources they consider for recovery can only be reused between certain process streams. Specifically, resource can only be transferred from a high quality stream to a low quality one, for example, from high to low temperature or high to low concentration. Therefore, determining the maximum amount resource that can be resued requires

1. Enumerating all the possible matches of resource streams, and
2. Assessing which of these matches are feasible.

We also need to ensure that the method selected to complete these steps applies to the resources type in the integration problem and can handle the complexity of and assumptions about the system.

The most straightfoward approach to complete these two steps is to perform them directly using a superstructure. These superstructure approaches, first introduced by Grossmann and Sargent for heat integration [43], optimize over all possible network configurations. These approaches are generalizable to a wide array of integration problems and can in theory obtain globally optimal solutions. However, to guarantee optimality, the superstructures must embed all possible configurations. For problems like heat and mass integration in which stream mixing is not allowed, the superstructure is divided into states to allow for partial matches between streams [97].

In addition, whether or not the superstructure is complete, the model sizes scale exponentially with the number of resource streams and the resulting optimization formulations require solving nonconvex, nonlinear programs that typically include binary variables [44, 41, 57]. Thus, superstructure approaches are useful for determining construction details for a particular system but are not computationally tractable for screening or optimizing across large numbers of designs.

As a result, many process integration methods approach the problem in two sequential steps: first, determining the minimum attainable fresh and waste resource flows for the process, and second, designing a network of stream connections for resource reuse that can approach these targets. This first step is called the targeting

method, and the results from this part of the problem can be used to efficiently screen or optimize process designs without needing to construct the full resource reuse network. Therefore, in this thesis, we exclusively consider targeting methods to develop scalable and efficient approaches to process integration.

To calculate external resource utilities without designing the resource reuse network, targeting approaches use pinch analysis theory. Pinch analysis reduces the complexity of the problem by combining the resource streams that are present at each quality to create representative composite streams for the resource sources and sinks. Then, targeting approaches use a variety of techniques to maximize resource recovery between these composite streams. More detail on the principles and theory of pinch analysis are given as background in Chapter 2.

The simplest class of targeting approaches are graphical pinch analysis and transshipment (also referred to as cascade) formulations, first proposed by Linnhoff et al. and Papoulias and Grossmann [61, 73]. Graphical approaches plot the combined streams as composite curves on a resource quantity versus quality axis and visually determine the maximum amount of overlap between the curves. While convenient for small problems, graphical pinch analysis is inexact and cannot be used to quickly assess the effects of changes to the system. Transshipment methods instead use linear programs to automatically minimize resource use. However, they still require process variables to be known a priori in order to construct the composite streams. As a result, they cannot be used to simulate systems with known resource targets or for simultaneous process integration and optimization.

Other approaches improve the flexibility of pinch analysis by using disjunctions to express the combined resource availability at each quality [45, 68]. Disjunctions allow these methods to solve for any process variables, but they are not compact enough to address large systems or be embedded in process optimization problems. These formulations solve MINLPs that scale quadratically and cubically, respectively, in the number of constraints and binary variables as the number of resource sources and sinks in the system increase.

Overall, traditional approaches to process integration present a tradeoff between

flexibility and scalability. In addition, all of these methods are specific to a certain resource type, and solving a process integration problem requires searching for and selecting the correct method for the integrated resource. And these methods are generally not flexble to changes in assumptions if the problem becomes more complex.

1.3 Nonsmooth Approaches to Process Integration

A promising method for developing process integration methods that are both flexible and scalable is to use explicity nonsmooth equations. Nonsmooth functions are functions that are continuous but are not differentiable at every point in their domain such as the abolute value function or minimum and maximum functions over a finite set of points. Nonsmooth equations and expressions can be useful in simplifying a wide variety of problems because they

1. Can compactly describe variations in functions, such as property relations, across different regions using a single expression instead of requiring disjunctions and binary variables, and

2. Can transform many optimization problems to equation-solving ones using minimum and maximum functions across finite sets, either by reformulating KKT conditions or incorporating knowledge of the physcial system being described.

Targeting problems are excellent candidates for nonsmooth formulations because the resource availability or requirements of the composite source and sink streams vary nonsmoothly with their quality; the resource flows change suddenly over quality regions as streams become present or disappear. Duran and Grossmann [29] developed the first nonsmooth approach for process integration called the "pinch location method." This approach constructs composite curves for heat integration problems by using nonsmooth "max" expressions to automatically select which streams are present at a given temperature. These expressions are used in inequalities to constrain the temperatures of the hot composite curve to be higher than those of the cold composite curve for feasible heat transfer. Because the pinch location method avoids the

need to explicitly construct composite curves before solving the integration problem, it can be used to solve for process variables such as unknown stream temperatures and flow rates. In addition, the optimization problem scales linearly in the number of constraints with the number of hot and cold streams in the system, and it does not require a mixed-integer formulation.

To avoid the need for optimization and improve the scaling of the problem size with the number of streams, Watson et al. [92] reformulated the inequalities in the pinch location method to develop an equation-solving approach that describes the conditions for optimal heat recovery. The resulting approach is a system of nonsmooth equations that retains only two equations regardless of the size of the system. Watson et al. were also able take advantage of new methods in nonsmooth equation solving to solve for any process variable with the same convergence properties as smooth approaches.

1.4 Thesis Goals and Outline

Given the advantages of these nonsmooth approaches for solving heat integration problems, the primary goal of this thesis is to extend these benefits to other forms of process integration. This work accomplishes this goal by contributing three novel methods that can be used to optimize recovery and reuse for systems with different resources or assumptions. Each of these methods adapts the nonsmooth heat integration approaches to more efficiently model and optimize these integrated processes. These three contributions are:

1. A generalized operator for integrating any resource with a single limiting quality,

2. A multicomponent mass and water integration operator for addressing systems with multiple contaminants that can limit transfer,

3. A nonsmooth optimization approach that uses heat integration to design variable-temperature cogeneration systems.

Each of these projects provide a tool to address a key type of integration problem. Together, they increase the applicability of computationally efficient process integration methods to a wide range of chemical processes.

The chapters of this thesis detail methods, case studies, and results for each contribution as outlined below:

Chapter 2: Background Chapter 2 contains the necessary background for understanding the methods in the subsequent chapters. It details the structure and assumptions of the integration problems we consider; explains pinch analysis theory and the existing nonsmooth heat integration approaches in more depth; and gives an overview of nonsmooth equation-solving and optimization methods.

Chapter 3: The General Integration Operator Chapter 3 presents a nonsmooth approach for solving general process integration problems. This approach extends the equation-solving method of Watson et al. so that it can integrate a wide variety of resources. In addition, our general integration formulation is uniquely able to integrate multiple resources simultaneously and can automatically handle threshold problems in which one of the external resource utilities is not present. The general integration operator also retains the benefits of Watson et al.'s heat integration approach and requires only two equations per resource and can solve for any unknown process variables.

This chapter details the formulation and use of our nonsmooth integration operator, including variable selection for different resource types. We follow with a series of examples with the operator being applied to a wide range of integration problems: carbon-constrained energy planning, a water threshold problem, a hydrogen conservation network with unknown process variables, and a combined mass and water integration problem with a process model.

Chapter 4: Multicomponent Mass and Water Integration Chapter 4 extends the general integration operator to systems in which multiple factors can limit resource transfer. Specifically, we consider mass and water integration problems where more than one material is present in the water or solvent streams. When multiple components are present, they each independently can limit the feasibility of mass

transfer and their transfer in mass exchange units is also interdependent. Therefore, in these problems, all the materials must be considered simultaneously to avoid infeasible results, further increasing the size and complexity of the integration problem and its existing solution methods.

Our multicomponent integration operator adapts the general integration operator to these new problem types by incorporating nonsmooth scaling techniques and considering pinch conditions over all components simultaneously. The result is still a nonsmooth system of two equations that can be used to determine any process variable and that scales compactly in both the number of sources and sinks in the problem as well as the number of components. Compared to the single-component operator, the solution to the multicomponent operator is not necessarily an attainable water or mass target. Nevertheless, it provides a rigorous lower bound to the minimum fresh resource requirements, making it well-suited to solve large-scale screening and optimization problems.

This chapter formally defines the multicomponent integration problem considered and introduces previous work on the nonsmooth scaling relations. It then discusses the formulation and implementation of our nonsmooth operator and analyzes the tightness of the lower bound it provides. The chapter concludes with a series of case studies of increasing complexity to demonstrate the flexibility and scalability of our approach.

Chapter 5: Optimization of Variable-Temperature Cogeneration Designs Chapter 5 applies these integration approaches to design real systems by incorporating them into a nonsmooth optimization formulation. The application we consider is process cogeneration, which is the recovery of process waste heat by using it to drive a power cycle and produce electricity. While cogeneration is a promising approach to valorizing industrial waste heat, current methods for designing cogeneration systems must assume a constant-temperature heat source. In real processes, waste heat is likely to be released across a large temperature range, and designing for a single temperature reduces the utilization of high quality heat and limits the potential power output.

We present an optimization approach to design cogeneration systems that recovers the high-temperature heat from a process by including multiple power cycles with different operating temperatures. With this approach, each cycle can be supplied with waste heat from the process or heat rejected from higher-temperature power cycles. Our optimization formulation uses nonsmooth heat integration approaches as constraints in an outer optimization problem to efficiently account for all of the possible methods for heat recovery without needing to design the full network of stream matches.

We have also developed an original approach for estimating the cost of our combined power cycles without having to design the full heat exchanger network. Since targeting approaches do not determine the network for the integrated process, they do not provide convenient information to estimate capital costs. We introduce nonsmooth expressions that automatically partition streams into multiple multistream heat exchangers by temperature. Then we can employ methods for calculating the multistream heat exchanger areas to account for how the equipment requirements vary with phase or temperature. Thus, we are able to improve the accuracy of the cost estimation without sacrificing efficiency to determine the full network design.

This chapter details our novel approaches for optimizing variable-temperature cogeneration systems and estimating the costs of heat integration networks. We then demonstrate the potential of these approaches and variable-temperature cogeneration by using them to design combined sCO_2 Brayton and steam Rankine cycle systems for two promising applications, sulfuric acid and cement production.

Chapter 2

Background

This chapter contains background on both process integration and nonsmooth analysis. It includes a formal description of the targeting problem that we solve in later chapters and details on the existing approaches for solving this problem. We focus on providing an overview of pinch analysis and an understanding of how it its used in current nonsmooth integration methods. This chapter concludes with a discussion of the nonsmooth equation-solving and optimization formulations that we use to solve our nonsmooth integration formulations.

2.1 The General Integration Problem

Each of the contributions in this thesis presents a solution approach or application for a version of the general integration problem. The general integration problem considers a set of resources, T, for integration. For each resource, there is a set of sources and a set of sinks, where each source or sink has a quality that changes with resource transfer and a constant state that determines the rate at which this quality changes. The source and sink qualities determine whether resource transfer is feasible between them based on enforced quality limits or driving force limitations. For each resource, the integration problem also incorporates a fresh utility that can supply any sink and a waste utility that can take in resource from any source. This system of resource sources and sinks is connected by a process model, which is dependent on the

resource utilities and process variables. The objective of the general resource-targeting problem is then to determine the system specifications, either resource targets or process variables, at which minimal feasible resource use and waste production occur. Note that the general resource-targeting problem does not include applications that select between multiple utilities with different costs and qualities. However, multiple external utilities can be incorporated in the general integration problem by including them in the set of sources.

Mathematically, the general integration problem can be represented by a system of equations describing a process model and a set of embedded optimization problems in parallel that minimize the fresh loads of each resource and are parametric in the process variables. For each resource type $n \in T$, we denote a vector of utilities, $\boldsymbol{y}_n = (R_{SR,n},\ r_{SK,n})$, where $R_{SR,n}$ is the fresh resource supply and $r_{SK,n}$ is the waste resource flow. Then, for a process model, $\boldsymbol{h}$, and a set of process variables, $\boldsymbol{x}$, an outline of the structure of the general integration problem is:

$$\left.\begin{aligned} \mathbf{0} &= \mathbf{h}(\boldsymbol{x}, \boldsymbol{y}_1, \ldots, \boldsymbol{y}_{|T|}), \\ \{\boldsymbol{y}_n\} &= \arg\min_{\boldsymbol{y}_n} R_{SR,n}(\boldsymbol{x}) \\ &\text{s.t.} \quad \text{Resource balance holds,} \\ &\qquad\ \ \text{Resource transfer is feasible,} \end{aligned}\right\} \quad \forall n \in T.$$

Note that the minimum for each embedded optimization problem is guaranteed to be unique because $R_{SR,n}$ is the objective function value and $r_{SK,n}$ is given explicitly in terms of $R_{SR,n}$ by the resource balance. The resource balance also guarantees that minimizing $R_{SR,n}$ is equivalent to minimizing $r_{SK,n}$.

Within this problem structure, we also make assumptions about the nature of the transfer of each resource. For each resource transferred from a set of sources SR_n to a set of sinks SK_n, using the notation presented by Foo [40], we assume the sources $i \in SR_n$ have constant states $S_{i,n}$ that change in quality from $Q_{i,n}^{\text{in}}$ to $Q_{i,n}^{\text{out}}$ for a resource output $R_{i,n}$ according to $R_{i,n} = S_{i,n}(Q_{i,n}^{\text{in}} - Q_{i,n}^{\text{out}})$. Correspondingly, the sinks $j \in SK_n$ have constant states $s_{j,n}$ that change in quality from $q_{j,n}^{\text{in}}$ to $q_{j,n}^{\text{out}}$ for

a resource input $r_{j,n}$ according to $r_{j,n} = s_{j,n}(q_{j,n}^{\text{out}} - q_{j,n}^{\text{in}})$. For resource transfer to be feasible between a source i and sink j, the source qualities must be higher than those of the sink by a minimum feasible quality difference $\Delta Q_{\min}$, i.e. $Q_{i,n}^{\text{out}} \geq q_{j,n}^{\text{in}} + \Delta Q_{\min}$ and $Q_{i,n}^{\text{in}} \geq q_{j,n}^{\text{out}} + \Delta Q_{\min}$.

2.2 Pinch Analysis

The solution to the general integration problem can be described by using pinch analysis theory. This theory is used as the basis for targeting approaches because it uses composite curves to avoid needing to design the resource exchange nework. In this section, we provide an overview of pinch analysis to help improve understanding of the nonsmooth integraion methods presented later in this work. For a more in-depth introduction to pinch analysis theory, we recommend Smith [80].

Source and sink composite curves are constructed by combining all of the sources or sinks, respectively, that are present at each quality. The state of the combined stream at a given quality is the sum of the states of all the streams that are present. Therefore, the total resource availability of the composite curve above or below each quality will be consistent with the individual sources and sinks. Because we assume the stream states are constant, the cumulative state of the composite curves will be constant within intervals partitioned by the inlet and outlet stream qualities. Therefore, with this assumption, the resource transferred by the combined streams is a piecewise affine function of the quality with nonsmooth points at the inlet and outlet qualities.

Once the sources and sinks are combined into composite curves, the aggregate data can be used assess the optimal resource transfer. Within a quality interval, resource can be transferred from the source to the sink composite curve. Any excess resource available from the sources can be cascaded down to be used in a lower quality interval. Any additional resource required to supply the sinks must come from higher quality intervals. Therefore, the fresh resource utility is cascaded through each quality inteveral until it is used up, and for feasibility, it must be large enough so that the

sinks are supplied in all intervals.

Pinch analysis theory shows that this fresh resource supply will be minimized when there is a pinch point in the system. This pinch point occurs when there is a quality interval that does not receive any resource from higher quality intervals. When a pinch point is present, the external fresh utility is not cascaded all the way through the quality intervals. It is only used to supply resource sinks above the pinch quality, and the external waste utility only receives excess resource from the sinks below it. If there is not a pinch point in the system, fresh utility is cascaded all the way down to the waste stream and both utilities can be reduced. When a pinch point is present, decreasing the utilities will cause an infeasible system where some resource is transferred from low to high quality intervals.

Note that, if there is a nonzero minimum feasible quality difference required for resource transfer to occur, such as a minimum temperature difference for heat transfer or concentration for mass transfer, then the qualities for the sinks must be shifted up by this minimum quality difference when constructing the composite curves and enthalpy intervals to ensure a feasible difference at the pinch point.

Here we present the transshipment formulation of Papoulias and Grossmann [73] as an example of how to fully express this pinch analysis approach. In addition to being one of the first numerical approaches to resource-targeting, the transshipment formulation is still commonly used. This approach first defines a set of K_n quality intervals for each resource, partitioned by the sorted inlet and outlet qualities of the sources and sinks so that interval k spans higher quality values than $k+1$. Thus, each interval with width $\Delta Q_{k,n}$, is predefined and independent of the current source or sink being considered. Given these quality intervals, we identify the sets $SR_{k,n} \subset SR_n$ and $SK_{k,n} \subset SK_n$, which are the sources and sinks, respectively, that have changes in quality that span interval k. The transfer constraints for each resource calculate the hypothetical resource flows $F_{k,n}$ that are available for transfer from interval k to the lower quality interval $k+1$ using resource balances. (Note these flows are distinct from the individual source outputs $R_{i,n}$ because they are net quantities that consider all of the sources and sinks in k.) Feasibility is enforced by constraining the flows $F_{k,n}$

to be nonnegative. Thus, the general integration problem, which we wish to solve for a selection of unknowns from $\boldsymbol{x}$ and $\boldsymbol{y}_n$, can be written as:

$$
\begin{aligned}
&\mathbf{0} = \mathbf{h}(\boldsymbol{x}, \boldsymbol{y}_1, \ldots, \boldsymbol{y}_{|T|}), \\
&\{\boldsymbol{y}_n\} = \underset{\boldsymbol{y}_n, F_{1,n}, \ldots, F_{|K_n|-1,n}}{\arg\min} \quad R_{SR,n}(\boldsymbol{x}), \\
&\quad \text{s.t.} \quad 0 = R_{SR,n} - F_{1,n} + \Delta Q_{1,n}\Big(\sum_{i \in SR_{1,n}} S_{i,n} - \sum_{j \in SK_{1,n}} s_{j,n} \Big), \\
&\qquad\quad 0 = F_{k-1,n} - F_{k,n} + \Delta Q_{k,n}\Big(\sum_{i \in SR_{k,n}} S_{i,n} - \sum_{j \in SK_{k,n}} s_{j,n} \Big), \\
&\qquad\qquad\qquad\qquad\qquad\qquad\qquad\qquad \forall k \in \{2, \ldots, |K_n| - 1\}, \\
&\qquad\quad 0 = F_{|K_n|-1,n} - r_{SK,n} + \Delta Q_{|K_n|,n}\Big(\sum_{i \in SR_{|K_n|,n}} S_{i,n} - \sum_{j \in SK_{|K_n|,n}} s_{j,n} \Big), \\
&\qquad\quad 0 \leq F_{k,n}, \quad \forall k \in \{1, \ldots, |K_n| - 1\},
\end{aligned}
\qquad \Bigg\} \quad \forall n \in T.
$$

For this formulation, the fresh resource flows $R_{SR,n}$ are minimized when a flow $F_{k,n}$, $k \in K_n$ is zero $\forall n \in T$, which indicates that a pinch point is present.

Although the above formulation is a complete representation of the general integration problem as embedded linear programs, when qualities are unknown, it is a nontrivial process to determine the quality intervals, k, and the mapping of the sources and sinks to these intervals to find $SR_{k,n}$ and $SK_{k,n}$ as functions of the qualities. Therefore, the qualities in the problem cannot be unknowns in $\boldsymbol{x}$ and must be known a priori.

An alternative approach to understanding and applying pinch analysis theory is graphical pinch analysis. This approach visualizes the comosite curves on resource quantity versus quality axes. Then, visually, the pinch point occurs when the composite curves touch. Because the curves touch at this point, there is no excess resource that can be cascaded down to the waste stream. The pinched system can also be thought of as the system in which the composite curves overlap as much as feasible possible, and thus the most resource is transfered between the sources and sinks. Figure 2-1 shows an example of composite curves plotted for a heat integration prob-

lem. While graphical pinch analysis can be intuitive and easy to implement for small problems, like transshipment approaches, the qualities must be known a priori. As a result, these traditional pinch analysis approaches cannot be applied to problems where these qualities may be decision variables, such as designing systems with given resource constraints or optimizing the design of an integrated system.

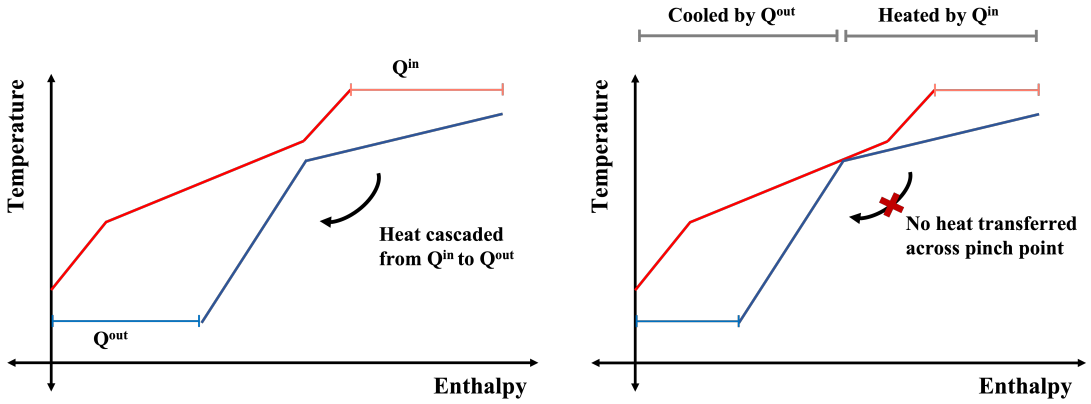

Figure 2-1: Composite curves for suboptimal (left) and optimal (right) integrated heat transfer systems. The hot and cold composite curves are shown in red and blue, respectively. When the system is not fully integrated, there is an enthalpy separation between the composite curves that shows the heat that is cascaded from the hot utility down to the cold. When a pinch point is present where there is no enthalpy separation, there is no heat from the hot utility transferred across it and supplied to the sink.

2.3 Nonsmooth Integration Approaches

Because of the limitations of other targeting methods, the work in this thesis develops nonsmooth approaches to solve integration problems. These approaches use nonsmooth functions to describe the naturally nonsmooth behavior of the composite curves, which avoids the need to explicitly construct quality intervals. In this section, we describe the previous nonsmooth integration methods that we draw on in our work.

These nonsmooth integration approaches solve a specific instance of the general integration problem for heat transfer. For heat integration, the resource quantities are the enthalpy transferred, Q, the streams states are their heat capacity flow rates

F, and the qualities that limit heat transfer are the temperatures T. In this case, the general integration problem becomes

$$\begin{aligned} \boldsymbol{y} \in \underset{\boldsymbol{y}=[Q^{\mathrm{H}} Q^{\mathrm{C}}]}{\arg\min}\ & Q^{\mathrm{H}} \\ \text{s.t.}\quad & \text{Energy balance holds,} \\ & \text{Heat transfer is feasible,} \end{aligned} \tag{2.1}$$

where Q^{H} and Q^{C} are the enthalpy requirements of the heating and cooling external utilities, respectively.

To solve this problem, Duran and Grossmann [29] developed the "pinch location method," which avoids the explicit construction of temperature intervals by using explicitly nonsmooth expressions to automatically select which streams should be included above potential pinch temperatures. These expressions are used in inequalities to constrain the total enthalpy of the hot streams to be greater than that of the cold streams at each temperature so that heat is cascaded only from high to low temperatures. One inequality is introduced for each potential pinch temperature in the system. Because the temperature-heat relationship is assumed to be affine for each stream, it is only feasible for pinch points to occurs at the finite set of inlet stream temperatures. Thus, the number constraints in the formulations scale linearly with the number of hot and cold streams in the process.

The resulting formulation is:

$$\begin{aligned} \boldsymbol{y} \in \underset{\boldsymbol{y}=[Q^{\mathrm{H}}, Q^{\mathrm{C}}]}{\arg\min}\ & Q^{\mathrm{H}} \\ \text{s.t}\quad & 0 = \sum_{i \in H} F_i (T_i^{\mathrm{in}} - T_i^{\mathrm{out}}) - \sum_{j \in C} f_j (t_j^{\mathrm{out}} - t_j^{\mathrm{in}}) + Q^{\mathrm{H}} - Q^{\mathrm{C}} \\ & 0 \leq EBP_C^p - EBP_H^p + Q^{\mathrm{C}}, \quad \forall p \in P, \end{aligned} \tag{2.2}$$

where $P = H \cup C$ is the index set of pinch point candidates and EBP_H^p and EBP_C^p

are the hot and cold stream balances below the pinch candidate p defined by

$$EBP_H^p := \sum_{i \in H} [\max\{0, T^p - T_i^{\text{out}}\} - \max\{0, T^p - T_i^{\text{in}}\}], \quad \forall p \in P, \tag{2.3}$$

$$EBP_C^p := \sum_{j \in C} [\max\{0, (T^p - \Delta T_{\min}) - t_j^{\text{in}}\} - \max\{0, (T^p - \Delta T_{\min}) - t_j^{\text{out}}\}], \quad \forall p \in P. \tag{2.4}$$

$\Delta T_{\min}$ is the minimum feasible temperature difference for heat transfer, and the temperatures of the pinch point candidates, T^p are given by

$$T^p = \begin{cases} T_i^{\text{in}} & \forall p = i \in H, \\ t_j^{\text{in}} + \Delta T_{\min}, & \forall p = j \in C. \end{cases}$$

Note that Duran and Grossmann's original formulation uses the enthalpy balances above candidate pinch temperatures. Here, we present the alternative enthalpy balances below the pinch candidates from Watson et al. [92] to stay consistent with the other methods used in this work.

Duran and Grossmann solve this nonsmooth optimization problem using a smoothing approximation, which requires a user-specified parameter that must be tuned to avoid inaccuracies and ill-conditioning. Alternatively, Vikse et al. [88] show success solving this problem directly using nonsmooth optimization approaches.

To avoid approximations and improve the scaling of the problem size with the number of streams, Watson et al. [92] reformulated the inequalities in the pinch location method to develop an equation-solving approach that describes the conditions for optimal heat recovery. The resulting approach is a system of two nonsmooth equations that enforce the existence of a pinch point at one of the potential pinch temperatures. For feasibility, at each of the potential pinch points, the enthalpy balance will be nonnegative, which is enforced by Duran and Grossman's constraints. In addition, for optimality, the constraint at the pinch temperature must be equal to zero so that the enthalpy balance is minimized at this point. These conditions therefore can be re-expressed using a single nonsmooth "min" function. An overall

energy balance is included to ensure the external utilities cover the additional heating and cooling requirements. The resulting system of equations is

$$0 = \sum_{i \in H} F_i(T_i^{\text{in}} - T_i^{\text{out}}) - \sum_{j \in C} f_j(t_j^{\text{out}} - t_j^{\text{in}}) + Q^{\text{H}} - Q^{\text{C}}, \tag{2.5}$$

$$0 = \min_{p \in P}\{EBP_C^p - EBP_H^p + EXT_C^p - EXT_H^p\} + Q^{\text{C}}. \tag{2.6}$$

Watson et al. also add non-physical curve extensions to the enthalpy balances so that their derivatives are defined for all temperatures. These extensions are defined by

$$EXT_H^p := \sum_{i \in H} F_i[\max\{0, T^p - T^{\max}\} - \max\{0, T^{\min} - T^p\}], \quad \forall p \in P,$$

$$EXT_C^p := \sum_{j \in C} f_j[\max\{0, (T^p - \Delta T_{\min}) - t^{\max}\} - \max\{0, t^{\min} - (T^p - \Delta T_{\min})\}],$$

$$\forall p \in P,$$

where $T^{\max}$ and $T^{\min}$ are the maximum and minimum temperatures, respectively, across the hot streams, and $t^{\max}$ and $t^{\min}$ and the maximum and minimum temperatures across the cold streams.

Watson et al. also introduce a third equation that can be used to estimate the area of the ideal multistream heat exchanger required to achieve the heat integration target calculated by Equations (2.5) and (2.6). This approach assumes that the overall exchanger area is the sum of the contributions from each enthalpy interval in the composite curves. At each nonsmooth point on the composite curves, Watson et al. implicitly solve for the unknown temperature on the other curve to fully define the enthalpy interval. Because the composite curves are affine within each enthalpy interval, the area contributions from each interval can be calculated by using the same approach as for a classic two-steam heat exchanger. Concretely, let K be the index set for the points at which the composite curves are nondifferentiable, as well as their endpoints. Then for $k \in K$, the enthalpy values at the nonsmooth points in

the composite curves are calculated using

$$0 = Q^k - \sum_{i \in H} F_i(\max\{0, T^k - T_i^{\text{out}}\} - \max\{0, T^k - T_i^{\text{in}}\}), \tag{2.7}$$

$$0 = Q^k - \sum_{j \in C} f_j(\max\{0, t^k - t_j^{\text{out}}\} - \max\{0, t^k - t_j^{\text{in}}\}), \tag{2.8}$$

where Equation (2.7) finds the corresponding enthalpies for the hot stream temperatures, $T^k \in \{T_i^{\text{in/out}} : i \in H\}$ and (2.8) finds the enthalpies for the cold stream temperatures $t^k \in \{t_j^{\text{in/out}} : j \in C\}$.

Once the enthalpies Q^k are defined, Equation (2.7) or (2.8) is solved for the remaining unknown hot or cold stream temperature, respectively. The enthalpy-temperature triplets (Q^k, T^k, t^k) for each nonsmooth point are sorted by their enthalpy values, and the resulting enthalpy intervals are used to calculate the heat exchanger area:

$$0 = UA - \sum_{k \in K, k \neq |K|} \frac{\Delta Q^k}{\Delta T_{\text{LM}}^k}, \tag{2.9}$$

where $\Delta Q^k = Q^{k+1} - Q^k$ and

$$\Delta T_{\text{LM}}^k(\Delta T^k, \Delta T^{k+1}) = \begin{cases} \frac{1}{2}(\Delta T^k + \Delta T^{k+1}), & \text{if } \Delta T^k = \Delta T^{k+1}, \\ \frac{\Delta T^{k+1} - \Delta T^k}{\ln(\Delta T^{k+1}) - \ln(\Delta T^k)}, & \text{otherwise,} \end{cases}$$

with $\Delta T^k = T^{k+1} - T^k$. If the sorting operation is performed using an explicitly nonsmooth method such as Bubble Sort, Watson et al.'s approach can be used not only to solve for the heat exchanger area, but also to solve for other variables in the system for a specified area value.

Compared to other approaches, the nonsmooth integration operator only requires an equation system instead of an optimization formulation and the number of equations remains the same regardless of the number of hot and cold streams in the system. These features make it an efficient choice for constraining heat transfer when optimizing an integrated system. Therefore, we adapt this approach to solve the general integration problems in this work.

2.4 Overview of Nonsmooth Analysis

This next section outlines the nonsmooth equation-solving and optimization methods that we use to handle nonsmooth functions in our work.

2.4.1 Equation Solving

Nonsmooth analysis is a well-developed field, and many algorithms for nonsmooth equation-solving have been defined with desirable theoretical properties that are even competitive with their smooth counterparts. Such algorithms include Newton-type methods such as semismooth or linear-programming (LP) Newton.

The semismooth Newton method is analogous to the smooth Newton method; however, the evaluation of a generalized derivative element, $\mathbf{F}(\boldsymbol{x}_k)$, is required at each iteration instead of the Jacobian matrix. Therefore, the k^{th} iteration is given by solving the linear equation

$$\mathbf{F}(\boldsymbol{x}_k)(\boldsymbol{x}_{k+1} - \boldsymbol{x}_k) = -\mathbf{f}(\boldsymbol{x}_k),$$

where $\mathbf{f}$ is semismooth and $\mathbf{F}(\boldsymbol{x}_k)$ is square and nonsingular.

The LP-Newton method relaxes the singularity requirement by iteratively solving the LP

$$\begin{aligned} \min_{\gamma\in\mathbb{R},\boldsymbol{x}\in X} \gamma \quad \text{s.t.} \quad & \|\mathbf{f}(\boldsymbol{x}_k) + \mathbf{F}(\boldsymbol{x}_k)(\boldsymbol{x} - \boldsymbol{x}_k)\|_\infty \leq \gamma \|\mathbf{f}(\boldsymbol{x}_k)\|_\infty^2, \\ & \|\boldsymbol{x} - \boldsymbol{x}_k\|_\infty \leq \gamma \|\mathbf{f}(\boldsymbol{x}_k)\|_\infty, \end{aligned}$$

where X is a polyhedral set [36]. For global convergence, a simple backtracking line search is performed after each LP iteration [37]. If $\mathbf{f}$ is piecewise differentiable [77], the generalized derivatives are elements of the Bouligand (B-) subdifferential (the set of limiting Jacobians), and certain regularity conditions are met, both of these methods exhibit local Q-quadratic convergence.

Despite both the desirable performance of these algorithms and the ability of

nonsmooth equations to describe many physical systems naturally and compactly, nonsmooth equation solving has generally been avoided due to the difficulty in calculating generalized derivative elements. Elements of the B-subdifferential cannot be found directly using automatic differentiation (AD) since they do not obey sharp calculus rules, nor can they be found from directional derivatives in the coordinate directions or component-wise limiting gradients [12].

However, Khan and Barton have recently defined the LD-derivative, which follows a sharp chain rule, and can therefore be calculated using the nested computations of AD [54]. Additionally, the LD-derivative can be used to compute the L-derivative elements of the B-subdifferential for piecewise differentiable functions. Combined, these properties allow for the automatic calculation of useful generalized derivative elements for nonsmooth equation solving in complex settings and make explicitly nonsmooth approaches to process simulation viable.

In this work, we solve nonsmooth equation systems using either the semismooth or LP Newton method as specified. We implemented these methods in MATLAB® 2019B. Both methods are supplied with generalized derivative elements calculated with vector forward AD for LD-derivatives as detailed by Khan and Barton and Barton et al. and implemented using operator overloading [54, 12]. Using this approach, each function evaluation will produce a LD-derivative in addition to the function value. These directional derivatives are transformed to generalized L-derivatives and provided as the Jacobian information to the equation-solving methods. For more information on performing operator overloading for automatic differentiation in MATLAB, we suggest referring to Neidinger [69].

2.4.2 Optimization

Current mathematical programming methods for handling general nonsmooth objectives and constraints are limited and not included in most optimization software. Nonsmooth optimization problems are particularly challenging because all elements of the Clarke generalized Jacobian $\partial_C f(\boldsymbol{x})$, which is the convex hull of the set of limiting Jacobians, must be considered to ensure that the KKT conditions are met. For a

constrained problem, the generalized KKT sufficient conditions are: for a convex objective $f : \mathbb{R}^n \to \mathbb{R}$ and convex constraints $g_i(\boldsymbol{x}) \leq 0, \quad g_i : \mathbb{R}^n \to \mathbb{R}, \quad i = 1, \ldots, m$, $\boldsymbol{x}^*$ is a global optimum of the problem if there exist multipliers $\lambda_i \geq 0, \quad i = 1, \ldots, m$ such that $\lambda_i g_i(\boldsymbol{x})^* = 0$ and $\mathbf{0} \in \partial_C f(\boldsymbol{x}^*) + \sum_{i=1}^m \lambda_i \partial_C g_i(\boldsymbol{x}^*)$. These conditions make it difficult to determine a descent direction and provide no implementable subgradient-based stopping criteria.

While there are specialized algorithms available for solving nonsmooth optimization problems with specific forms, most generalizable nonsmooth optimization algorithms fall into two categories: subgradient methods or bundle methods [11], [51]. Subgradient approaches are local solvers that adapt smooth gradient-based methods by replacing derivatives with a single element of the subdifferential or other generalized derivative for nonconvex functions. Both these and other nonsmooth optimization solvers typically handle constraints using barrier functions. These methods are easy to implement by adapting smooth local solvers and can take advantage of the flexibility and robustness of these established codes. Nevertheless, subgradient algorithms do not guarantee a descent direction at each iteration, which can result in a poor convergence rate. In addition, it is traditionally challenging to calculate a generalized derivative element at each step. However, Watson et al. [93] had success adopting a new type generalized derivative for subgradient descent. This LD-derivative can be calculated using automatic differentiation [54] making it easy to supply subgradient elements to a smooth solver.

Bundle methods use a "bundle" of subgradients from previous iterations to approximate the whole subdifferential instead of using one arbitrary subgradient and to provide more information about the local behavior of the function. The subgradients are used in a quadratic programming subproblem to find the next search direction. Bundle methods have been shown to have global convergence for a limited number of stored subgradients and are more efficient than simpler subgradient approaches. However, the size of the subproblems can increase quickly with the number of variables, making them ill-suited to large-scale nonsmooth problems [10]. For nonconvex problems, additional relaxations are also required in the subproblem, which can decrease

the rate of convergence.

While the subgradient and bundle methods are the most common approaches to nonsmooth optimization, we also note that recent work in gradient sampling methods, which randomly sample subgradients around the current iterations, suggests that they have the potential to outperform bundle methods [11].

For this work, we chose to use the method presented by Watson et al., which was developed to optimize a system similarly constrained by the nonsmooth equality constraints in Formulation (5.2). For this problem type, Watson et al. were unable to achieve convergence with a bundle method. However, they had success with a subgradient-type method that uses the LD-derivative to calculate generalized derivative elements at nonsmooth points. LD-derivatives are a form of generalized directional derivatives which follow a sharp chain rule, and can therefore be calculated using the nested computations of automatic differentiation [54]. They also follow an implicit function theorem that can be used to find derivatives from the implicit functions in this work [54, 12], which are part of the steam property model and the multistream heat exchanger area calculations.

Watson et al. solve nonconvex, nonsmooth optimization problems by using LD-derivatives to provide generalized Jacobian information to the smooth solver IPOPT, which uses a primal dual interior point method. The built-in IPOPT methods are used to estimate the Hamiltonians from these generalized derivative elements. Watson et al. note that this approach is not guaranteed to converge to a local minimum if the minimum is at a nonsmooth point. Nevertheless, in practice, they were able to still reach minima at nonsmooth points with slightly relaxed tolerances.

We also implemented this optimization approach in MATLAB® 2019B and generated LD-derivatives using operator overloading. These directional derivatives are transformed to generalized L-derivatives and provided as the gradient and Jacobian information to the IPOPT-MATLAB interface.

Chapter 3

General Integration Operator

This chapter presents a nonsmooth approach for solving general process integration problems that extends the integration approach from Watson et al. [92]. Watson et al.'s nonsmooth approach, which is detailed in the Background chapter, is simple, compact, and able to solve for any process variables. However, it is only applied to heat integration problems, specifically for multistream heat exchangers. Therefore, in this work, we generalize the variables in Watson et al.'s formulation to extend its benefits to integrating any pinch-constrained resource.

Our method scales well with problem size, requires only equation-solving approaches, and can solve for process variables while simultaneously considering the integration of multiple resources. We also present a simple modification that identifies and solves threshold problems automatically. To our knowledge, this is the only approach to the targeting problem that has all of these properties, and the only solution presented explicitly for the general problem.

In the sections below, we detail the formulation of our nonsmooth integration operator, including variable selection for different resource types and modifications for the threshold problem. We follow with a series of examples with the operator being applied to a wide range of integration problems: carbon-constrained energy planning, a water threshold problem, a hydrogen conservation network with unknown process variables, and a combined mass and water integration problem with a process model. We conclude with a discussion of the features and limitations of our approach and

possible avenues for future work.

The work presented in this chapter has been published in Nielsen and Barton [72].

3.1 Problem Structure and Assumptions

The method presented in this chapter solves the "general integration problem" detailed in the Background chapter. The general integration problem describes the simultaneous minimization of the fresh supplies of an arbitrary number of resources. Each resource type $n \in T$, has utilities, $\boldsymbol{y}_n = (R_{SR,n},\ r_{SK,n})$, where $R_{SR,n}$ is the fresh resource supply and $r_{SK,n}$ is the waste resource flow, which are minimized by transferring resource from a set of sources SR_n to a set of sinks SK_n. We assume the sources $i \in SR_n$ have constant states $S_{i,n}$ that change in quality from $Q_{i,n}^{\text{in}}$ to $Q_{i,n}^{\text{out}}$ for a resource output $R_{i,n}$ according to $R_{i,n} = S_{i,n}(Q_{i,n}^{\text{in}} - Q_{i,n}^{\text{out}})$. Correspondingly, the sinks $j \in SK_n$ have constant states $s_{j,n}$ that change in quality from $q_{j,n}^{\text{in}}$ to $q_{j,n}^{\text{out}}$ for a resource input $r_{j,n}$ according to $r_{j,n} = s_{j,n}(q_{j,n}^{\text{out}} - q_{j,n}^{\text{in}})$. For resource transfer to be feasible between a source i and sink j, the source qualities must be higher than those of the sink by a minimum feasible quality difference $\Delta Q_{\min}$. The general integration problem can also include a process model $\mathbf{h}(\boldsymbol{x}, \boldsymbol{y}_1, \ldots, \boldsymbol{y}_{|T|})$ that is a function of the set of process variables $\boldsymbol{x}$ and the utilities $\boldsymbol{y}_n$.

There is a significant body of work proposing different integration types, each of which can be described by the general integration problem. The resources, states, and qualities for a representative sample of integration types are summarized in Table 3.1. Note that the same terminology is often used to refer to integration formulations with different selections of resources, and formulations that are fundamentally the same are referred to in different ways. For example, water integration approaches can be of either the "fixed-load" or "fixed-flow rate" type. The former problem considers process units with constant water flow rates and is treated the same as a mass integration problem with the contaminant mass as the integrated resource; whereas, the latter directly integrates the water flows [39]. Similarly, carbon integration can either integrate power production with different emission quantities, or flows between CO_2

Table 3.1: Resources, qualities, and states for a sample of integration formulations (adapted from Foo [40]).

Integration Types	**Resource Quantity**	**Quality**	**State**
Heat[61]	heat transfer rate	temperature	heat capacity flow rate
Mass[31] Fixed-load water[91]	contaminant mass load flow rate	concentration in reference stream	scaled solvent mass flow rate
RCN[52] Fixed-flow water [33] Hydrogen [7] Oxygen [99] Carbon [67]	mass flow rate	cumulative difference in property loads (e.g. contaminant mass flow rate)	reciprocal of a linear mixing property, sorted by increasing property value (e.g. contaminant concentration)
Carbon-constrained energy[82]	electrical power	cumulative difference in emission masses	reciprocal emission factor, sorted by increasing emissions
Inventory[19]	time	cumulative volume	usage or production rate

sources and sinks [82, 67]. In addition, both of the latter water and carbon formulations are types of resource conservation networks (RCNs), in which the resource is a material flow that can be reused directly without considering heat or mass transfer [40].

3.2 Generalized Nonsmooth Operator Formulation

In this section, we introduce a new approach to solving the general resource-targeting problem that uses explicitly nonsmooth equations to improve scaling compared to current approaches and retain the ability to solve for unknown process variables including qualities. Our method also has the flexibility to automatically identify threshold problems. As an alternative to the nonsmooth LPs of the transshipment formulation and the MINLPs or nonsmooth NLPs of the pinch location method formulations, our nonsmooth approach uses systems of equations to express the solutions of the

embedded minimization problems. Each of these nonsmooth systems, or nonsmooth integration operators, consists of two equations per integrated resource: an overall resource balance, which ensures that resource transfer is feasible based on availability, and a resource balance below potential resource transfer pinch points, which enforces optimal transfer given quality limits or driving force limitations. The nonsmooth integration operators for each resource are coupled with the process model, and the resulting system can be solved efficiently using the nonsmooth equation-solving methods described in the Background.

As in Watson et al.'s heat integration approach, the pinch point balance uses a simple nonsmooth expression to enforce both the feasibility of resource transfer due to quality constraints and minimal resource use. For resource transfer to be feasible, at each pinch candidate quality, the total resource quantity produced by the lower quality sources must be less than or equal to the capacity of the sinks (including the waste resource flow) that can accommodate resource at these qualities. This feasibility requirement is given explicitly by the inequality constraints in the pinch location formulation from Duran and Grossmann and is expressed in the transshipment formulation by the directionally-constrained resource flows from high to low quality.

In addition, according to pinch analysis theory, for resource transfer to be optimal, there must exist at least one quality pinch point for the resource, below which the source production and sink capacities are equal. Otherwise, fresh resource must be used to fulfill the sink demands below each quality level and is cascaded down to the waste resource sink. Therefore, both the feasibility and optimality criteria can be easily expressed using an explicitly nonsmooth equation by setting the minimum resource balance over the problem qualities to zero.

Because the general integration operator assumes constant state sources and sinks, this property can be equivalently enforced with a pinch point balance that considers a finite set of potential pinch points. Again drawing on pinch analysis, for constant state sources and sinks, the potential pinch point candidates are the inlet source and sink qualities that define distinct quality intervals for the problem. Additionally, enforcing feasibility at each of these points ensures feasibility at all qualities between

them. Therefore, the pinch point balance in our nonsmooth integration operator considers potential pinch points in this set.

Then, neglecting the index n for clarity, the resulting nonsmooth integration operator for a single given resource is:

$$0 = \sum_{i \in SR} S_i (Q_i^{\text{in}} - Q_i^{\text{out}}) - \sum_{j \in SK} s_j (q_j^{\text{out}} - q_j^{\text{in}}) + R_{SR} - r_{SK}, \tag{3.1}$$

$$0 = \min_{p \in P} \{RBP_{SK}^p - RBP_{SR}^p\} + r_{SK}, \tag{3.2}$$

where P is the finite index set of pinch point candidates and

$$\begin{aligned} RBP_{SR}^p := & \sum_{i \in SR} S_i [\max\{0, Q^p - Q_i^{\text{out}}\} - \max\{0, Q^p - Q_i^{\text{in}}\} \\ & - \max\{0, Q^{\min} - Q^p\} + \max\{0, Q^p - Q^{\max}\}], \quad \forall p \in P, \\ RBP_{SK}^p := & \sum_{j \in SK} s_j [\max\{0, (Q^p - \Delta Q_{\min}) - q_j^{in}\} \\ & - \max\{0, (Q^p - \Delta Q_{\min}) - q_j^{\text{out}}\} + \max\{0, (Q^p - \Delta Q_{\min}) - q^{\max}\} \\ & - \max\{0, q^{\min} - (Q^p - \Delta Q_{\min})\}], \quad \forall p \in P, \end{aligned}$$

where $\Delta Q_{\min}$ is the minimum feasible quality difference between a source and sink at which resource transfer can occur and the source qualities at the potential pinch points are

$$Q^p = \begin{cases} Q_i^{\text{in}}, & \forall p = i \in SR, \\ q_j^{\text{in}} + \Delta Q_{\min}, & \forall p = j \in SK. \end{cases}$$

The expressions RBP_{SR}^p and RBP_{SK}^p are the cumulative source and sink resource quantities that can be exchanged at qualities lower than Q^p. The nonsmooth max terms capture the position of the inlet and outlet qualities of each source or sink in relation to the potential pinch point quality, and therefore whether the source or sink should be, either partially or wholly, included in the resource balance. Thus, these expressions allow us to avoid the explicit ordering and construction of quality

intervals as required in the transshipment formulation. $Q^{\min,\max}$ and $q^{\min,\max}$ are the minimum and maximum qualities across the sources or the sinks, respectively, and the max terms containing these variables create nonphysical extensions to the cumulative resource quantities, which avoid additional singular regions or infinite solutions by ensuring the difference between the source and sink resource balances is always defined. Note that, so the pinch point balance correctly selects resources transferred below the pinch quality, we define the inlet and outlet qualities such that $Q_{\text{in}} \geq Q_{\text{out}}$ and $q_{\text{out}} \geq q_{\text{in}}$.

For the case of heat integration, Watson et al. provide a detailed justification for why this system of equations enforces the existence of a pinch point [92]. This analysis can be applied analogously to the case of a general resource whose transfer obeys the linear relations $R_{i,n} = S_{i,n}(Q_{i,n}^{\text{in}} - Q_{i,n}^{\text{out}})$ and $r_{j,n} = s_{j,n}(q_{j,n}^{\text{out}} - q_{j,n}^{\text{in}})$ where the qualities have values that increase with increasing purity as described in the section below. Therefore, for any pinch-constrained resource transfer with this property, Equations (3.1) and (3.2) will enforce a pinch point and thus describe optimal resource transfer.

Graphically, the source and sink balances define quality versus quantity composite curves, and Equations (3.1) and (3.2) ensure that the source composite curve is always at higher qualities than the sink composite curve and that the composite curves touch at a pinch point. Figure 3-1 illustrates this graphical conceptualization of the resource balances and nonsmooth integration operator.

3.2.1 Determining Integration Variables

Before the nonsmooth operator can be used to solve a general integration problem, qualities and states must be defined for each resource, and often the provided data must be preprocessed in order to calculate these state and quality values. The sections below present some special considerations when defining and calculating integration variables, particularly for RCNs.

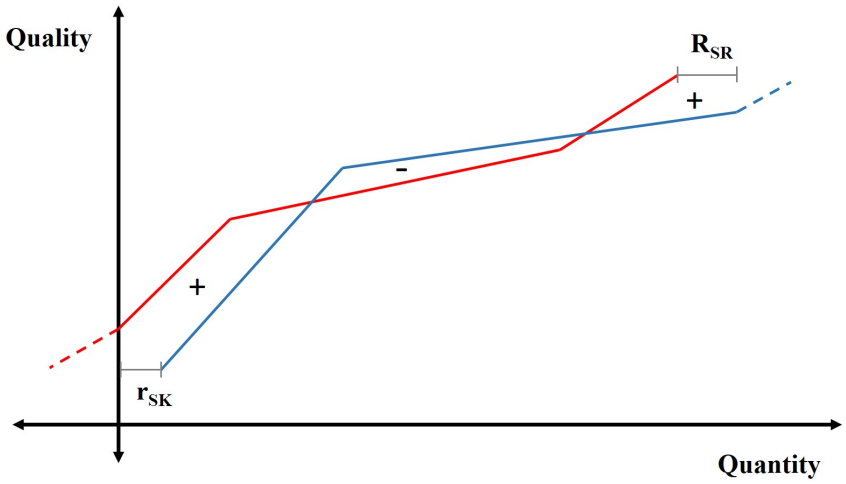

Figure 3-1: Graphical illustration of the nonsmooth integration operator. The red and blue plots are the source and sink composite curves whose qualities are generated by RBP^p_{SR} and RBP^p_{SK}, respectively, at each potential pinch point, and the dashed lines show the curve extensions. The sign of $RBP^p_{SK} - RBP^p_{SR} + r_{SK}$ is indicated for each region. These particular curves do not satisfy Equations (3.1) and (3.2) because $RBP^p_{SK} - RBP^p_{SR} + r_{SK}$ is not constrained to be nonnegative.

Quality Sign Selection

The pinch point balance as defined above calculates net quantity of resource transferred at qualities below the pinch point quality, including the waste resource quantity. Therefore, our formulation requires the waste resource flow to have the lowest quality value of all the sources and sinks and the fresh resource to have the highest. Thus, while the equations as written are applicable to any general integration problem, the qualities used here may need to be transformed from those presented in other works. For example, in many types of integration problems, including common RCNs, the qualities are cumulative values such as property loads. In the typical RCN formulation, summarized by Foo [40], the cumulative property loads, P_i and p_j, are determined by summing up changes in load from a selected fresh resource load

$P^{\min} = p^{\min}$ according to

$$P_1^{\text{out}} = P^{\min}, \tag{3.3}$$

$$P_i^{\text{in}} = P_i^{\text{out}} + \Delta P_i, \quad \forall i \in SR, \tag{3.4}$$

$$P_i^{\text{out}} = P_{i-1}^{\text{in}}, \quad \forall i \in SR, \quad i \neq 1 \tag{3.5}$$

for the source loads and

$$p_1^{\text{in}} = p^{\min}, \tag{3.6}$$

$$p_j^{\text{out}} = p_j^{\text{in}} + \Delta p_j, \quad \forall j \in SK, \tag{3.7}$$

$$p_j^{\text{in}} = p_{j-1}^{\text{in}}, \quad \forall j \in SK, \quad j \neq 1, \tag{3.8}$$

for the sinks. $P^{\min}$ is usually chosen to be zero; however, the actual value is arbitrary since only the changes in property load are relevant. Therefore, in this formulation, the source exists at the lowest property load and the sink at the highest, so our nonsmooth operator cannot use this definition of the property load as the quality in the integration problem.

Instead, for RCNs, we define the qualities by subtracting the changes in property load from a selected fresh resource quality $Q^{\max} = q^{\max}$. For the source qualities,

$$Q_1^{\text{in}} = Q^{\max}, \tag{3.9}$$

$$Q_i^{\text{out}} = Q_i^{\text{in}} - \Delta Q_i, \quad i = 1, \ldots, |SR|, \tag{3.10}$$

$$Q_i^{\text{in}} = Q_{i-1}^{\text{out}}, \quad i = 2, \ldots, |SR|, \tag{3.11}$$

and for sink qualities,

$$q_1^{\text{out}} = q^{\max}, \tag{3.12}$$

$$q_j^{\text{in}} = q_j^{\text{out}} - \Delta q_j, \quad j = 1, \ldots, |SK|, \tag{3.13}$$

$$q_j^{\text{out}} = q_{j-1}^{\text{in}}, \quad j = 2, \ldots, |SK|, \tag{3.14}$$

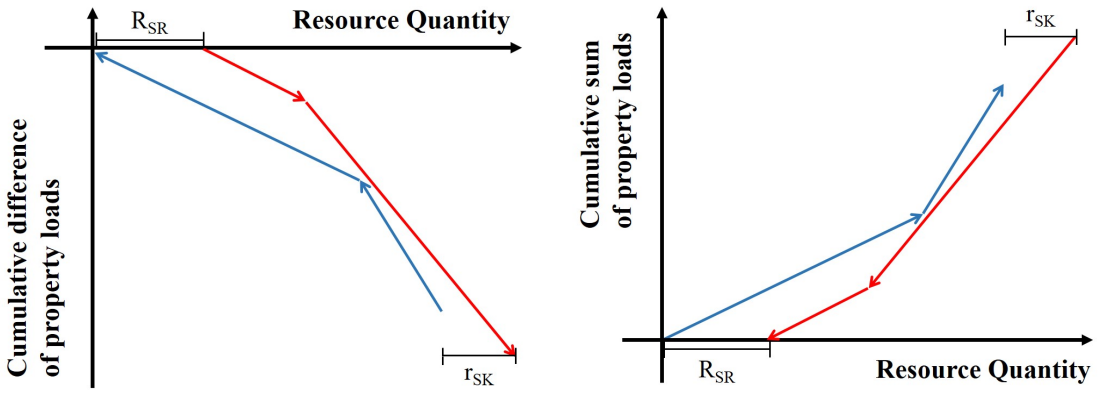

(a) Defining qualities through a cumulative difference so the source is at the highest quality value and the sink at the lowest.

(b) Reformulating the integration operator to include the fresh resource below the pinch point.

Figure 3-2: Illustration of approaches to determining problem qualities that can be used in our approach. The source and sink composite curves are red and blue, respectively.

where $\Delta Q_i = \Delta P_i$ and $\Delta q_j = \Delta p_j$. Again, the value of $Q^{\max}$ is arbitrary and is usually set to zero. Now, the source is at the highest quality value, the sink is at the lowest, and we maintain $Q_i^{\text{in}} \geq Q_i^{\text{out}}$ and $q_j^{\text{out}} \geq q_j^{\text{in}}$. Thus, we can apply the nonsmooth integration operator to these qualities.

In order to easily transfer the nonsmooth integration operator between problems, in this work, for cases where the high purity streams have low property loads, we always use this approach of defining the qualities through a cumulative difference so that they are consistent with the operator formulation. If desired, an alternative approach is to interchange the source and sink variables in the operator. With this change, the pinch point balance now includes the fresh resource source instead of the waste resource sink in the resource exchanged below the pinch point. Figure 3-2 visually demonstrates the difference between these two approaches. Figure 3-2a shows the transformation of the cumulative loads so that the waste sink is correctly included below the potential pinch point qualities, and Figure 3-2b shows swapping the sources and sinks so that the qualities of the source composite curve are lower than those of the sinks.

Sorting Property Values

In the integration problems such as RCNs discussed above, in which the qualities are cumulative values, the qualities, and thus the calculated resource targets, are highly dependent on the ordering of the sources and sinks. For RCNs where resource reuse is limited by composition, El-Halwagi et al. prove that resource targets are minimized if the sources and sinks are each sorted by increasing concentration [33], and Kazantzi and El-Halwagi extend this principle to general property integration where the sources and sinks are also sorted by their property values according to decreasing purity [52]. To perform this sorting, most approaches to RCNs require all source and sink properties, which are the states S_i or s_j in the general integration problem and are usually the reciprocal of the property value, to be known a priori. The few formulations that can solve for the properties are typically superstructures that must be solved with MINLPs that scale poorly with problem size. However, many sorting algorithms are inherently continuous but nonsmooth with respect to the sorted elements because the sorted order only changes at the finite set of points where two elements are equal. Thus, they can be incorporated directly into the nonsmooth integration operator so that we can solve for properties and states in RCNs using only equation-solving methods.

To incorporate sorting when it is required, we treat the sorting algorithm as a nonsmooth function that maps the unsorted input to a sorted output. Then, the overall nonsmooth system that simulates the integrated process is the composition of the integration operator and the sorting operation. In practice, we preprocess the problem data to create lists of property and property load pairs for the sources and sinks and sort each list in order of nonincreasing purity (e.g. nondecreasing contaminant concentration).

By selecting a sorting algorithm for which we can calculate LD-derivatives, because they obey a sharp chain rule, we can find the generalized derivative elements for the composite function by supplying the derivatives for the sorted pairs with respect to the unknown variables to the integration operators. Then these generalized

Input: An unsorted list, A, with entries $A[1], \ldots, A[m]$
Output: The list A, with the m entries sorted in order of increasing values
for $i \leftarrow 1$ **to** m **do**
  for $j \leftarrow 1$ **to** $m - 1$ **do**
    $a \leftarrow \min(A[j], A[j+1])$
    $b \leftarrow \max(A[j], A[j+1])$
    $A[j] \leftarrow a$
    $A[j+1] \leftarrow b$
return A

Figure 3-3: A simple bubble sort algorithm.

derivative elements can be used to solve the equation system using the nonsmooth equation-solving methods detailed above. For all of the examples in this work, we have used a simple bubble sort algorithm as shown in Figure 3-3. Because the only operations required are taking the max or min of two functions and these operations are performed the same number of times for any input of a given size, we can easily incorporate this sorting algorithm into code for the nonsmooth integration operator and apply AD methods to calculate the LD-derivatives for both the sorting process and the composite integration equations. Therefore, using this method, the nonsmooth integration operator can solve for property values in RCNs, a feature unique to our approach.

3.2.2 Extension to the Threshold Problem

Another significant advantage of modeling integrated systems using nonsmooth equations is the ability to easily incorporate additional scenarios such as threshold problems. A threshold scenario can occur for a resource when the resource utilities are unknowns and all other variables that the resources flows depend on, the process variables, are fixed, i.e. the traditional targeting problem. For this problem type, it may be infeasible for a pinch point to occur, in which case, resource usage will be optimal when the fresh or waste resource flow is zero and the pinch point balance in Equation (3.2) will be positive instead of zero. To capture this behavior, a simple

min function wrapper can be added to Equation (3.2) so it becomes:

$$0 = \min\{\min_{p \in P}\{RBP^p_{SK} - RBP^p_{SR}\} + r_{SK}, R_{SR}, r_{SK}\}. \tag{3.15}$$

This expression captures all possible cases for the basic resource-targeting problem: either a pinch point exists, so the pinch point balance is zero and the utilities are nonnegative, or a pinch point does not exist, so the pinch point balance is positive, and one of the utilities is zero and the other is nonnegative. Therefore, when the process variables related to a resource are known, Equation (3.15) should be used in place of Equation (3.2) for that resource. Then, unlike other approaches to process integration, the nonsmooth operator will identify threshold cases even if they are not known a priori.

It is important to note that Equation (3.15) should not be applied when process variables are unknown. In this case, the free process variables ensure that a pinch point is obtainable. Thus, if a pinch point is not enforced at the solution, both the fresh and waste resource flows could feasibly be reduced, and the solution does not describe a system under optimal resource reuse. Additionally, if one of the external resource utilities is specified to be zero, the integration operator will be underdetermined because Equation (3.15) will automatically be satisfied. Therefore, we use Equation (3.2) in these scenarios to ensure the existence of a pinch point.

3.2.3 Nonsmooth Operator Implementation

To solve the general integration problem using the nonsmooth integration operator, one operator is constructed for each integrated resource using the specifications detailed above. The states and qualities for each resource are identified along with any operations, including sorting, required to calculate them from the problem data and unknowns. Then, the appropriate pinch point balance is selected from Equations (3.2) and (3.15) depending on whether the resource states and qualities are dependent on any unknown process variables. Once the integration operators are constructed, they are combined with a process model to form a system of nonsmooth equations.

The resulting system can be solved for different selections of unknowns, where the degrees of freedom are determined by the size of the equation system, using the nonsmooth equation-solving methods described in the Background section. Regardless of the number of sources and sinks in the problem, the integration operator for each resource contributes only two equations to the system. This feature results in a problem formulation that scales compactly with problem size. In comparison, the optimization formulations for the pinch location method are either MINLPs that scale at best quadratically with both the number of constraints and binary variables or nonconvex, NLPs that scale linearly in the number of constraints but require smoothing approximations or nonsmooth solvers. Additionally, this strategy is applicable to any generalized integration problem, and we show its implementation for a variety of specific problems in the examples below.

3.3 Example Problems

In this section, we present a series of examples that demonstrate the use and potential of the nonsmooth integration operator. These examples begin with a classic resource-targeting problem and increase in complexity to include unknown process variables, process models, and the simultaneous integration of multiple resources. They also cover a wide range of resource types to show the utility of a truly generalizable approach to the integration problem.

3.3.1 Example 1: Carbon-constrained Energy Planning

In this example, we demonstrate the ability of the nonsmooth integration operator to solve for fresh and waste targets for any general integration problem where the resource transfer is limited by a pinch point. We consider the carbon-constrained energy-planning problem presented by Tan and Foo [82], which examines how best to utilize energy sources under carbon limits during the transition to clean energy. In this scenario, there is a set of geographical regions, which each have an expected energy consumption and a CO_2 emission limit for the planning horizon, and a set of

Table 3.2: Problem data for Example 1.[82]

Energy resource	**Emission factor (t CO_2/TJ)**	**Available resource (10^6 TJ)**	**Demand region**	**Expected demand (10^6 TJ)**	**Emission limit (10^6 t CO_2)**
Coal	105	0.6	Region I	1.0	20
Oil	75	0.8	Region II	0.4	20
Natural gas	55	0.2	Region III	0.6	60

energy resources with different emission factors (tonnes CO_2 emitted per TJ of energy produced) and availabilities. The provided data for this example is given in Table 3.2. We need to determine the quantity of emission-free renewable energy sources required to meet the emission targets for each region and the quantity of high-emission sources that will go unused.

The first step in solving this problem with the generalized nonsmooth operator is determining the problem states and qualities. Here, the energy is the resource transferred from the production sources to the different regions where it is consumed, and Tan and Foo use cumulative emission versus energy pinch plots to solve the integration problem for optimal energy transfer. As for standard RCNs, the cumulative emission loads are determined by sorting and source and sinks by increasing emission factor. This approach suggests that the cumulative emission loads and reciprocal emission factors can be considered as the qualities and states for this problem, respectively, which is consistent with our definitions since the energy transfer is constrained by the net carbon loads released from the energy sources and gained by the different geographic regions and the change in carbon load for each source or sink is proportional to its limiting emission factor. However, Tan and Foo's approach to calculating the cumulative emission loads, as in Equations (3.3)-(3.8), results in the zero-emission energy source having the lowest cumulative load and the excess power sink the highest. Therefore, for this problem, to be consistent with the nonsmooth integration operator, we chose to use Equations (3.9)-(3.14) to calculate the qualities as the cumulative difference of the changes in emission load.

We then transformed the problem data to these states and qualities to be used

Table 3.3: Calculated states and qualities used in the nonsmooth integration operator for Example 1.

Energy resource	$\mathbf{S_i}$ (10^{-3} TJ/ t CO_2)	$\mathbf{Q_i^{in}}$ (10^6 t CO_2)	$\mathbf{Q_i^{out}}$ (10^6 t CO_2)	**Demand region**	$\mathbf{s_j}$ (10^{-3} TJ/ t CO_2)	$\mathbf{q_j^{in}}$ (10^6 t CO_2)	$\mathbf{q_j^{out}}$ (10^6 t CO_2)
Natural gas	18.2	0	-11	Region I	50	-20	0
Oil	13.3	-11	-71	Region II	20	-40	-20
Coal	9.5	-71	-134	Region III	10	-100	-40

with the integration operator. The resulting values are shown in Table 3.3. For the energy resources, the states can be calculated directly as the reciprocals of the emission factors. Then, the changes in emission load for each source can be found from the known energy flows, R_i, according to $\Delta Q_i = R_i/S_i$. Using these values, we sorted the $(S_i,\ \Delta Q_i)$ pairs by nonincreasing state (nondecreasing emission load) to be used in Equations (3.9)-(3.11) to find Q_i^{out} and Q_i^{in}. Here, the sources can be sorted using any algorithm since the emission factors can be calculated explicitly from the problem data. Note that the sorting procedure changes the order of the energy resources as shown in Table 3.3. For the demand regions, we are given r_j and Δq_j, so we determined the states from $s_j = r_j/\Delta q_j$ and found q_j^{in} and q_j^{out} from the sorted $(s_j,\ \Delta q_j)$ pairs and Equations (3.12)-(3.14). We also set $\Delta Q_{\min} = 0$ since no driving force is required for power transfer between the energy resources and demand regions.

Once the states and qualities are calculated, the appropriate operator equations can be applied to these state and quality values, and the system can be solved using one of the nonsmooth equation-solving methods described above. For this problem, since all process variables are known, we used Equation (3.15) in addition to Equation (3.1) to ensure potential threshold problems are identified. We solved this system for R_{SR} and r_{SK} using the semismooth Newton method to give $R_{SR} = 0.81 \times 10^6$ TJ and $r_{SK} = 0.81 \times 10^6$ TJ as expected. Figure 3-4 shows the pinch plot at the solution both in terms of the qualities used in the integration operator and using the standard representation for this problem type.

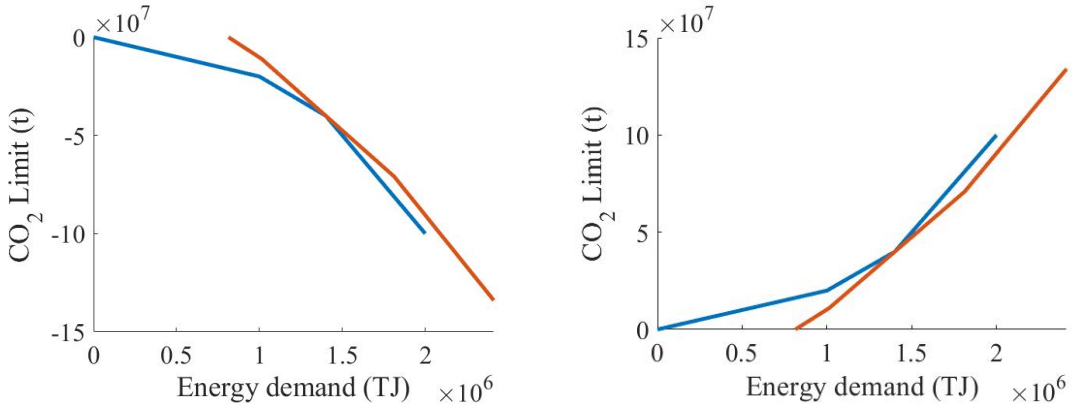

(a) Quality versus quantity plot showing the negative qualities used in the integration operator.

(b) Standard pinch representation.

Figure 3-4: Pinch plots for Example 1. The source and sink composite curves are red and blue, respectively.

Semismooth Newton is a good equation-solving method for any application where all unknowns are resource targets because the resource targets are not present in any nonsmooth terms, and therefore, the algorithm cannot encounter any singular generalized derivative elements along its solution path. Accordingly, in this example, semismooth Newton converged to the solution for all initial guesses tested in only 1 or 2 iterations.

3.3.2 Example 2: Water Threshold Problem

The next example shows the use of our integration operator to automatically identify and solve threshold problems. Here, we consider two cases presented by Foo for fixed-flow water integration with the flow rates and concentrations given in Tables 3.4 and 3.5 [38]. The first data set describes a zero-discharge network in which all of the source water can be used by the system, and the second a water network that requires no fresh water feed.

Analogous to the carbon integration problem in Example 1, since Foo approaches these problems using cascade tables with water and cumulative contaminant flow rates sorted by increasing contaminant concentration, we selected the cumulative difference of the contaminant flow rates and the reciprocal source and sink concentrations as

Table 3.4: Zero discharge problem data for Example 2.[38]

Water source	**Flowrate (g/min)**	**Concentration (ppm)**	**Water sink**	**Flowrate (g/min)**	**Concentration (ppm)**
1	20	20	1	50	20
2	50	100	2	20	50
3	40	250	3	100	400

Table 3.5: Zero fresh resource problem data for Example 2.[38]

Water source	**Flowrate (t/h)**	**Concentration (ppm)**	**Water sink**	**Flowrate (t/h)**	**Concentration (ppm)**
1	500	100	1	1200	120
2	2000	110	2	800	105
3	400	110	3	500	80
4	300	60			

the qualities and states, respectively. We then transformed the problem data to these states and qualities and applied Equations (3.1) and (3.15) with $\Delta Q_{\min} = 0$ since no driving force is required for resource transfer. For both problems, we solved for the fresh and waste water flow rates using the semismooth Newton method, and we converged to the solutions in 1 to 2 iterations across a wide range of initial guesses. As desired, for the zero-discharge problem, the integration operator determined the correct zero waste water flow rate and a fresh water flow rate of 60 g/min, and for the other, it found a zero fresh water flow rate and a waste water flow rate of 700 t/h.

In comparison, using Equation (3.2) for these targeting problems does not correctly identify threshold cases, giving infeasible waste and fresh water flow rates of -26 g/min and -9.1 t/h for the zero-discharge and zero fresh flow cases, respectively. Pinch plots comparing the results from using Equations (3.2) and (3.15) for the zero-discharge problem are given in Figure 3-5. Although not appropriate for identifying threshold problems in resource-targeting cases, when solving for process variables, using Equation (3.2) enforces pinch points in the system to ensure resources are used as efficiently as possible as demonstrated in the examples below.

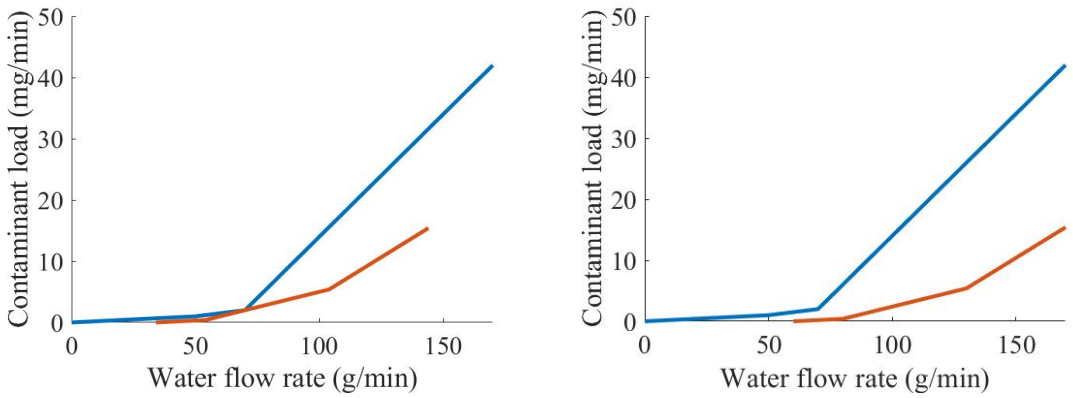

(a) Equation (3.2) enforces a pinch point.

(b) Equation (3.15) correctly identifies the solution in the threshold case.

Figure 3-5: Comparison of approaching the zero-discharge threshold problem using Equations (3.2) and (3.15). The source and sink composite curves are red and blue, respectively.

3.3.3 Example 3: Hydrogen Conservation Network

The next example highlights the ability of our formulation to solve for process variables in integration problems, particularly properties that must be sorted to determine optimal resource transfer. In this example, we examine a refinery hydrogen recovery network similar to that from Alves and Towler [7, 40]. The network contains four hydrogen-consuming processes, a hydrocraking unit (HCU), a naphtha hydrotreater (NHT), a cracked naphtha hydrotreater (CNHT), and a diesel hydrotreater (DHT), and two in-plant hydrogen-producing facilities, a catalytic reforming unit (CRU) and a steam-reforming unit (SRU). There is also an external feed of hydrogen that can be purchased with an impurity content of 6.5%. The limiting data for the hydrogen network is given in Table 3.6. We assume there is potential to upgrade the SRU to produce higher-purity hydrogen, and we wish to determine the required flow rate of external hydrogen and purity of the hydrogen produced by the SRU to achieve a waste flow rate of 100 mol/s.

To solve this problem using the integration operator, we note that the system is a RCN of the same form as the water networks in Example 2. Therefore, we again selected qualities that are the cumulative differences of the impurity loads and states that are the reciprocal concentrations. In this case, because the external hydrogen

Table 3.6: Problem data for Example 3.[40]

Sink	**Hydrogen consumption (mol/s)**	**Concentration (mol %)**	**Source**	**Hydrogen production (mol/s)**	**Concentration limit (mol %)**
HCU	2495.0	19.39	HCU	1801.9	25.0
NHT	180.2	21.15	NHT	138.6	25.0
CNHT	720.7	24.86	CNHT	457.4	30.0
DHT	554.4	22.43	DHT	346.5	27.0
			SRU	623.8	-
			CRU	415.8	20.0

source has a fixed impurity concentration and is not the highest possible purity, we treated it as an additional source stream with an unknown flow rate and set $R_{SR} = 0$. Because process variables are unknown, we applied Equations (3.1) and (3.2), and to solve for the SRU concentration, we used the bubble-sort algorithm presented in Figure 3-3 to determine the generalized derivatives of the functions composed with the sorting process. Using these generalized derivatives in the semismooth Newton algorithm gave a SRU hydrogen purity of 7.00 mol % and an external hydrogen feed of 268.8 mol/s in 1 to 2 iterations. Figure 3-6 gives the pinch plot for this result, which shows the node corresponding to the SRU correctly sorted among the other hydrogen sources to achieve a pinch point in the optimally integrated system.

In comparison to our approach, most other integration methods are unable easily to solve for quality variables in RCNs due to the complexity of the sorting operations. Historically, determining these variables has required repeatedly solving the integration problem at different quality values or using large mixed-integer programs [7, 6]. Instead, our approach allows for the efficient identification of network properties by solving only a single system of equations. However, when using the nonsmooth integration operators to solve for process variables, to ensure the system is well-defined, it is important to be mindful of where the process variables are present in the operator equations when they are transformed to the appropriate qualities and quantities. For example, when using flow rate and property data for a RCN, the overall resource balance in Equation (3.1) is only a function of the resource flow rates, so the integration

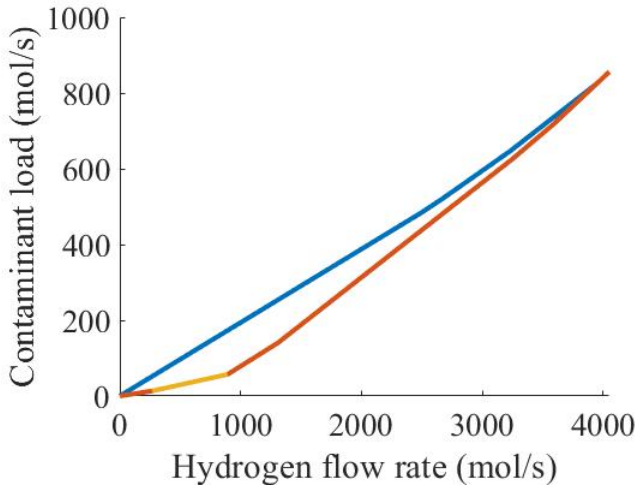

Figure 3-6: Pinch plot for Example 3. The source and sink composite curves are red and blue, respectively. The source node corresponding to the SRU is highlighted in yellow.

operator is only able to solve for one quality value. As demonstrated in the next example, this limitation can be mitigated by including a process model or integration operators for other resources to fix unknown properties.

3.3.4 Example 4: Dephenolization and Recycling of Aqueous Wastes

This final example extends the use of the integration operator to a problem that includes both a process model and the joint integration of multiple resources whose flows are dependent on the process variables. We have adapted a problem presented by El-Halwagi [30], which involves an oil recycling facility that uses steam strippers to remove sulfur and other light compounds from the oil streams. The main contaminant of concern in the stripper condensates is phenol, which can be removed through transfer to the oil streams in a MEN. Here, we analyze a proposed retrofit of a facility that processes lube oil, which considers both adding capacity for recycling gas oil and the possibility of reuse of the stripper condensate after dephenolization to reduce both fresh water consumption and wastewater production. The proposed plant therefore includes two steam strippers, a mass integration network for reducing the condensate

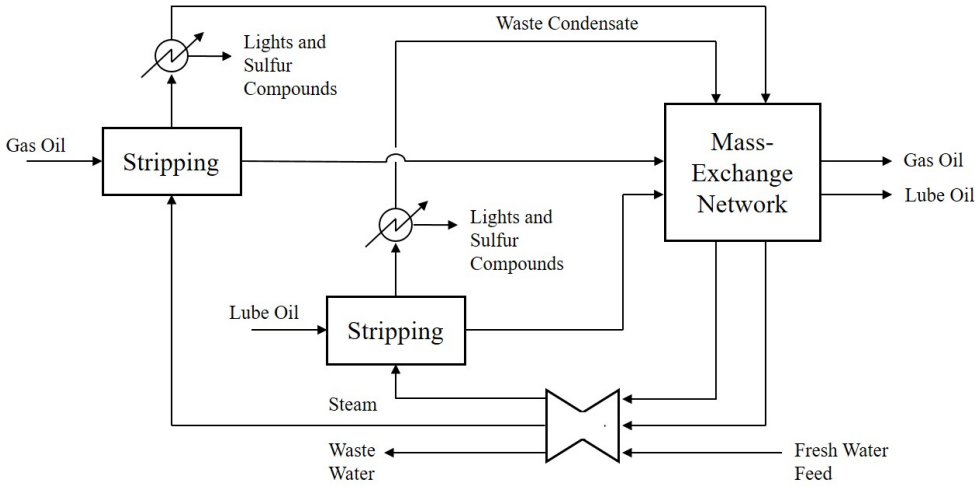

Figure 3-7: Simplified process diagram for the proposed process in Example 4.

phenol concentration, and a water network to reuse the water output in the strippers. Figure 3-7 shows a simplified process diagram for the plant.

We wish to determine the minimum attainable fresh and waste water flow rates as well as the phenol concentrations and water flow rates throughout the system, particularly in the new gas oil stripper. We require that no external utilities are used in the MEN and that the concentrations of the two stripper condensates are the same when they exit the MEN. We also assume that there are phenol concentration limits in the boilers that limit the inlet concentrations to the strippers and that the mass of phenol transferred in each stripper is constant. (This assumption can be replaced by more complex stripper models if desired.) The parameters for this system are given in Table 3.7.

To solve this problem, we applied two integration operators, one for the allocation of water and one for the mass exchange of phenol. As in Example 2, the water network qualities and states were taken as the cumulative differences in contaminant (phenol) load and the reciprocal contaminant concentration, respectively. Again, we obtained the sorted mass fractions required to determine these states and qualities using the bubble sort algorithm. For mass integration, the qualities and states are analogous to those defined in the common heat integration problem; as shown in Table 3.1, the qualities are the stream contaminant concentrations, and the states are the stream

Table 3.7: System parameters for Example 4. Lube oil is processed in stripper 1, and gas oil in stripper 2.

Stream	**Flow rate (kg/h)**	**Inlet mass fraction**	**Outlet mass fraction**
Lube Oil	5	0.005	0.015
Gas Oil	3	0.010	0.030
Stripper 1 steam	2.5	0.005	z_2
Stripper 2 steam	z_1	0.002	z_4
Stripper 1 wastewater	2.50	z_2	z_3
Stripper 2 wastewater	z_1	z_4	z_5
Fresh water	z_6	-	-
Wastewater	z_7	-	-
Stripper 1 mass load: 0.11 kg/h Stripper 2 mass load: 0.03 kg/h			
Equilibrium relation for lube oil: $y = 2.00x_1$ Equilibrium relation for gas oil: $y = 1.53x_2$ Minimum MEN concentration difference in oil streams: $\epsilon = 0.001$			

flow rates. However, to ensure that concentrations can be compared in a meaningful way, the equilibrium expressions must be used to transform the stream concentrations to their equivalent values in a selected reference stream, which we chose as the stripper condensate. The stream flow rates in the system must also be transformed to ensure the overall resource balance holds. Additionally, in this problem, the minimum MEN concentration difference is given in reference to the oil streams, so we included this concentration difference in our transformations, i.e. $y = m(x+\epsilon)$, and set $\Delta Q_{\min} = 0$.

In addition to the two integration operators, we also included process equations describing the constant mass transfer in the strippers and equating the MEN water outlet concentrations:

$$m_1 = V_1(z_2 - y_{0,1}),$$
$$m_2 = z_1(z_4 - y_{0,2}),$$
$$z_3 = z_5,$$

where $m_{1,2}$ are the mass loads of phenol transferred in each stripper, V_1 is the steam

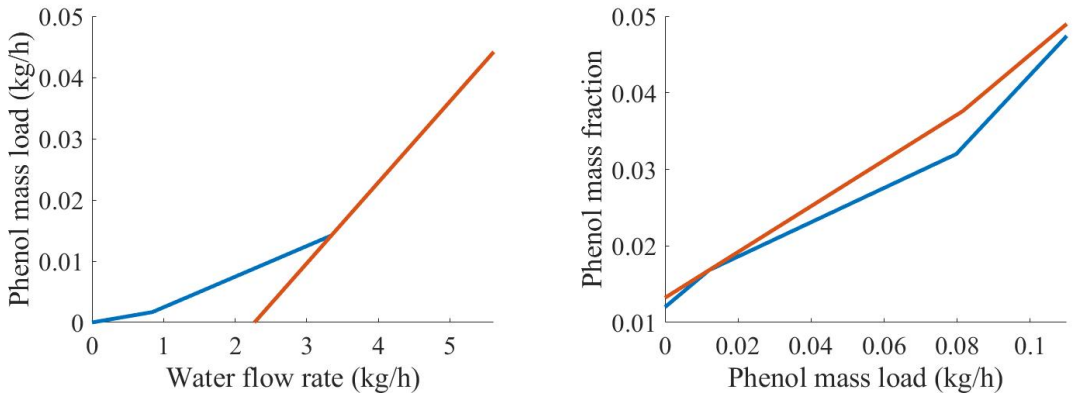

(a) Water allocation network.

(b) Mass integration network.

Figure 3-8: Composite curves for the optimized dephenolization system. The source and sink curves are red and blue, respectively.

flow rate through Stripper 1, and $y_{0,1}$ and $y_{0,2}$ are the inlet steam concentrations to the strippers.

With these process equations, we obtained a nonsmooth system of 7 equations which we solved for 7 unknowns using a semismooth Newton method to give $\boldsymbol{z} = (0.84,\ 0.049,\ 0.013,\ 0.038,\ 0.013,\ 2.27,\ 2.27)$. For a range of initial guesses, the semismooth Newton method quickly converged to the solution in 3 to 9 iterations. The mass and water composite curves for this solution are given in Figure 3-8 and demonstrate that our solution method produces the optimal pinch behavior. These results highlight the unique ability of our approach to simultaneously integrate multiple resources that are coupled through process variables.

3.4 Conclusions

In this work, we present a new, generalizable, and efficient approach for solving resource-targeting problems using compact, nonsmooth operators. These operators are nonsmooth systems of only two equations per integrated resource, regardless of the number of sources and sinks in the system. New methods in AD for LD-derivatives make it easy to solve these operators, in combination with process models, for resource targets or any process variable, including qualities that require sorting. We

include a series of examples that, together, demonstrate the ability of our approach to automatically identify threshold problems, solve for sorted qualities, include process models, and be applied to any pinch-constrained resource, including multiple resources simultaneously.

The current formulation is only applicable to problems with preclassified sources and sinks and can only consider a single contaminant for each resource. However, because our approach is nonsmooth, there is the potential to easily incorporate other work that uses explicit max and min expressions to address unclassified streams and multicontaminant problems while retaining the desirable features of our methods [88, 6]. We have begun this work by extending our formulation to a class of multicontaminant mass and water integration problems, which is discussed in Chapter 4.

Additionally, the method presented in this chapter is only applicable to process integration, not optimization, and has degrees of freedom limited by the size of the equation system. Nevertheless, with advances in nonsmooth optimization methods, nonsmooth integration operators can be embedded in mathematical programming problems to perform simultaneous process integration and optimization and increase the degrees of freedom. This approach promises significant improvements in scaling and efficiency compared to existing methods because nonsmooth operators introduce two equality constraints per resource regardless of the size of the process without requiring embedded optimization problems or large numbers of constraints and binary variables that increase rapidly with the number of sources and sinks. Chapter 5 describes how we have initially applied this optimization approach to integrate heat in cogeneration systems.

Our nonsmooth formulation is the only approach to the resource-targeting problem that can solve for any unknown quantity while scaling compactly, only requires equation-solving methods, and is explicitly generalizable to multiple resources. Therefore, the nonsmooth integration approach is a good candidate for performing integration for large, even interplant, systems and can be easily extended as pinch analysis is applied to new problems. Thus, we have formulated a readily adaptable approach

that significantly reduces problem complexity and can provide computationally practical solutions to a wide variety of new integration problems to improve resource use and sustainability in chemical processes.

Chapter 4

Multicomponent Mass and Water Integration

In the previous chapter, we presented a general integration operator that uses non-smooth equations to improve the adaptability and scaling of current approaches to process integration. However, the general integration operator assumes that resource transfer is limited by a single quality of the resource streams. Therefore, this chapter extends the benefits of the general integration operator by adapting it to systems in which multiple factors can limit resource transfer.

This characteristic is particularly common in mass integration problems because there are typically multiple materials present in each solvent stream. In these mass integration problems, the goal is to utilize a set of solvent streams that are lean in some components to remove those components from a set of rich streams. When multiple components are present, they not only each independently limit the feasibility of mass transfer and reuse, but they are also transferred dependently in mass exchange operations. Therefore, in these problems, all the materials must be considered simultaneously to avoid infeasible results, further increasing the size and complexity of the integration problem. To address these challenges, this work presents a new, tailored approach to the multicomponent mass integration problem that both improves upon the limitations of traditional integration strategies and also accounts for the unique complications in real world systems.

Of the existing approaches to mass integration, superstructures have been the primary technique adapted to solve multicomponent problems as first proposed by Takama et al. [81] These methods solve the targeting and network design portions of the integration problem simultaneously by creating a superstructure of potential resource stream pairings and exchange units. These superstructures are then solved using a mixed-integer or global nonlinear programing formulation.

For integration problems, this superstucture approach is flexible and easy to set up, making it simple to adopt for the multicomponent problem by adding new constraints to address the mass transfer and limits of the additional components. Therefore, there has been a significant amount of previous work investigating variations to the superstructure setup, its mixed-integer reformulation, and optimization strategies to improve the solution efficiency. Improvements to the superstructure include using pinch insights to reduce the number of constraints [18] and incorporating necessary conditions for optimality [9, 76]. There has also been work reformulating the superstructure problem to a nonlinear program without integer variables by including all possible matches and later eliminating matches with negligible flowrates [21, 13]; however, while these approaches can make the mathematical programs easier to solve, they often also introduce numerical issues without careful tuning. For each of these formulations, methods have been proposed to improve the robustness and efficiency of optimization such as initialization heuristics [21, 60, 84], linearization approaches [89, 83], and the application of heuristic algorithms [58, 86, 74, 63].

In addition, due to their flexibility, superstructure methods have been extended to heat integrated water networks, total water networks and regeneration systems, integration under uncertainty, batch processes, etc. However, we will not go into these extensions in detail here because they are out of the scope of this work. For a comprehensive review of these and other mass integration approaches, we recommend Jezowski [50]. Note that although the review focuses on approaches that have been applied to water integration, any fixed-load water integration approach can be applied to the class of mass integration problems considered in this work.

However, even with these improvements, the superstructure approach scales poorly

in the number of constraints and variables with both the number of resource streams and components in the problem, making them ill-suited for addressing large systems or being embedded in screening and optimization problems. In addition, because these methods must limit the superstructure to a finite number of possible exchange units and connections, it is not guaranteed that they will produce an optimal utility target.

As an alternative to the superstructure approach, pinch-based techniques are simpler and scale better because they only address the targeting problem. However, although there has been significant success using pinch-based approaches for the single-contaminant problem [31, 32], the extension of these methods to the multicomponent problem has been limited. Any multicomponent pinch-based approach must incorporate methods to describe mass transfer relationships between the components since this interdependence makes it unlikely that all the concentration limits specified in the problem can be achieved simultaneously. Additionally, multicomponent approaches must consider all of the components when prioritizing the use of the sources and sinks. Wang and Smith first introduced these considerations in the case of the fixed-load water integration problem, a subset of the mass integration problem in which the lean solvent streams are water [92]. They developed a heuristic approach for scaling and shifting the rich stream concentrations that uses both mass transfer relations and comparisons of the limits introduced by each component. Liu et al. also presented a variation of these heuristics with comparable results but using simpler calculations [62]. Alva-Argaez et al. subsequently refined this method by proposing nonsmooth scaling relations for the rich stream outlet concentrations that simultaneously relate the mass transfer of the components in each rich stream and also identify the limiting component [5]. These scalings are included in a transshipment formulation to identify a pinch point in one of the scaled components.

In both Wang and Smith's and Alva-Argaez et al.'s approaches, the scalings can be easily modified to describe any mass transfer relation. However, the scope of these scaling techniques is slightly limited compared to superstructure methods because they are only applicable to systems with a single lean solvent stream or, as in the

case of fixed-load water integration, systems in which the lean solvent streams are miscible. Nevertheless, since these types of systems are common, the main limitation of pinch-based multicontaminant approaches is still the same as that for most single-component pinch approaches, the inability to solve for most process variables.

Our goal with this work was to overcome this limitation of pinch-based integration methods and provide a tractable and flexible solution to the multicomponent mass integration problem. Because our nonsmooth approach was successful in addressing these limitations for the single-component problem, our strategy was to extend the generalized integration operator by incorporating scaling techniques and considering pinch conditions over all components simultaneously. The result is still a nonsmooth system of two equations that now scales compactly in both the number of sources and sinks in the problem as well as the number of components. Like other pinch-based approaches, our method applies to any mass integration problem with a single or miscible lean streams, including fixed-load water integration problems. However, unlike other approaches, our multicomponent integration operator can be used to determine any process variable, even component concentrations that are arguments of the nonsmooth scaling relations.

The remainder of this chapter provides the background and details necessary to understand and implement our novel approach to the multicontaminant problem. We begin by formally defining the problem we are addressing, and then introduce previous work on scaling relations that we drew on to develop our approach. The main body of the chapter presents the details of the multicomponent integration operator and applies it to a literature case study to demonstrate its use and its success as a tractable and flexible approach to this challenging problem.

At the time of writing, the work in this chapter is in preparation for publication [71].

4.1 Problem Definition

In this work, we consider a common subset of the multicomponent mass integration problem in which a single lean solvent stream is used to remove material from a series of rich streams. In mass integration targeting problems, often we assume that there are no concentration-independent mass utilities available and solve for the system parameters that would make these utilities zero with maximum resource recovery. Commonly, there is assumed to be a single fresh solvent stream in the system that is used as a concentration-dependent mass sink. Using this framework, the fresh solvent can be treated as a lean stream, and its minimum flow rate, L, for feasible mass recovery from the rich streams is determined.

To understand this multicomponent problem, we begin by defining the equivalent single-component mass integration problem, which is an instance of the general integration problem described in both Chapters 2 and 3 of this thesis. In this problem there is a system with a set of source solvent streams, R, that are rich in a given component and a set of sink streams, S, that are lean in that component. For each stream, the qualities that limit resource transfer are the component concentrations. Here, we denote the inlet and outlet concentrations of a rich stream, $i \in R$ as y_i^{in} and y_i^{out}, respectively, its flow rate as G_i, and the mass transferred from the stream as $M_{R,i}$. Analogously, the concentrations for the lean solvent stream are x^{in} and x^{out}, the flow rate is L, and the mass transferred to the stream is M_L. We determine the mass of material transferred from a rich stream or to the lean stream by the linear relations $M_{R,i} = G_i(y_i^{\text{in}} - y_i^{\text{out}})$ and $M_L = L(x^{\text{out}} - x^{\text{in}})$, respectively. We also assume that for mass to be transferred from a rich stream to the lean stream, the rich stream concentrations must be larger than those in the lean stream.

To meaningfully compare concentrations when solving these mass integration problems, the concentrations and flow rates we refer to above are scaled according to their equilibrium relations. Given a set of expressions describing the equilibrium concentration y_i in rich stream i corresponding to a concentration x in the lean stream, we can transform each concentration in the problem to a corresponding concentra-

tion in the lean reference stream. Then, the stream flow rates are also transformed using these equilibrium expressions so that the mass loads transferred do not change from their original values. These scaled quantities are used to solve the integration problem, and the equilibrium relations are again used to transform the solution back to real values.

For example, for affine equilibrium relations

$$y_i = m_i x + b_i \tag{4.1}$$

and a minimum feasible concentration difference for mass transfer ϵ_i, the concentrations in the lean stream are

$$\hat{y}_i = \frac{1}{m_i}(y_i - b_i) - \epsilon_i, \tag{4.2}$$

and the scaled flow rates are given by

$$\hat{G}_i = m_i G_i. \tag{4.3}$$

Using this procedure, equilibrium relations of any form can also be applied to perform the transformations [31].

The goal of the mass integration problems in this work is to minimize the flow rate of the lean stream required to feasibly meet the rich stream concentration requirements. Mathematically, we can express this problem as

$$\begin{aligned} &\mathbf{h}(\boldsymbol{x}, \boldsymbol{y}) = \mathbf{0}, \\ &\boldsymbol{y} \in \underset{\boldsymbol{y}=[L\ x^{\text{out}}]}{\arg\min}\ L \\ &\text{s.t.} \quad \text{Mass balance holds,} \\ &\qquad \text{Mass transfer is feasible,} \\ &\qquad \text{External utilities are zero.} \end{aligned} \tag{4.4}$$

While these single-component mass integration problems can provide useful lower bounds on the utility requirements, most real systems have multiple components present in the rich and lean solvent streams. In these systems, the mass loads transferred must now meet the rich and lean stream requirements for each of the components present. In addition, for feasible mass transfer, the concentrations of every component in the rich stream must exceed the concentration of the corresponding component in the lean stream. Another consideration in these multicomponent systems is that the mass transfer of each component cannot be controlled independently meaning that the concentration requirements cannot be met simultaneously. Instead, to meaningfully solve the integration problem, mass transfer relations must be used to determine the actual concentration removal or gain that meets the given limits. Together, these new requirements make it likely that failing to consider all components simultaneously will result in an infeasible solution. Therefore, to address these multicomponent systems, we extend Problem (4.4) to the following optimization problem, where the set C is introduced to describe the different components present.

$$
\begin{aligned}
&\mathbf{h}(\boldsymbol{x}, \boldsymbol{y}) = \mathbf{0}, && (4.5)\\
&\boldsymbol{y} \in \underset{\boldsymbol{y}=[L\ x_1^{\text{out}} \ldots\ x_{|C|}^{\text{out}}]}{\arg\min} \quad L\\
&\text{s.t.} \quad \text{Mass balance holds,}\\
&\qquad \text{Mass transfer is feasible,} && \forall c \in C\\
&\qquad \text{Mass transfer is consistent,}\\
&\qquad \text{External utilities are zero.}
\end{aligned}
$$

This multicomponent formulation, like the single-component problem, includes a process model and considers the concentrations and flow rates that have been scaled by the equilibrium relations shown above. The first two sets of constraints are also equivalent to the single-component case but are now applied $\forall c \in C$ to ensure mass transfer and feasibility holds across all components. The third set of constraints introduces the interdependence of mass transfer and defines the component concen-

trations such that they can be achieved simultaneously within the limits given by the problem and considered in the final constraints. For the multicomponent problem, we only consider the case where there are no external utilities because there is generally no physically meaningful way to consider independent external utilities for each component.

While the multicomponent problem has been solved before, having to consider the interactions between each rich and lean stream pair and then each component within those matches typically results in approaches that scaled very quickly with both the number of streams and components and are ill-suited to address large systems. In the rest of this work, we address this limitation by introducing a new approach for solving the multicomponent mass integration problem, which uses nonsmooth equations to maintain a compact and tractable formulation that is simultaneously flexible enough to determine any system parameters.

4.1.1 Extension to Water Integration

The mass integration problem as it is presented here can also be used to solve a class of water integration problems called "fixed-mass" problems [91, 39]. These problems consider a series of water-using operations that have constant water flow rates throughout the unit. The rich streams in the system are the process streams in the water-using operations that transfer mass to the water streams, and the lean stream is the fresh water required to supply the units. Typically, the data given for the rich streams in these problems is transformed to equivalent concentration and flow rate limits for the water supplied to each operation, which is called the limiting water curve.

In many works, the problem of fixed-mass water integration is considered distinct from mass integration because this type of data analysis can extend to a wide range of processes beyond mass exchangers, including utility use, filtration, washing or evaporation. However, once the data is transformed to a limiting water curve, the targeting problem for fixed-mass water integration problem can be solved using the mass integration approaches presented below.

Nevertheless, it is useful to note that the results of the network design problem can look significantly different between mass and water integration because water streams are usually allowed to mix while this may not be feasible for the different solvents in a more general mass integration problem. For a multicomponent problem with multiple lean or fresh streams, the inability of general solvents to mix can also introduce additional mass transfer limits. Therefore, our assumption of a single fresh solvent source in this work is important when extending it to water integration problems.

4.2 Background: The Single-component Mass Integration Operator

As a starting point for designing a multicomponent integration approach, we used our previous work on the generalized, nonsmooth integration operator. This approach was developed to solve a general class of integration problems, which includes the single-component mass integration problem. The details of this general approach can be found in Chapter 3, but the following section provides the specific formulation for the type of mass integration problems considered in this chapter.

The nonsmooth integration operator uses a nonsmooth system of two equations to describe solutions to the single-component problem detailed under Problem (4.4). The first equation is a simple resource balance, ensuring the total mass produced by the rich streams can be accommodated by the lean stream. The second equation guarantees that the mass transfer is both feasible and optimal by enforcing the presence of a pinch point in the system. According to pinch analysis theory, a pinch point occurs in a mass integration problem at a concentration where the mass balance holds independently for both the concentrations above and below the pinch point. The presence of a pinch point indicates optimal mass reuse because decreasing the lean stream flow rate further past this point would require mass at the pinch point to be transferred infeasibly from a low to high concentration. Pinch analysis theory has also shown that the pinch point must occur at one of the stream inlet concentrations. Therefore,

we can express this pinch condition using a single nonsmooth equation by calculating the mass balance below each of these inlet concentrations, or potential pinch points, and setting the minimum balance to zero at the pinch point. This condition also ensures that mass transfer is feasible at the other potential pinch points by keeping the mass balance nonnegative.

The equation system for a mass integration problem with a single concentration-dependent mass sink is:

$$0 = \sum_{i \in R} \hat{G}_i(\hat{y}_i^{\text{in}} - \hat{y}_i^{\text{out}}) + L(x^{\text{in}} - x^{\text{out}}), \tag{4.6}$$

$$0 = \min_{p \in P}\{MBP_S^p - MBP_R^p\}, \tag{4.7}$$

where P is the finite index set of pinch point candidates that give the potential pinch concentrations

$$z^p = \begin{cases} \hat{y}_i^{\text{in}}, & \forall p = i \in R, \\ x^{\text{in}}. \end{cases} \tag{4.8}$$

These potential pinch points are used to calculate the source and sink mass balances below the corresponding concentrations:

$$MBP_R^p := \sum_{i \in R} \hat{G}_i[\max\{0, z^p - \hat{y}_i^{\text{out}}\} - \max\{0, z^p - \hat{y}_i^{\text{in}}\} + EXT_R^p], \quad \forall p \in P, \tag{4.9}$$

$$MBP_S^p := L[\max\{0, z^p - x^{\text{in}}\} - \max\{0, z^p - x^{\text{out}}\} + EXT_S^p], \quad \forall p \in P. \tag{4.10}$$

The EXT terms create nonphysical extensions to the mass balances to ensure the difference between the rich and lean stream balances is always defined and are given by

$$EXT_R^p = \max\{0, z^p - \hat{y}^{\max}\} - \max\{0, \hat{y}^{\min} - z^p\}, \quad \forall p \in P, \tag{4.11}$$

$$EXT_R^p = \max\{0, z^p - x^{\max}\} - \max\{0, x^{\min} - z^p\}, \quad \forall p \in P, \tag{4.12}$$

where $\hat{y}^{\min,\max}$ and $x^{\min,\max}$ are the minimum and maximum concentrations across the rich and lean streams, respectively. Here, $x^{\min} = x^{\text{in}}$ is known a priori.

We solve the nonsmooth system of equations using the techniques described in the Background chapter.

As discussed in Chapter 3, this approach to solving the integration problem has unique benefits. The nonsmooth equation system is only two equations regardless of the system size, resulting in superior scaling and tractability for large systems. And because we use an equation-solving approach instead of optimization, we can also solve the system for any process variable, which allows us to design systems for specified resource targets. However, although these benefits make the nonsmooth integration operator a good approach for single-component mass integration problems, it cannot address the multicomponent case. Specifically, while the integration operators for multiple resources can be used in parallel, combining the single-component operators for multiple components assumes that each material can be optimally integrated simultaneously. However, because the component concentrations cannot be manipulated independently, we are only guaranteed optimal resource transfer for one material and feasibility for the others. Additionally, the integration operator does not provide a way to describe how the component concentrations vary due to the interdependent mass transfer. Therefore, this work focuses on addressing these limitations in order to extend the nonsmooth integration operator to multicomponent mass integration problems.

4.3 Solution Method

4.3.1 Concentration Shifting for Multicomponent Mass Transfer

While our approach to single-component integration provides tools to describe the conditions for optimal mass reuse, a key barrier limiting its extension to multiple components is that it does not include a strategy to describe their dependent mass

transfer. To incorporate these strategies, we have adopted a method proposed by Alva-Argaez et al. that uses nonsmooth expressions to determine the limiting component in each operation and to scale the component concentrations accordingly. Below, we provide the background required to implement our multicomponent integration approach, but we recommend referring to Alva-Argaez et al. for details on the derivation and applications of the scaling method [5].

This approach begins by assuming a mass transfer relation that governs the dependent mass transfer of the different components. Common mass transfer assumptions discussed by Alva-Argaez et al. are a fixed mass load distribution, where the mass of a component transferred is proportional to its rich stream inlet concentration, and proportional mass transfer, where the proportion of the mass load transferred is constant between components. The selection of the mass transfer relation depends on the process. For mass-exchange units, the fixed-mass load assumption is usually more accurate, but for some water-using operations like washing, proportional mass transfer may be a better choice. It is also important to note that these mass transfer assumptions do not limit the utility of this approach; any mass transfer relation can be incorporated, and different relations can be selected for each operating unit.

When selecting and using a mass transfer relation, it is also important to consider which pieces of data are physically relevant. For a system, data on the rich streams may be given as the inlet and outlet concentration limits, flow rates, or mass removal requirements. Because these four factors are interdependent, only three are necessary to fully define the problem. Typically, the concentration limits are given because they are important operating constraints. Our definition of the mass integration problem assumes that the additional data is given as the solvent flow rates for each operating unit. If the operating units are mass exchange units where the rich streams have real, physical flow rates, this choice of variables is a good representation of the system. However, in a washing-type operation, there is not a physical flow rate to use, and the relevant data is the mass of each component that is removed. In this case, the mass removal requirements can be used to calculate a representative limiting flow rate, which is described in more detail below. While these limiting flow rates are a

good method for describing operations without a physical rich stream, we caution against using limiting flow rates when a rich stream is present. If mass removal and concentrations are given as limits or requirements, the limiting flow rates calculated may be different than the real rich stream flow rate, and these variations will affect the result of the mass transfer scalings that are used.

Below, we present mass transfer scalings for the two cases described above. Note that because these scalings describe the behavior of the comomponents in the rich streams, they should generally be performed before the equilibrium adjustments described under Problem Definition. However, if the equilibrium concentrations are proportional, which is a common assumption in mass integration problems, then the ordering of the scaling processes is interchangable.

Fixed Mass Load

In a unit described by a fixed mass load mass transfer relation, the rich stream inlet concentrations are the real system concentrations, but the outlet concentrations are the minimum concentration removal limits. Because the materials in the system are transferred together during mass exchange, it is likely not physically possible for each component to reach its outlet concentration limit simultaneously. However, because these concentrations are upper bounds, we can instead transfer mass from the rich stream until just one component is at its limit and the others are at or below theirs. Alva-Argaez et al.'s scaling approach can be used to determine the real outlet concentrations of each component in this limiting case.

Presenting the scaling results from Alva-Argaez et al., the mass loads of contaminants c and c' from a rich stream i can be related by

$$\frac{M_{i,c}}{y_{i,c}^{\text{in}}} = \frac{M_{i,c'}}{y_{i,c'}^{\text{in}}}. \tag{4.13}$$

Alva-Argaez et al. show that when the lean stream concentrations are negligible compared to the rich stream outlet concentrations, this relation can described by a con-

stant relative use across all the components:

$$Ru_{i,c} = \frac{y_{i,c}^{\text{out}}}{y_{i,c}^{\text{in}}} = \frac{y_{i,c'}^{\text{out}}}{y_{i,c'}^{\text{in}}}. \tag{4.14}$$

Thus, the component requiring the lowest relative use will determine the use of the other components, and the actual concentrations $y_{i,c}^{\text{out}}$ that allow all the components to reach or exceed their given limits $y_{i,c}^{\text{out, max}}$ are

$$Ru_i = \min_{c \in C} \frac{y_{i,c}^{\text{out, max}}}{y_{i,c}^{\text{in}}}, \tag{4.15}$$

$$y_{i,c}^{\text{out}} = y_{i,c}^{\text{in}} Ru_i. \tag{4.16}$$

A visual representation of this scaling argument is shown in Figure 4-1.

Now that the concentration limits are scaled so they are consistent between components, they can be used to calculate an improved fresh solvent target for the system. This updated target is the maximum target calculated across all the components using the scaled concentrations, where the individual component targets can be calculated using any integration approach. In Alva-Argaez et al.'s work, these component targets are found by solving a MILP transshipment formulation.

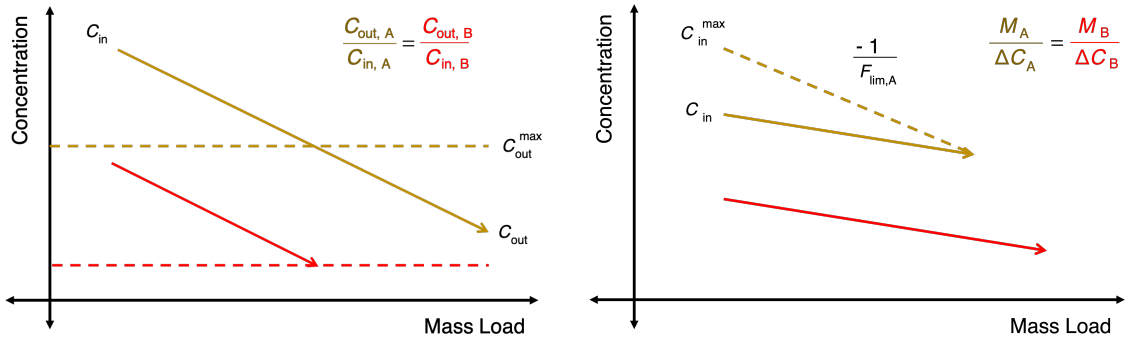

(a) Fixed-mass-load scaling. $C_{\text{out, A}}$ is decreased to meet the same concentration ratio as component B.

(b) Proportional mass transfer scaling. $C_{\text{in, A}}$ is decreased so that the limiting flow rate for component A is the same as for B.

Figure 4-1: Visual representation of the scalings for the two mass transfer relations presented in this work.

Proportional mass transfer

The next mass transfer relation that we consider is proportional mass transfer. Alva-Argaez et al. also show the results of their method for this case, but do not show the corresponding scaling relation used to obtain these results. Therefore, we have derived our own scaling relations from our interpretation of this mass transfer relation as shown below.

Under the assumption of proportional mass transfer, the mass loads of contaminants transferred from a rich stream i to the fresh solvent stream are fixed at their given values for the system. For given concentration limits and a required mass load, an effective rich stream flow rate can be calculated for each component. This effective flow rate is the maximum lean solvent flow rate needed to remove the required mass load of the component. Therefore, the maximum lean solvent flow rate for an operation is the maximum over the components:

$$F_{\text{lim},i} = \max_{c \in C} \frac{M_{i,c}}{y_{i,c}^{\text{in,max}} - y_{i,c}^{\text{out}}}. \tag{4.17}$$

Then, the concentration scaling for this assumption reduces y_i^{in} for each component in a unit so that its mass transfer reaches the desired value for the effective flow rate $F_{\text{lim},i}$. If the flow rates calcuated for each component are the same, the concentrations will remain unchanged relative to the given limits.

$$y_{i,c}^{\text{in}} = \frac{M_{i,c}}{F_{\text{lim},i}} + y_{i,c}^{\text{out}}. \tag{4.18}$$

A visual representation of this scaling argument is shown in Figure 4-1.

This scaling is equivalent to decreasing the allowable lean solvent outlet concentrations. The smaller concentration limits will increase the required lean solvent flow rates so they can handle the higher effective rich stream flow rate enforced by the limiting component. As for the assumption of a fixed mass load, these scaled concentrations can then be used in an integration approach in place of the original concentration limits, and the maximum target over the components is a valid fresh

solvent target for the overall system.

Tightness of the Fresh Solvent Target

This scaling approach introduced by Alva-Argaez et al. offers significant advantages over the alternative heuristic scalings first developed by Wang and Smith. Alva-Argaez et al.'s approach only requires modifying a single concentration instead of both the inlet and outlet concentrations in Wang and Smith's method. In addition, Alva-Argaez et al.'s scaling can be performed separately for each unit, while Wang and Smith's concentration adjustments for an operation are dependent on the adjusted concentrations of all the upstream units.

Neglecting the dependence between the operating units makes the targeting problem significantly easier to solve. The fresh solvent target can be calculated automatically without requiring a superstructure and can be used to quickly screen design alternatives or be embedded in larger problems. This approach is also guarenteed to give a valid lower bound for the fresh solvent flow rate as long as the mass transfer scalings accurately describe the physics in the system. Pinch theory results for the single-component problem show that the pinched fresh solvent flow rates are lower bounds for these systems. The addition of multiple components increases the constraints on how water can be reused and can only increase the fresh solvent required. Therefore, maximizing the pinched targets across each component will still give a lower bound for the system. The scaling arguments given above represent physical limits of the rich streams that are present due to the interdependent mass transfer between the components. The fixed mass load scaling accounts for the additional mass that must be transferred to meet the concentration targets across all components, and the proportional mass scaling keeps the fresh solvent flow rate consistent for a given washing unit. If these or other scalings correctly describe the physical constraints, the lower bound argument above still holds.

Nevertheless, neglecting this dependence between operating units does have the potential to decrease the tightness of the lower bound. In other words, while the target will be a valid lower bound, it is no longer guaranteed to be a tight lower

bound. In this case, it is not possible to design a solvent network that exactly meets the calculated target. Because Alva-Argaez et al.'s work does not discuss the tightness of their calculated target, we present our analysis supporting these conclusions below. First, we examined the case study Alva-Argaez et al. use to demonstrate their method and found that the target they calculate for this scenario is smaller than the minimum fresh water flow rate that can be feasibly achieved by a water network design.

To determine the minimum attainable fresh water flow rate, we used the NLP superstructure formulation from Doyle and Smith [27]. Because Doyle and Smith assume constant mass or constant outlet concentration to calculate their network designs, we added the constraint

$$\frac{\Delta m_{i,c}}{C_{i,c}^{\text{out,max}}} = \frac{\Delta m_{i,c+1}}{C_{i,c+1}^{\text{out,max}}}, \quad \forall c \in C, c \neq |C| \tag{4.19}$$

for consistency with Alva-Argaez et al.'s fixed-mass-load mass transfer assumption. Here, the notation for the concentrations is different than that in Equation (4.13) because Doyle and Smith's model is written in terms of the solvent concentrations instead of the rich stream concentrations. With the addition of this equality constraint, the mass loads calculated in Constraints 16 and 17 are variables in the formulation instead of parameters for the system.

We implemented this NLP in GAMS [2] and solved it to global optimality for the system in Alva-Argaez et al. Example 1 using the software Antigone [1]. We found a minimum fresh water flow rate of 129.6 t/h which is obtained by the water reuse network shown in Figure 4-2. The target of 109.5 t/h calculated by Alva-Argaez et al. is 15.5% lower than this attainable flow rate. Therefore, our results show that the target produced by Alva-Argaez et al.'s concentration scaling procedure is not guaranteed to be a feasible, tight lower bound.

Seemingly conflicting with our results, Alva-Argaez et al. present a water network that has a fresh water flow rate equivalent to their target of 109.5 t/h. A representation of this network is shown in Figure 4-2. This network meets the water inlet and outlet concentration limits given in the original data, and the fixed-mass-load ratio

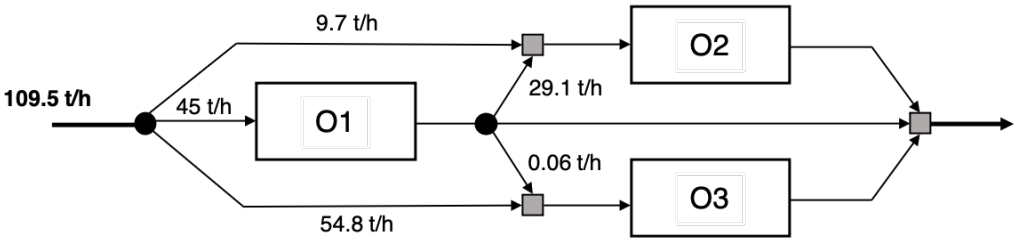

(a) Network from Alva-Argaez et al..

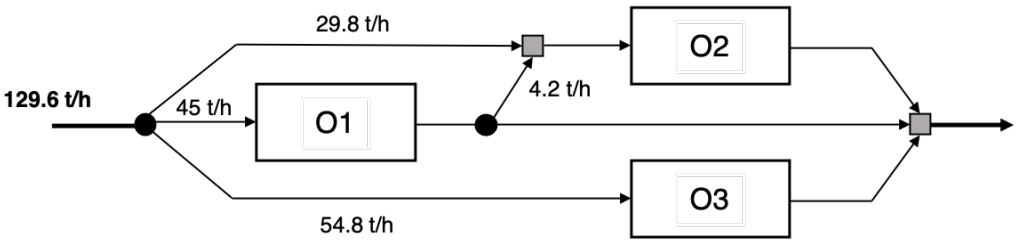

(b) Network developed using Doyle and Smith's superstructure approach.

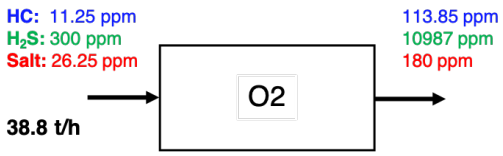

(c) Operation 2 in Alva-Argaez et al.'s network.

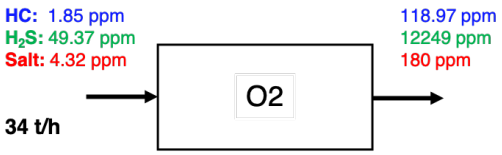

(d) Operation 2 in our superstructure-derived network.

Figure 4-2: Comparison of the water reuse networks developed for Alva-Argaez et al. Example 1. For clarity, only the water flows are shown.

holds for the rich streams in each operation. However, on closer inspection, the mass transfer in this potential network is infeasible.

The infeasibility occurs because the water flow rate in Operation 2 is larger than the limiting water flow rate. Alva-Argaez et al. present the rich stream data as a limiting water profile, which means that its concentrations have been transformed to their equivalent concentrations in the water reference stream. This data is given in terms of minimum mass loads and concentration limits, so Equation (4.17) can be used to calculate the rich stream flow rates (in terms of the water reference) that Alva-Argaez et al. use in their transshipment formulation. This limiting water flow rate for Operation 2 is 34 t/h, which represents both the physical rich stream flow rate and the maximum water flow rate required to meet the mass and concentration

removal requirements.

Because the water flow rate through Operation 2 is larger than the limiting flow rate at 38.8 t/h, using the water inlet and outlet cocentrations provide by Alva-Argaez et al., the mass loads of each component that are transferred in the operation are $\mathbf{\Delta m} = [4.0\ 414.7\ 6.0]$ in kg/h for HC, H_2S, and salt respectively. The rich stream enters Operation 2 at the equivalent water concentrations $\hat{\boldsymbol{y}}^{\mathbf{in}} = [120\ 12500\ 180]$ ppm. Then, for a rich stream flow rate of 34 t/h, the outlet concentrations are $\hat{\boldsymbol{y}}^{\mathbf{out}} = [2.9\ 304.2\ 4.5]$. Although these concentrations meet the removal limits, the excess mass removal from a higher water flow rate means that now the inlet water concentrations given for both HC and salt are larger than their outlet rich stream concentrations, which makes mass transfer infeasible.

We can also see the effects of this flow rate increase in the concentrations of the water stream into Operation 2. Here, both the hydrocarbon and salt inlet concentrations exceed the inlet concentration limits found from the scaling procedure despite the unit meeting the mass load ratio in Equation (4.13).

To confirm that this infeasibility is the result of an increase in the water flow rate above its limiting value, we also solved the superstructure formulation while allowing the rich stream flow rate to vary, which resulted in the same water network presented by Alva-Argaez et al.

Intuitively, the target calculated by Alva-Argaez et al.'s scaling approach is not guaranteed to be tight because it assumes that the target water inlet concentrations for each component can be achieved simultaneously. However, because the flow rates in the network are nonnegative, there may not be a feasible combination of the recycled and fresh water streams that reaches the optimal concentrations in each component at an operation's inlet. To demonstrate this limitation, we look at the inlet to Operation 2 in the example above. The fixed-mass-load scalings for this operation give a rich stream outlet composition of 2.8 ppm hydrocarbons, 300 ppm H_2S, and 4.3 ppm salt. Therefore, using the water outlet concentrations from Operations 1 and

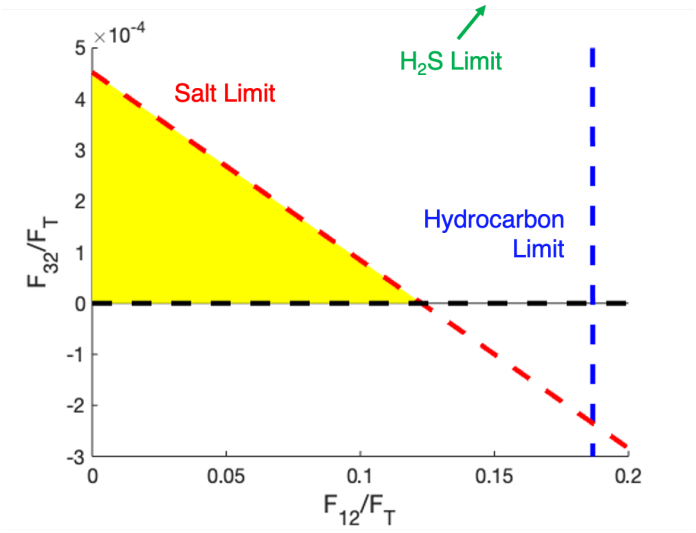

Figure 4-3: Plot of the constraints on the recyled water flow rates to Operation 2 in Alva-Argaez et al. Example 1. Limits on the hydrocarbon and salt concentrations from Equations (4.21) and (4.23) are blue and red, respectively, and the feasible region is shown in yellow. The H_2S limit is out of the bounds of this plot.

3 given in Figure 4-2, the inlet water stream must satisfy the inequalities

$$F_{ij} \geq 0, \quad \forall i, j \in R, i \neq j, \tag{4.20}$$

$$\frac{F_{32}}{F_T} \leq \frac{2.8}{220} - \frac{15}{220}\frac{F_{12}}{F_T}, \tag{4.21}$$

$$\frac{F_{32}}{F_T} \leq \frac{300}{45} - \frac{400}{45}\frac{F_{12}}{F_T}, \tag{4.22}$$

$$\frac{F_{32}}{F_T} \leq \frac{4.3}{9500} - \frac{35}{9500}\frac{F_{12}}{F_T}, \tag{4.23}$$

where $F_T = \sum_{i \in R} F_{i2} + F_{fw}$, F_{12} and F_{32} are the flow rates of the water recycled from Operations 1 and 3, respectively, and F_{fw} is the fresh water flow rate to Operation 2. Figure 4-3 shows the resulting feasible region. Because not all three inequalities in Equations (4.21)-(4.23) can be active at the same time, the feasible water inlet concentrations will be less than the scaled rich-stream outlet concentrations in at least one component, which can further increase the achievable fresh water target compared to the target found from the scaled outlet concentrations. Here, the maximum water reuse by Operation 2 occurs for $\frac{F_{12}}{F_T} = 0.12$ and $\frac{F_{12}}{F_T} = 0$ which gives an inlet water composition of 1.8 ppm hydrocarbons, 49 ppm H_2S, and 4.3 ppm salt. These

reduced concentrations increase the mass load of hydrocarbons below the pinch point, increasing the fresh water requirement. The adjusted composite curves are shown in Figure 4-4.

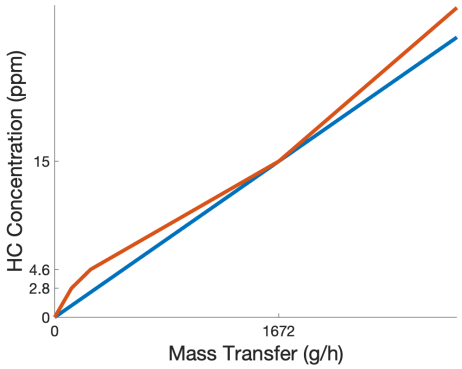

(a) Results from Alva-Argaez et al.'s scaling approach. The required fresh water flow rate in 109.5 t/h.

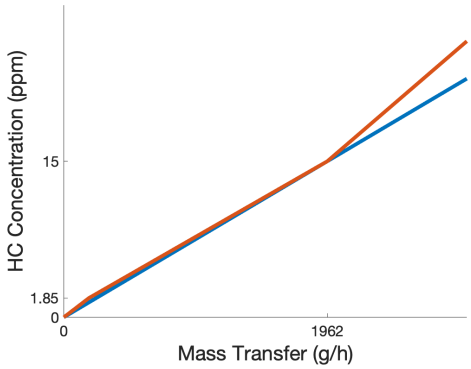

(b) Results from solving the network superstructure. The required fresh water flow rate in 129.6 t/h.

Figure 4-4: Comparison of composite curves for the solutions to Alva-Argaez et al. Example 1. The rich and lean streams are shown in red and blue, respectively.

4.3.2 The Multicomponent Nonsmooth Operator

The mass-transfer scaling presented above identifies the limiting component for each rich stream or water-using operation and uses this information to ensure that all of the concentration limits in these mass sources are consistent. However, in order to calculate the minimum lean solvent flowrate or mass utilities, we also need to determine the overall limiting component for the system. Therefore, we have extended our previous work on the nonsmooth integration operator to develop an approach that automatically identifies and solves the mass integration problem for the limiting component.

In this section, we introduce this extension to the integration operator. This formulation assumes that the process variables have been transformed to account for both the different solvents and simultaneous mass transfer in the system. Specifically, the flow rates and concentration values have been transformed to a single reference stream using equilibrium relations like those in Equations (4.2) and (4.3) (or an appro-

priate limiting water curve has been constructed), and these reference concentrations have been adjusted to be consistent with the limiting contaminant in each rich stream using a selected mass transfer relation, as described in the Concentration Scalining section above.

Our discussion of the target tightness demonstrates that a valid lower bound on the fresh solvent flow rate can be found by taking the maximum fresh solvent flow rate or utility after performing integration for each component [5]. Therefore, one feasible strategy to solve the multicomponent problem is to apply our single-component integration operator to each component and include an additional nonsmooth equation that sets the solvent flowrate to be the maximum solution across the component set. This method would result in an equation system whose size remains the same with the number of rich streams in the system and scales linearly with the number of components, which is a significant improvement in scaling over other approaches.

While this maximization approach can be useful to provide an intuitive understanding of the limiting component and pinch behavior in the system, we have found that we can further take advantage of the nonsmooth behavior of the system to formulate an approach that also scales compactly in the number of the components. Using the maximization method, the minimum fresh solvent flow rate calculated for each component is the flow rate that will result in a pinch point in that component. Taking the maximum over these flow rates therefore guarantees that at least one component will be pinched in the resulting system, while the others will remain feasible. Thus, an equivalent method to minimize the feasible fresh solvent flow rate is to enforce just one pinch point across all of the components. The example composite plots shown in Figure 4-5 visually demonstrate this argument.

Mathematically, we can ensure a single pinch point by using the same pinch point balance presented in Equation (4.7) for the single-component integration operator but extending the set of candidate pinch points so that includes the potential pinch points for all components. This pinch point balance is combined with an overall resource balance in a single component. Any component can be selected for this overall balance and used to directly calculate the concentrations of other components

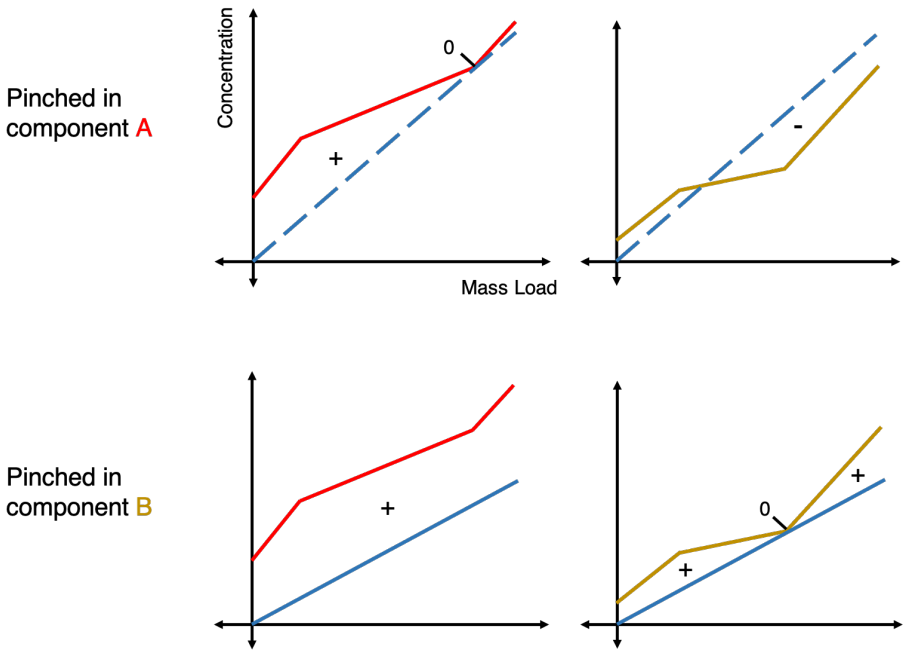

Figure 4-5: Enforcing a single pinch point across components and feasibility elsewhere will select the minimum feasible water flow rate for the system. In the scenario above, component B (gold) can be identified as the limiting component because enforcing a pinch point in B results in feasible water flow rate for A (red). Conversely, the pinched flow rate for A is not feasible for component B and cannot satisfy this condition.

of interest during post processing. The resulting equation system is:

$$0 = \sum_{i \in R} \hat{G}_i(\hat{y}_{i,c}^{\text{in}} - \hat{y}_{i,c}^{\text{out}}) + L(x_c^{\text{in}} - x_c^{\text{out}}), \quad c = C_{\text{ref}} \tag{4.24}$$

$$0 = \min_{p \in P, c \in C} \{MBP_{S,c}^p - MBP_{R,c}^p\}. \tag{4.25}$$

Now, the balances included in the minimization are those below the sets of candidate pinch points P whose concentrations for a given component c are:

$$z_c^p = \begin{cases} \hat{y}_{i,c}^{\text{in}}, & \forall p = i \in R, \\ x_c^{\text{in}}. \end{cases} , \tag{4.26}$$

As in the single component case, the balances below these pinch concentrations

are:

$$MBP^p_{R,c} := \sum_{i \in R} \hat{G}_i[\max\{0, z^p_c - \hat{y}^{\text{out}}_{i,c}\} - \max\{0, z^p_c - \hat{y}^{\text{in}}_{i,c}\} + EXT^p_{R,c}], \quad \forall p \in P, \forall c \in C, \tag{4.27}$$

$$MBP^p_{S,c} := L[\max\{0, z^p_c - x^{\text{in}}_c\} - \max\{0, z^p_c - x^{\text{out}}_c\} + EXT^p_{S,c}], \quad \forall p \in P, \forall c \in C. \tag{4.28}$$

However, here, x^{out}_c, $c \neq C_{\text{ref}}$ are functions of the other variables such that $x^{\text{out}}_c = \sum_{i \in R} \hat{G}_i / L(\hat{y}^{\text{in}}_{i,c} - \hat{y}^{\text{out}}_{i,c})$. The EXT nonphysical extensions are given by

$$EXT^p_{R,c} = \max\{0, z^p_c - \hat{y}^{\max}_c\} - \max\{0, \hat{y}^{\min}_c - z^p_c\}, \quad \forall p \in P, \forall c \in C, \tag{4.29}$$

$$EXT^p_{S,c} = \max\{0, z^p_c - x^{\max}_c\} - \max\{0, x^{\min}_c - z^p_c\}, \quad \forall p \in P, \forall c \in C, \tag{4.30}$$

where $\hat{y}^{\min,\max}_c$ and $x^{\min,\max}_c$ are now the minimum and maximum concentrations of component c across the rich and lean streams, respectively. Because the problems in this work consider a single lean stream, $x^{\min}_c = x^{\text{in}}_c$ and $x^{\max}_c = x^{\text{out}}_c$.

Because this approach uses a combined pinch point balance to identify the limiting component automatically instead of determining it explicitly, the resulting equation system remains only two equations regardless of both the number of rich streams and the number of components in the system. To our knowledge, our method is thus the only approach to the multicomponent integration problem that can achieve the same scaling and efficiency as a single-component method. (Although, the complexity of the function evaluation for Equation (4.25) now scales with $|P||C|$.) The nonsmooth equation system can also be solved for any process variable, including concentrations that are arguments of the nonsmooth mass transfer scalings, using the efficient nonsmooth equation solving methods outlined in the Background.

4.4 Examples

The following section demonstrates the use and benefits of our nonsmooth approach by applying it to a series of example problems.

4.4.1 Example 1, Fixed Mass Load

This first example, adapted from Wang and Smith and Alva-Argaez et al., is a water integration problem from the petroleum refining industry. Petroleum refining requires large quantities of water for steam stripping, washing away contaminants from hydrocarbon streams, etc. This example includes three such units that introduce three different contaminants into the wastewater streams. Table 4.1 gives the limiting water curve that has been derived for this process. In the cases below, we use this data to demonstrate how to use our methods both to include different mass transfer assumptions and to solve for different types of process variables.

Table 4.1: Concentration scaling for Example 1.

	$\hat{\boldsymbol{G}}$ (t/h)		$\hat{\boldsymbol{y}}^{\mathbf{in}}$ (ppm)	$\hat{\boldsymbol{y}}^{\mathbf{out,max}}$ (ppm)	$\boldsymbol{Ru}$	$\hat{\boldsymbol{y}}^{\mathbf{out}}$ (ppm)
Steam Stripper	45	HC	225	0	0	0
		H_2S	400	0	0	0
		Salt	150	0	0	0
Hydro-desulphurisation	34	HC	240	30	**0.125**	30
		H_2S	800	200	0.25	100
		Salt	320	80	0.25	40
Desalter	56	HC	300	100	0.33	60
		H_2S	100	50	0.5	20
		Salt	1500	300	**0.2**	300

Scenario 1, Calculation of Water Target

In this first case, we assume that the transfer of mass from the water-using operations to the water streams follows a fixed mass load distribution. As detailed in the Concentration Scaling section above, under this assumption, each contaminant

in a given operation must have the same relative recovery, and each component at the operation outlet must be at or below the desired concentration limit (or here the equivalent concentration in the limiting water profile). The resulting scaling for these assumptions is given in Equation (4.16).

First, we use this assumption to determine the minimum required freshwater flow rate for the concentration limits given in Table 4.1. For each unit, we use Equation (4.16) to calculate the limiting contaminant, fix the relative recovery for the unit, and calculate the actual outlet concentration for each contaminant. These scaled concentrations are also given in Table 4.1. The scaled concentrations are used in the nonsmooth equation system given by Equations (4.25) and (4.24), which is then solved using the semismooth Newton's method with LD derivatives as the generalized derivative elements. Here, we selected the hydrocarbon concentrations to use for the overall mass balance in Equation (4.24), but any choice of contaminant gives equivalent results.

We solved the system of two equations for the minimum freshwater requirement and the corresponding concentration of hydrocarbons in the wastewater stream, which were found to be 115.5 t/h and 265.8 ppm, respectively. Using a variety of initial guesses resulted in convergence of the semismooth Newton's method in 2-5 iterations. If needed, the outlet concentrations of the other components can be calculated directly from these results using the overall mass balances from Equation (4.24) for each of these components. Figure 4-6 gives the composite curves for each component. These plots show a pinch point in the hydrocarbon composite curves while the curves for the other components are feasible but not pinched. This result demonstrates that hydrocarbons are the overall limiting factor in the system and also how our method can automattically identify this pinched component.

We also solved this problem using the MILP1 formulation from Alva-Argaez et al. to confirm these results. We note that we also get consistent results to Alva-Argaez et al. when using our method to solve their instance of the petroleum refining problem; we have only modified the concentration limits used here to improve the visual comparison with subsequent parts of this example. While Alva-Argaez et al.'s approach

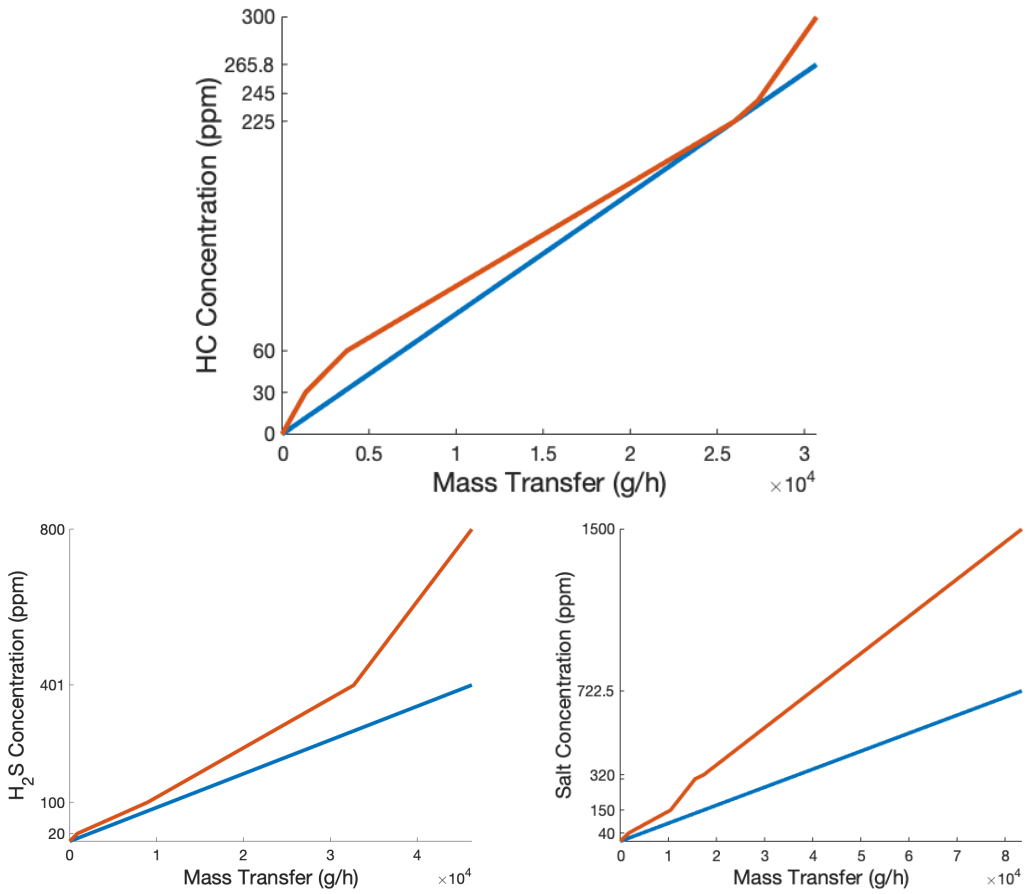

Figure 4-6: Results for Example 1, Scenario 1. The rich-stream composite curves are plotted using the adjusted outlet concentrations given in Table 4.1

uses a MILP that can be solved relatively efficiently compared to other mathematical programming problems, even for this simple system, it requires 60 constraints and 100 continuous variables, which will grow quadratically with the number of solvent-using operations in the system. As written, Alva-Argaez et al.'s formulation also includes 21 binary variables; however, for this problem with one water stream, there is only one feasible set of binary variables, which can be determined during preprocessing. In comparison, our nonsmooth approach only involves solving a two-equation system, regardless of the process size.

As explained above, the fresh water requirement calculated by both our approach and Alva-Argaez et al.'s MILP1 is not guaranteed to be a tight lower bound. Similar to the results for the original data in Alva-Argaez et al., for this modified problem,

solving the water network superstructure gives an attainable fresh water flow rate of 116.7 t/h, which is about 1 % higher than our calculated limit. While our limiting flow rate is not as tight those that can be calculated for a single-component problem, it still represents a significant improvement over results that do not account for the interdependence of the species concentrations during mass transfer. For this example, calculating the fresh water flow rate using the unscaled concentration limits gives a target of 105.6 kg/h, 9.5 % below the feasible target. Figure 4-7 compares the hydrocarbon composite curves for the unscaled concentration limits and the corrected concentrations. When the interdependent mass transfer is considered, the outlet concentration of hydrocarbons in the desalter decreases from 100 to 60 ppm to allow salt to reach its maximum outlet concentration. This change increases the hydrocarbon load for the system, which also increases the required fresh water flow rate. Because the unscaled approach does not account for how the hydrocarbon concentrations must change, the results it produces are much lower than the feasible target for the system.

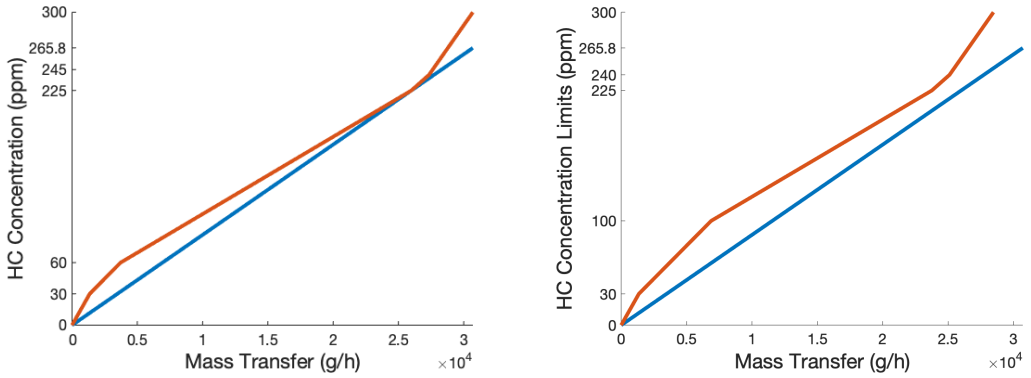

Figure 4-7: Comparison of results for Example 1, Scenario 1 using scaled (left) and unscaled (right) rich stream outlet concentrations. The scaled fresh water target is used for both plots, and the lack of pinch point for the unscaled concentration limits shows how the consideration of interdependent mass transfer increases the calculated target.

Scenario 2, Calculation of Concentration Limit

Next, instead of determining the minimum water requirements for a given process, we design a process to meet a specific water limit. We now assume that there is

freshwater limit of 100 t/h for the petroleum refining process, possibly due to local availability and climate, government regulations, or capacity of a water regeneration or desalination process. In this example, the process engineers have identified that there may be room to improve the performance of the process so the concentration of hydrocarbons entering the steam stripper decreases from its current value of 225 ppm. Therefore, we used our approach to determine how much the inlet concentration requirement of hydrocarbons in the steam stripper would need to be reduced to give a freshwater flow rate of 100 t/h.

We used semismooth Newton's method to solve Equations (4.25) and (4.24), using hydrocarbons for the system balance, for the concentration of hydrocarbons into the steam stripper and the outlet concentration of hydrocarbons in the wastewater stream. Note that now, the concentration scalings are composed in the evaluation of the equations rather than computed as a preprocessing step before solving the equations.

All other component concentrations remained the same as those given in Table 4.1. The results were 125.1 and 262.1 ppm for the inlet and wastewater hydrocarbon concentrations, respectively. Figure 4-8 shows how the pinch plot for the system changes for this solution compared to Scenario 1. This inlet hydrocarbon concentration is the maximum allowable concentration to achieve a freshwater flow rate of 100 t/h because our integration operator will identify the system for which 100 t/h is the minimum attainable flow rate. Therefore, increasing the inlet hydrocarbon concentration any further will make a freshwater flow rate of 100 t/h infeasible.

The ability to solve this type of integration problem is a significant benefit of our approach. Other pinch-based approaches to the multicomponent problem are not able to solve for any concentration process variables because these concentrations are the arguments of nonsmooth functions. The concentrations are both sorted to determine concentration intervals for mass transfer and are arguments of the "min" and "max" functions used to determine the limiting component in the concentration scalings. Derivatives cannot be calculated for these algorithms to be used in optimization solvers, and therefore, these other pinch-based approaches require all

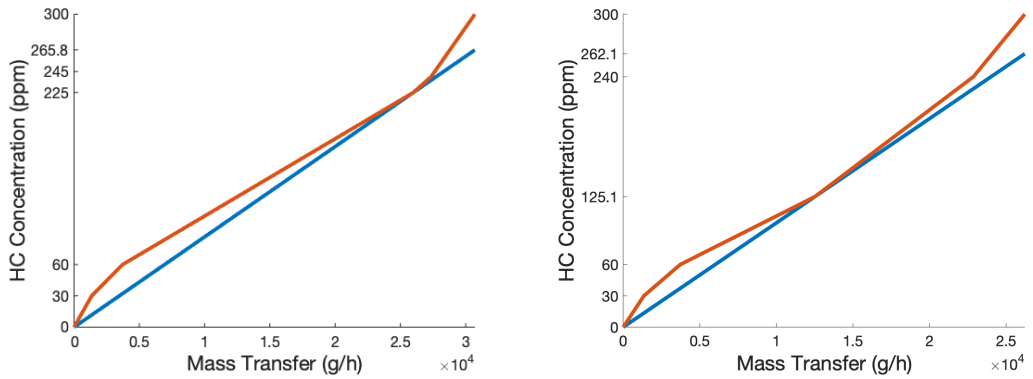

Figure 4-8: Comparison of results for Example 1, Scenario 1 (left) and Scenario 2 (right).

concentration values to be known a priori. As a result, superstructures were previously the only methods capable of solving for these process variables. But because our integration operator is explicitly nonsmooth, we can solve for any process variable while maintaining significantly better scaling than a superstructure.

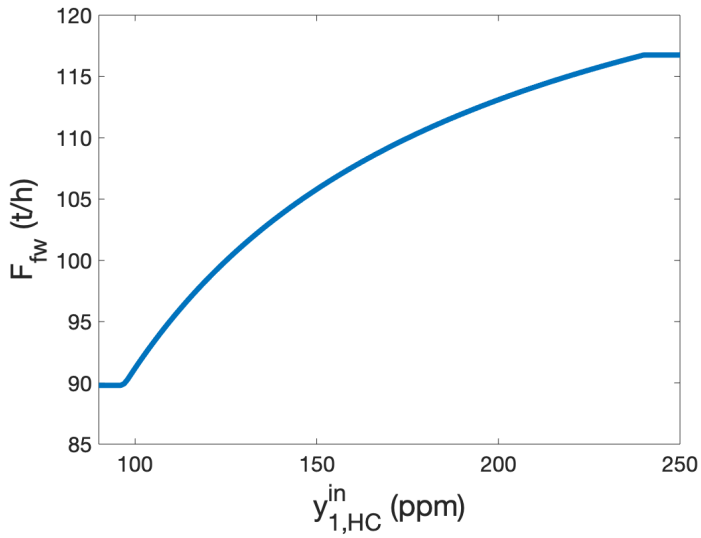

Figure 4-9: Changes to the limiting water flow rate with the inlet concentration of hydrocarbons to the steam stripper. When this concentration is no longer pinched, it does not affect the fresh water target.

One challenge with our nonsmooth integration operator is that the nonsmooth system of two equations only allows for two free variables. Therefore, selecting the appropriate unknown concentrations to reach a given fresh solvent flow rate requires

prior knowledge of the limiting components and operations in the process. Additionally, even if an appropriate unknown is determined, it is possible that this variable is no longer limiting at the solution, meaning that the Jacobian will become singular along the solution path. Figure 4-9 shows how the limiting water flow rate changes with the inlet concentration of hydrocarbons to the steam stripper. When this concentration goes below 96 ppm or above 240 ppm, the pinched concentration in the system changes and varying the concentration of hydrocarbons into the steam stripper no longer changes the fresh water target. A potential area of future work is incorporating additional nonsmooth expressions to switch automatically to the current limiting component. However, although it currently cannot be accomplished automatically, an advantage of using a pinch-based approach is that it is easy to both determine and visually observe the limiting processes and components.

4.4.2 Example 2, Proportional Mass Transfer

In this example, we consider the same system for integration and the same concentration data as in Example 1 above. However, we assume that the water-using operations are washing units in which the mass loads of each component remain constant. Thus, physical rich streams with the flow rates in Table 4.1 are no longer present, and the relevant data for the problem is now the mass loads of each component, which are given in Table 4.2. To address this different mass transfer scenario, we scale the inlet concentrations using Equation (4.18) so that the effective, limiting flow rates are consistent across components. The results of this scaling are also given in Table 4.2.

As for the case of a fixed mass load distribution, in this scenario, we determine the minimum required fresh water flow rate using the two-equation system given by Equations (4.24) and (4.25). Now, in these equations, $\hat{y}_{i,c}^{\text{in}}$ are the scaled inlet concentrations and rich stream flow rates are the limiting values $\hat{G}_i = F_{\text{lim},i}$. With this new mass transfer assumption, the minimum fresh water requirement decreases to 101.9 t/h and the hydrocarbon outlet concentration in the water stream is 250.3 ppm. The composite curves for the pinched hydrocarbons are shown in Figure 4-10. Changing the mass transfer assumption for this problem did not change the number of

Table 4.2: Concentration scaling for Example 2.

		$\boldsymbol{M}$ (g/h)	$\hat{\boldsymbol{y}}^{\mathbf{in,max}}$ (ppm)	$\hat{\boldsymbol{y}}^{\mathbf{out}}$ (ppm)	$\boldsymbol{F}_{\mathbf{lim}}$ (t/h)	$\hat{\boldsymbol{y}}^{\mathbf{in}}$ (ppm)
Steam Stripper	HC	9000	225	0	40	200
	H_2S	18000	400	0	**45**	400
	Salt	6000	150	0	40	133.3
Hydro-desulphurisation	HC	6510	240	30	31	221.5
	H_2S	20400	800	200	**34**	800
	Salt	8000	320	80	33.3	315.3
Desalter	HC	10000	300	100	50	278.6
	H_2S	2600	100	50	52	96.4
	Salt	67200	1500	300	**56**	1500

equations required to describe the system nor the rate of convergence of the Newton solver.

The fresh water flow rate calculated is again a lower bound for the minimum attainable flow rate but is not guaranteed to be tight. To evaluate the tightness of the bound, we calculated the minimum attainable flow rate for this system using the superstructure approach from Doyle and Smith. For a constant mass load, their formulation can be used directly, and the additional constraint in Equation (4.19) is no longer required. Solving the superstrucutre to global optimality gave an attainable flow rate of 111.8 t/h, making our bound 9% lower than the feasible target.

Although our lower bound is not always tight, this example demonstrates that the flexibility provided by treating the units separately. We can easiliy modify mass transfer assumptions without changing the structure or scaling of our method. In addition, changing these assumptions does not impact our ability to solve for any process variables. For example, we can once again calculate the concentration requirements in the stream stripper needed to decrease the fresh water bound to 100 t/h. Although the system is pinched in hydrocarbons, in this case, decreasing the inlet hydrocarbon limit to the stream stripper will not initially decrease the water target because the scaled inlet concentration is limited by the effective flow rate of H_2S. Thus, we instead solve for the inlet concentration of H_2S required to reach 100

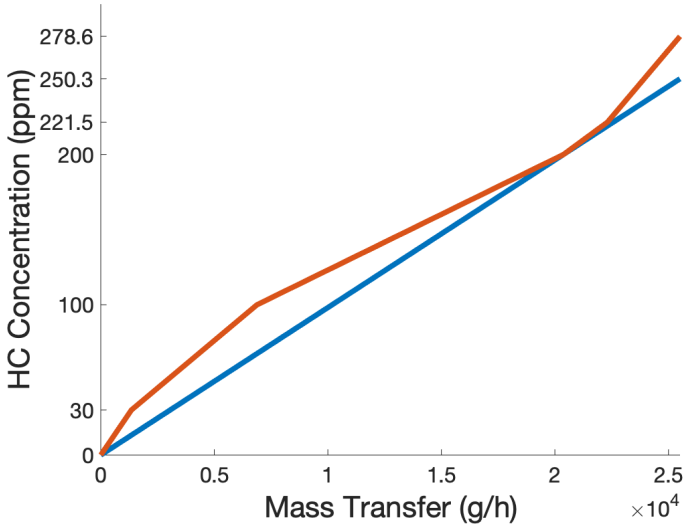

Figure 4-10: Composite curves for Example 2 using the data in Table 4.2

t/h. Solving Equations (4.24) and (4.25) using this limit gives a H_2S inlet requirement of 476 ppm H_2S to the steam stripper and a hydrocarbon waste concentration of 255.1 ppm. Because the 100 t/h target is not a tight limit, these results mean that the system must be modified so that the water exiting the steam stripper is allowed to reach at least 476 ppm H_2S, but additional changes to the system may also be required. For instance, at 476 ppm H_2S, the limiting component in the steam stripper changes, and decreasing our target flow rate past this point will require adjusting the limits for other components.

4.4.3 Example 3, Expanded System

The final example in this work extends the system in Example 1 to include additional operating units and an additional component. The results demonstrate how our nonsmooth approach solves integration problems just as efficiently as the size of the system increases. The data used for this example is modified from the examples in Chang and Li [21].

Scenario 1, Additional Units

In this first scenario, we consider two additional water-using units whose data is given in Table 4.3. To solve this problem, we will return to the assumption of fixed mass load mass transfer and use the concentration scaling given in Equation (4.16). We again solve the system of Equations (4.24) and (4.25) for the minimum fresh water flow rate using a semismooth Newton's method, which converged in 2-4 iterations for a variety of initial guesses. These calculations gave us a minimum fresh water flow rate of 121.3 t/h and a corresponding hydrocarbon outlet concentration of 263.8 ppm. We also solved this system using Alva-Argaez et al.'s MILP1 and achieved equivalent results. Figure 4-11 shows the composite curves for the pinched component in this solution. To examine the tightness of this lower bound, we also solved this problem using the superstructure approach described under "Concentration Scaling." This approach gave a minimum attainable fresh water flow rate of 131.3 t/h, which indicates that our target is low by 7.6%.

Table 4.3: Additional data for Example 3, Scenario 1

	$\hat{\boldsymbol{G}}$ (t/h)		$\hat{\boldsymbol{y}}^{\mathbf{in}}$ (ppm)	$\hat{\boldsymbol{y}}^{\mathbf{out,max}}$ (ppm)
Vacuum Ejector	8	HC	50	0
		H_2S	400	0
		Salt	60	0
Hydro-desulphurisation 2	8	HC	150	20
		H_2S	8000	60
		Salt	120	20

Scenario 2, Additional Component

In the next scenario, we analyze the same five units from Scenario 1 above, but now consider the suspended solids present in the rich streams as an additional contaminant in the system. The suspended solid concentrations for each unit are given in Table 4.4. To solve this problem, we repeat the process form Scenario 1 to get a minimum fresh water flow rate of 143.4 t/h and a corresponding hydrocarbon outlet concentration of

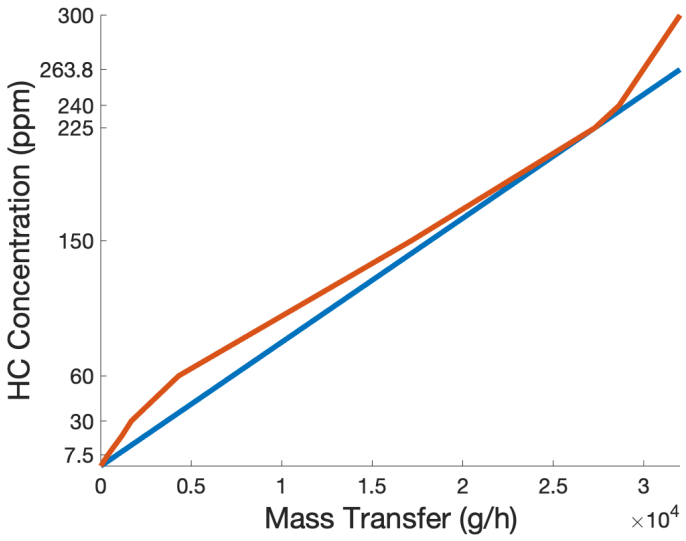

Figure 4-11: Composite curves for Example 3, Scenario 1 using the data in Tables 4.1 and 4.3

246.9 ppm in 2-5 iterations. We again verified our result using Alva-Argaez et al.'s MILP1. Figure 4-12 shows the composite curves for this solution. The superstructure solution for this problem gives an attainable fresh water flow rate of 144.4 t/h, so our lower bound underestimates the feasible solution by only 0.8%.

Table 4.4: Suspended solid concentrations for Example 3, Scenario 2

	$\hat{\boldsymbol{y}}^{\mathbf{in}}$ (ppm)	$\hat{\boldsymbol{y}}^{\mathbf{out}}$ (ppm)
Steam Stripper	60	10
Hydro-desulphurisation 1	100	30
Desalter	75	0
Vacuum Ejector	70	50
Hydro-desulphurisation 2	100	25

Note that with the additional consideration of the suspended solids, it becomes the limiting component in the overall system instead of hydrocarbons. Thus, this example demonstrates how important it is to be able to include all components when solving an integration problem, even when their concentrations seem relatively small. By enforcing the pinch point across all components in Equation (4.25), our nonsmooth approach automatically identifies this change without requiring any prior knowledge

of the limiting component.

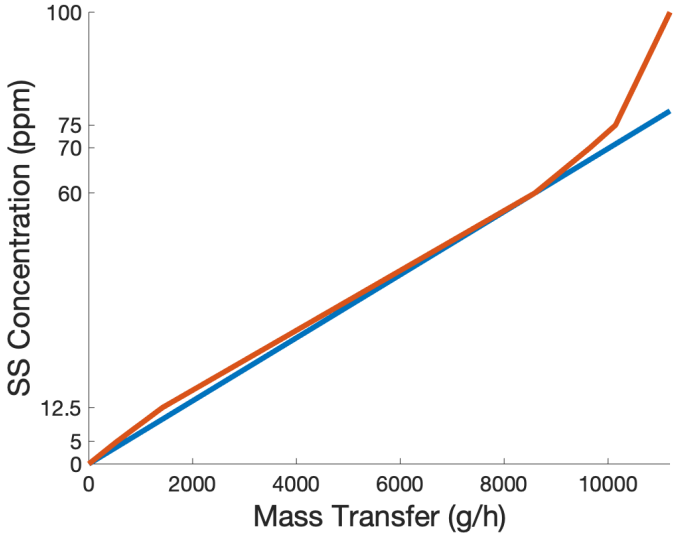

Figure 4-12: Composite curves for Example 3, Scenario 2 using the data in Tables 4.1, 4.3, and 4.4

In addition, our nonsmooth approach shows increasing benefits in efficiency as the size of the system increases. Although the size of the system has increased in both the number of components and process units, our approach still only requires solving a system of two equations, and the equation-solving process converges at a similar rate as it does for the smaller system in Example 1. In comparison, Alva-Argaez et al.'s approach to calculate the same lower bound requires 188 constraints, 301 continuous variables, and 45 binary variables (if the formulation is not simplified during preprocessing). Calculating the rigorous lower bound from the network superstructure used 162 constraints and 91 continuous variables and also required a global optimization approach to solve the nonconvex program with 40 bilinear terms. In addition, while this data allows for the use of an NLP to represent the superstructure, this is not guaranteed, and in some problems, additional binary variables may be required for numerical stability.

Scenario 3, Combining Mass Transfer Relations

Finally, we also use this example to demonstrate the ability of our method to tailor the mass transfer assumptions to each unit. Let us now assume that the relation between the components in the hydrodesulphurization units can better be described by proportional mass transfer with the mass loads given in Table 4.5. We also still assume that the concentrations in the other three units vary according to a fixed mass load distribution. To solve the system, we simply apply Equation (4.18) to scale the inlet concentrations to the hydrodesulphurization units and Equation (4.16) to scale the outlet concentrations for the remaining units. Then, these scaled concentrations are used in Equations (4.24) and (4.25) to solve for the fresh water target.

Solving this system gives a fresh water flow rate of 134.5 t/h and a waste water hydrocarbon concentration of 225.3 ppm. The system is now pinched in hydrocarbons, and the pinch plot is given in Figure 4-13. The superstructure solution for this problem gives an attainable fresh water flow rate of 137.4 t/h, so our lower bound underestimates the feasible solution by 2%.

Table 4.5: Mass loads for Example 3, Scenario 3

		$\boldsymbol{M}$ (g/h)
Hydro-desulphurization 1	HC	6510
	H_2S	20400
	Salt	8000
	SS	2240
Hydro-desulphurization 2	HC	750
	H_2S	60800
	Salt	440
	SS	550

4.5 Discussion

Our goal with this work was to develop a new approach that can provide tractable and flexible solutions to the multicomponent mass integration problem. The result

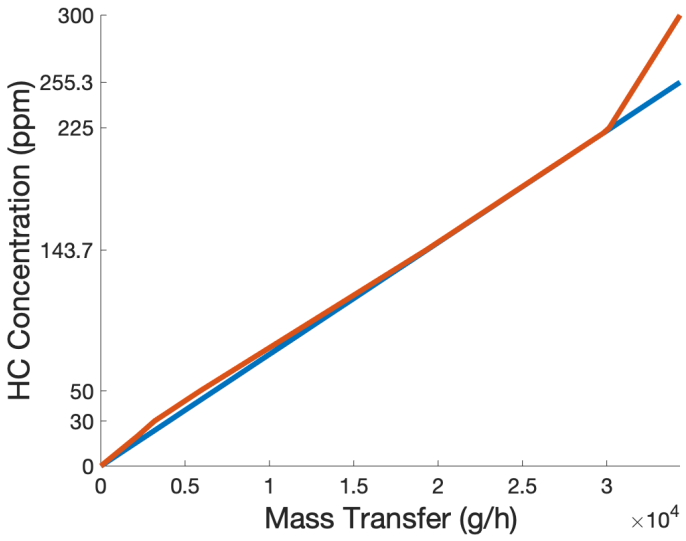

Figure 4-13: Composite curves for Example 3, Scenario 3 using the data in Tables 4.1, 4.3, 4.4, and 4.5.

is a nonsmooth integration operator that uses a system of two nonsmooth equations to enforce a single pinch point across the components. This system can be solved efficiently using new advances in nonsmooth equation solving to give a target fresh solvent flow rate that is a lower bound on the minimum attainable flow rate for the system. Our integration operator incorporates concentration scaling techniques to account for different mass transfer relations within the operating units and to increase the tightness of the lower bound.

We have applied our integration operator to a series of examples that show its success in calculating fresh solvent targets that capture the potential for reuse in a mass transfer system. A summary of these results is given in Table 4.6. These examples also demonstrate the unique benefits of our approach which include

- Compact scaling: Regardless of the number of operations or components in a mass transfer system, our integration operator only requires two equations. This ability to retain the same number of equations for any system makes this approach better equiped to handle large-scale systems than the existing methods that scale at least polynomially with the system size.

- Ease of varying mass transfer assumptions: This compact structure of our ap-

proach also remains the same no matter which mass transfer assumptions are used in the problem. Using the scaling approach, different mass transfer relations can easily be substituted for different problems or units without changing the size or complexity of our equation system.

- Ability to solve for any process variable: Because our approach only requires equation-solving instead of optimization, we are able to take advantage of nonsmooth equation-solving methods to solve for variables that are arguments of nonsmooth functions. In existing heuristic and transshipment approaches to multicomponent integration, like those from Wang and Smith and Alva-Argaez et al., the concentrations and rich stream flow rates must be known *a priori* in order to perform nonsmooth scalings or sorting. Therefore, unlike these methods, our nonsmooth operator can be embedded in outer optimization problems to perform simultaneous integration and optimization.

Table 4.6: Summary of calculated fresh water targets. The unscaled flow rate is calculated using Equations (4.24) and (4.25) without accounting for the mass transfer interactions. The minimum attainable flow rates are the results from solving the network superstructure to global optimality, and the once-through flow rates are the fresh water requirements without water reuse. All units are in t/h.

	Unscaled Target	Our Approach	Minimum Attainable	Once through
Ex 1, S1	105.6	115.5	116.7	119.6
Ex 2	94.6	101.9	111.8	119.6
Ex 3, S1	109.8	121.3	131.3	135.2
Ex 3, S2	116.5	143.3	144.4	146.3
Ex 3, S3	115.1	134.5	137.4	143.7

Another important result from this work is our analysis of the target tightness for multicomponent integration problems. We show that targets calculated for multicomponent systems using pinch analysis are not guarenteed to be tight lower bounds as they are for single-component integration problems. To our knowledge, this limitation is inherent to pinch-based methods, meaning it is unlikely that there is another approach that can both guarantee exactness of the bound and tractably be embedded in optimization problems. Efficiently calculating exact lower bounds will likely

require potential improvements to superstructure methods to decrease the system size and avoid the need for global optimization.

While our nonsmooth approach has many unique benefits, it can continue to be improved by further increasing its flexibility and relaxing assumptions on the system. Currently, to solve a design problem for a given solvent flow rate, our method requires the selection of the correct process variable as an unknown in the system. To address this challange, we believe that additional nonsmooth expressions could be used to automatically select the process variable that will affect the solvent target. This issue may be less relevant when the integration operator is used for simultaneous integration and there are more free variables in the system.

It would also be beneficial to extend our results to additional types of mass and water integration problems. There is potential to adapt our method to problems with multiple fresh solvent streams by deriving new scaling relations. However, we think that the most useful extension of our work would be to fixed-flow water integration problems. This problem formulation often describes real world systems better than fixed-load water integration because it allows the water flow rates to vary within a unit. This additional complexity can also make fixed-load water integration problems more difficult to solve; to prioritize the water sources and sinks in the problem, they must be sorted by concentration. But when multiple components are present, these priorities may conflict. For this reason, there are very few fixed-flow multicomponent water integration approaches that do not use a superstructure technique. However, recent work from Chin et al. presents a heuristic for sorting sources and sinks by their limiting components so the pinch problems can be solved separately by component to get a total fresh water requirement [24]. Therefore, our plan for our future work includes describing these sorting operations using nonsmooth expressions so we can incorporate this method into our nonsmooth approach.

Although there is room for improvement, our method is well tailored to solve screening and optimization problems, especially for large-scale systems, and this work significantly improves our ability to design and operate mass transfer systems with the smallest possible costs.

Chapter 5

Design of Variable-temperature Cogeneration Systems

This chapter applies the nonsmooth integration approaches discussed earlier in this thesis to design real systems. The application we consider is process cogeneration, which is the recovery of process waste heat by using it to drive a power cycle and produce electricity.

Waste heat from chemical processes is a significant and underutilized energy resource. Many processes involve exothermic reactions or require high temperatures to achieve conversion. The global industrial waste heat availability is estimated to be 14.6 GW with 8.8 GW released at temperatures above 450 °C [34, 17]. Major heat sources include sulfuric acid production, steel and aluminum mills, cement plants, and turbine and engine exhaust. This high-temperature, high-quality heat is a promising energy source for generating electricity using power cogeneration systems. Cogeneration systems produce power without additional emissions and can also decrease energy costs for chemical producers. However, currently, less than 800 MW of waste heat is converted to electricity.

In addition, when cogeneration systems are implemented, they are designed to take in heat at a single temperature and cannot optimally recover heat from a variable-temperature heat source [34]. This type of design does not take advantage of the high-temperature waste heat, which increases exergy losses and limits the useful heat

recovery. To address this limitation and increase the benefits from cogeneration, we propose a power system design that includes multiple power cycles with different operating temperatures. With this approach, heat recovery is improved because each cycle can be supplied with waste heat from the process or heat rejected from higher-temperature power cycles. While cascading power cycles have been widely proposed as bottoming cycles in power generation systems, no other approach has considered optimizing these systems for a variable-temperature heat source.

In this chapter, we present an efficient optimization formulation to determine design parameters for these types of variable-temperature cogeneration systems. This problem is challenging because we need to account for all possible methods of heat recovery to ensure the design is optimal, including heating of all cycles using the process streams, cascading heat between power cycles, and recuperation within power cycles. We also need to constrain this heat transfer so it only occurs between high and low temperatures. One approach to solving this problem is to fully design the heat transfer network so we can enforce feasibility in each heat exchanger. However, this approach requires creating a superstructure of all possible interactions and thus, the numbers of constraints and variables grow exponentially with the number of heat streams.

An alternative approach is to avoid network design by solving the heat integration targeting problem using the methods described earlier in this thesis. Of these approaches, the nonsmooth methods of Duran and Grossmann [29] and Watson et al. [92] are able to solve for any process variable and also scale most favorably with the number of hot and cold streams. Therefore, we adopt these nonsmooth methods to optimize cogeneration designs. By appropriately classifying the heat sources and sinks in the power cycles and variable temperature heat source, we use these heat integration approaches as constraints in an outer optimization problem with a selected design objective. Unlike work and heat exchange problems as in Holiastos and Manousiouthakis [49] that also incorporate engines into heat exchange networks, our approach considers and designs real power generation cycles rather than ideal Carnot cycles and includes multiple different-temperature streams in a single power

cycle. The result is a scalable and tractable approach to designing optimal and implementable cogeneration systems.

We have also developed an original approach for estimating the cost of our combined power cycles without having to design the full heat exchanger network. A traditional challenge when using a targeting approach to solve integration problems is that it cannot be used to estimate capital costs of the system required to achieve heat recovery. Since targeting approaches do not determine the network of stream matches and heat exchangers for the integrated process, they do not provide convenient information on the required equipment that could be used to estimate capital costs. As a result, in previous work, targeting approaches have only been used to calculate utility operating costs and superstructures are used to assess equipment needs.

To obtain information on the relative network requirements, [92] develop a nonsmooth equation to estimate the heat exchanger area necessary for integration, assuming a multistream heat exchanger is used. We extend this method with additional nonsmooth expressions to partition the network into multiple multistream heat exchangers by the temperatures of the fluid streams. By partitioning the network, we can account for how the equipment requirements vary with phase or temperature and improve the accuracy of the cost estimation without needing to determine the full network design. Thus, we are able to screen and optimize power generation systems by their capital costs while retaining the efficiency of the targeting method.

In the sections below, we detail our novel approaches for optimizing variable-temperature cogeneration systems and estimating the costs of heat integration networks. We then use these approaches to design combined sCO_2 Brayton and steam Rankine cycle cogeneration systems for two promising applications, sulfuric acid and cement production.

At the time of writing, the work in this chapter is in preparation for publication [70].

5.1 Problem Definition

The objective of this work is to determine the optimal power cycle parameters for a cogeneration system.

Given a set of heat flows from a chemical process and a set of power cycles, S, a sketch of the optimization problem we are trying to solve is

$$\begin{aligned} \boldsymbol{x} \in \arg\min_{\boldsymbol{x}} & \, g(\boldsymbol{x}) \\ \text{s.t.} \quad & \text{Process models hold,} \quad \forall s \in S, \\ & \text{Energy balance holds,} \\ & \text{Heat transfer is feasible,} \end{aligned} \tag{5.1}$$

where $\boldsymbol{x}$ is a set of design variables for the cogeneration system and $g(\boldsymbol{x})$ is any objective function for the design. In this problem, the energy balance constrains the optimization to the given waste heat input.

To define the heat input, we assume that we have complete stream data for the chemical process being considered for cogeneration. These streams include any waste heat that can be used for cogeneration (that have temperatures above the minimum power cycle heat input temperature). They can also consider cold streams in the chemical process that must be heated by the waste heat. Note that if these cold streams are included in our problem formulation, their heating takes precedent over the power cycles. For all streams, we use stream data in the form of inlet and outlet temperatures and heat capacity flow rates, and we assume that these quantities are linearly related. Thus, we have a set of hot streams, H, that vary in temperature from T_i^{in} to T_i^{out} for a heat output $\Delta Q_i = F_i(T_i^{\text{in}} - T_i^{\text{out}})$, and a set of cold streams, C, that vary in temperature from t_j^{in} to t_j^{out} for a heat input $\Delta Q_j = f_j(t_j^{\text{out}} - t_j^{\text{in}})$. If the heat-temperature relationships for the process streams are nonlinear, they can be linearized by subdividing them into as many substeams as necessary using the method presented by Watson et al. [92]. Note that in this chapter, Q refers only to enthalpy, which is the resource quantity, not quality as it does in the general

integration operator in Chapter 3.

When solving this design problem, we also assume that the designer has selected the set of power cycles S with a variety of working fluids. For best results, the working temperatures of these fluids will cover as much of the range of the hot stream temperatures as possible As detailed below, our method enforces a pinch point in the system to optimize heat recovery. Figure 5-1 illustrates that if the working temperatures for the power cycles are not high enough relative to the hot stream temperatures, then this pinch point is not attainable. On the other hand, the working fluids also should also reach low enough temperatures to recover all the waste heat from the process and rejected by higher-temperature cycles. Increasing the number of cycles will improve the heat recovery for the system because their temperatures can be tuned to better match the hot stream temperatures. However, it is likely a trade-off will be reached with the high capital costs required to install many smaller power cycles.

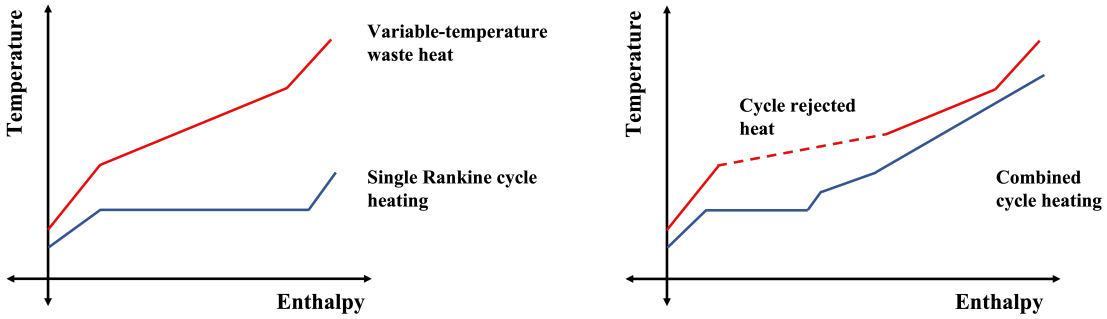

Figure 5-1: Composite curves comparing the heat transfer for a Rankine-only cogeneration system (left) and a combined-cycle system (right). The hot and cold composite curves are shown in red and blue, respectively, and represent the availability of the waste heat sources and the requirements of the cycle heat intake. For this example heat source, a Rankine cycle cannot reach the high temperatures of the heat source, so heat recovery is supoptimal. However, when a higher-temperature cycle is added, the rejected heat is high enough quality to be recovered by the Rankine cycle, which increases the amount of heat that can be recovered. Minimizing the distance between the hot and cold composite curves increases the temperature of the rejected heat and maximizes the heat recovery.

Finally, we assume that the user provides a model for the operation of each candidate power cycle. In the example section, we will demonstrate how we have modeled both steam Rankine and sCO_2 Brayton cycles. However, our approach is not limited

to these cycle types, and can be extended to any realistic power cycle by including appropriate property models for the working fluid. We assume the models provide the necessary temperature and enthalpy data to define the heat flows to and from the cycles in the form specified for the process streams above. The models should also output any other variables required to calculate the objective function. Additionally, we assume knowledge of any fixed parameters in the objective function, such as cost correlations for cycle equipment when optimizing the system costs.

5.2 Methods

5.2.1 Cogeneration Constraints

This work presents an efficient approach to solving the cogeneration design problem given by Equation (5.1). To our knowledge, this is the only approach presented in the literature that explicitly considers temperature variations in the heat source for power generation. And therefore, our method has the potential to improve the recovery of waste heat from a wide variety of sources and processes. Designing for variable-temperature heat sources is challenging because it requires:

1. Considering all possible heat flows both from the heat sources to the power cycles and cascaded between power cycles,
2. Evaluating the feasibility of these potential heat flows,
3. Determining the optimal selection of feasible heat flows.

However, heat integration methods are formulated to solve this problem of optimal heat recovery.

Superstructure approaches to heat integration systematically consider all possible heat transfer networks and scale exponentially with the number of sources and sinks. Therefore, they quickly become infeasible to use for design problems with many waste heat streams or multiple power cycles. However, incorporating targeting methods for heat integration addresses these challenges because they determine the system

parameters for optimal heat recovery without requiring the full design of the heat exchanger network.

Because targeting methods combine heat sources and sinks into composite curves, they automatically assess all potential modes of heat recovery, which for the cogeneration problem include transfer to any power cycle and heat cascading between power cycles. In addition, because composite curves do not distinguish between the different origins of the waste heat or requirements, if both the heating and cooling for an individual cycle are included for integration, the targeting method must also encompass reheating (recuperation) within that cycle. Thus, we present two optimization formulations for solving the variable-temperature cogeneration design problem that utilize the nonsmooth targeting approaches of Duran and Grossmann and Watson et al., which are described in the Background chapter.

For the cogeneration design problem, we set the external heating and cooling loads in the heat integration problem to zero. This constraint ensures both that the process heat is the only energy source considered and that all of the process heat is utilized by the cogeneration system. Then, these formulations are:

$$\begin{aligned} \boldsymbol{x} \in \arg\min_{\boldsymbol{x}} \quad & g(\boldsymbol{x}) \\ \text{s.t.} \quad & 0 = h_s(\boldsymbol{x}), \quad \forall s \in S, \\ & 0 = \sum_{i \in H} F_i(\boldsymbol{x})(T_i^{\text{in}}(\boldsymbol{x}) - T_i^{\text{out}}(\boldsymbol{x})) - \sum_{j \in C} f_j(\boldsymbol{x})(t_j^{\text{out}}(\boldsymbol{x}) - t_j^{\text{in}}(\boldsymbol{x})), \\ & 0 = \min_{p \in P} \{EBP_C^p - EBP_H^p + EXT_C^p - EXT_H^p\}, \end{aligned} \tag{5.2}$$

and

$$\begin{aligned} \boldsymbol{x} \in \arg\min_{\boldsymbol{x}} \quad & g(\boldsymbol{x}) \\ \text{s.t.} \quad & 0 = h_s(\boldsymbol{x}), \quad \forall s \in S, \\ & 0 = \sum_{i \in H} F_i(\boldsymbol{x})(T_i^{\text{in}}(\boldsymbol{x}) - T_i^{\text{out}}(\boldsymbol{x})) - \sum_{j \in C} f_j(\boldsymbol{x})(t_j^{\text{out}}(\boldsymbol{x}) - t_j^{\text{in}}(\boldsymbol{x})), \\ & 0 \leq EBP_C^p - EBP_H^p, \quad \forall p \in P, \end{aligned} \tag{5.3}$$

where $h_s(\boldsymbol{x})$ are the process models describing the behavior of the power cycles and $\boldsymbol{x}$ are the design decision variables for the power cycles. Alternatively, these process models can be used to explicitly determine the required cycle parameters and be incorporated directly into the objective function and the hot and cold stream data calculations. The set of hot streams, $H = (\cup_{s \in S} H_s) \cup H_w$, includes

- The set of fixed waste heat streams, H_w, that describe the variable temperature heat source. Note that fixing the magnitude of the heat sources constrains the optimization problem so that the resulting cogeneration designs are comparable.

- The sets of rejected hot streams, H_s, from power cycle coolers or condensers that have the potential for reuse. This criterion implies that the upper bound of the hot stream outlet temperature is higher than the lower bound of any of the cold stream inlet temperatures: $\max_i\{T_i^{\text{out}}\} \geq \min_j\{t_j^{\text{in}}\}$. Any of the stream variables, F_i, T_i^{in} or T_i^{out}, in H_s can be functions of the design variables $\boldsymbol{x}$.

The set of cold streams, $C = (\cup_{s \in S} C_s) \cup C_w$, contains

- The set of cold process streams, C_w, that must be heated using the process waste heat,

- The sets of power cycle heat inputs, C_s, to the heaters or evaporators. These stream variables can also be functions of $\boldsymbol{x}$.

If any of the streams in H or C do not follow the linear relationship between temperature and enthalpy transfer, these streams can be subdivided into multiple streams with different heat capacity flow rates until the linearity assumption is reasonable for each substream. All substreams are then included in H or C and the overall formulation remains unchanged. More details on this process can be found in Watson et al. [92].

Formulation (5.2) using the Watson et al. constraints is advantageous because the number of constraints will remain the same regardless of the complexity of the heat source or the power system design. This property also means that there is no penalty for subdividing hot and cold streams to achieve linearity. Regardless of how

many divisions occur, the number of constraints will remain unchanged. While the Duran and Grossmann formulation in (5.3) does not scale as well in the number of constraints, because inequalities are used instead of just equality constraints, in practice, it can sometimes be easier to converge to an optimal solution for some solvers or objective functions.

The decision variables, $\boldsymbol{x}$, in the optimization formulation can be any unknowns in the cycle designs. To fully design the cogeneration system, there will typically be nine unknowns for each power cycle in S: the temperatures and pressures at the inlets of each of the cycle components as shown in Figure 5-2 and the mass flow rate of the working fluid in the cycle. If the power cycle process models are incorporated into the objective and heat integration operator instead of expressed explicitly as separate constraints, then the number of free variables decreases by one per process component. A typical choice is to explicitly calculate the outlet temperatures of the compressor or pump and the turbine. Then, since pressures are fixed across the heat exchangers, a potential vector of unknowns is $\boldsymbol{x} = [\dot{m}_s, t_{2,s}, T_{4,s}, P_{2,s}, P_{3,s}, \ \forall s \in S]$.

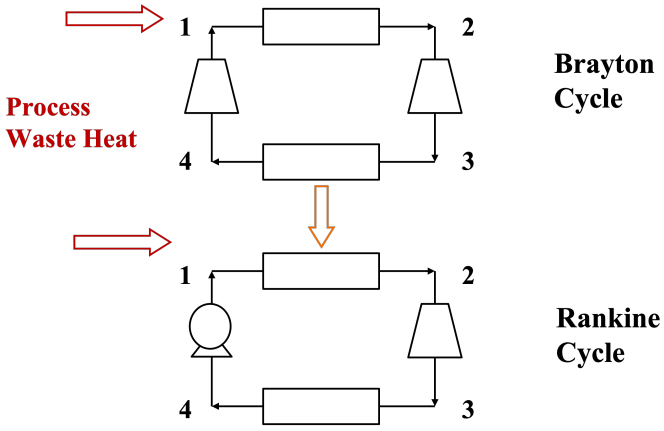

Figure 5-2: Representation of a cogeneration design using a Brayton and Rankine cycle. The numbering indicates the locations of potential unknown temperatures and pressures in the system.

When using Formulation (5.2) with the equality constraints from Watson et al., it may also be necessary to include $\Delta T_{\min}$ as a decision variable. In the Duran and Grossmann formulation, the inequalities ensure that the temperature approach between the hot and cold streams will never be smaller than $\Delta T_{\min}$ and thus, that the

heat transfer network is feasible. However, for an objective function that is nonlinear, it is not guaranteed that a pinch point will be present at the solution. On the other hand, the equalities from Watson et al. enforce a pinch point in the system. This property allows the designer to specify the minimum difference to optimize a fully integrated system instead of just a feasible one. If the goal is to explore the full space of feasible cogeneration systems, we can allow the temperature difference between the curves to vary by treating $\Delta T_{\min}$ as a design variable and using the minimum feasible temperature difference as a lower bound.

Note that if the objective for the cogeneration design is to maximize power generation, then $\Delta T_{\min}$ can be specified even when considering all feasible designs. A system with maximum power generation will have optimal heat recovery and thus a pinch point is present. If there is no pinch point in the system, then there is the potential to add additional source and sink capacity to the system to increase the heat recovery. Because the process heat source is fixed, these increases in capacity correspond to increases in size of the power cycles. Since the power output of a given power cycle increases monotonically with the heat input to the cycle, the total power generated by the system must also increase. Thus, a pinch point will be present in a system with optimal power generation. In practice, our results are consistent with this argument. When maximizing power generation using the Watson et al. formulation, we consistently see $\Delta T_{\min}$ reach its lower bound at the solution.

5.2.2 Heat Exchanger Costing

We have also developed an original approach for estimating the cost of our combined power cycles without having to design the full heat exchanger network. One of the benefits of our optimization approach is that we avoid needing to determine the structure of the heat exchanger network by using targeting methods for heat integration. However, this approach makes it difficult to estimate the capital costs of the heat exchanger networks because cost correlations for these systems typically require knowledge of the heat exchanger area, A, or the product of the area and the heat transfer coefficient, UA. These quantities are usually calculated for individual

two-stream heat exchangers, which requires knowledge of the heat exchanger network. Therefore, we need a unique approach for costing a heat exchanger network without needing to know the network connections.

Our approach to this problem has been to assume the heat exchange for the system is accomplished using one or more multistream heat exchangers. Multistream heat exchangers approach the ideal heat recovery for a system by transferring heat between multiple streams simultaneously instead of requiring individual connections between hot and cold stream pairs. Therefore, we can estimate the heat exchanger area or UA for a multistream heat exchanger by assuming this ideal heat recovery, which does not require designing the multistream heat exchanger. To calculate the multistream heat exchanger area, we adapt the methods of Watson et al. [92] and Hewitt and Pugh [47].

As described in Chapter 2, for a multistream heat exchanger with ideal heat recovery, heat is transferred directly between streams at the same enthalpy value in the pinched composite curves. Therefore, the product of the heat exchanger area and its heat exchanger coefficient, UA, can be estimated by treating each enthalpy interval between nonsmooth points as a separate two-stream heat exchanger. Watson et al. use nonsmooth expressions to automatically determine these enthalpy intervals and calculate the overall UA for the multistream heat exchanger by summing the contributions from each interval as given in Equation (2.9). Thus, for heat exchanger cost correlations that scale with UA, we utilize Equation (2.9). We note that in practice, both for this method and the modifications described below, we find it more robust to calculate the unknown temperatures using a seach and linear interpolation procedure. Then, these values are used with the implicit equations to find their LD-derivatives.

However, some cost correlations for heat exchangers use area as a scaling factor instead of UA. In this case, we incorporate insights from Hewitt and Pugh to estimate the area contributions from each interval. Given the enthalpy intervals for a set of composite curves, Hewitt and Pugh [47] proposed a method for combining volumetric heat transfer coefficients for individual streams to calculate an overall volumetric heat

transfer coefficient for each interval. They then use these heat transfer coefficients to calculate the contributions to the heat exchanger volume from each interval. In the absence of volumetric costing data, we chose to adapt Hewitt and Pugh's approach by using area-based heat transfer coefficients to calculate the heat exchanger area. Therefore, Equation (2.9) becomes

$$0 = A - \sum_{k \in K, k \neq |K|} \frac{\Delta \beta^k}{\Delta T^k_{\mathrm{LM}}}, \tag{5.4}$$

where $\Delta \beta^k = \beta^{k+1} - \beta^k$ is the enthalpy contribution from the interval weighted by the inverse heat transfer coefficients of the streams in the interval. The process of calculating $\Delta \beta^k$ for each enthalpy interval is similar to finding ΔQ^k for UA. For each stream inlet or outlet temperature in T^k and t^k, we still calculate the corresponding unknown temperature and enthalpy values with Equations (2.7) and (2.8). Now, we also define β^k using

$$\begin{aligned} \beta^k := & \sum_{i \in H} \frac{F_i}{U_i} (\max\{0, T^k - T_i^{\mathrm{out}}\} - \max\{0, T^k - T_i^{\mathrm{in}}\}) \\ & + \sum_{j \in C} \frac{f_j}{U_j} (\max\{0, t^k - t_j^{\mathrm{out}}\} - \max\{0, t^k - t_j^{\mathrm{in}}\}), \end{aligned} \tag{5.5}$$

where $U_{i/j}$ are the individual heat transfer coefficients for each hot or cold stream. The (Q^k, T^k, t^k, β^k) quadruples are sorted by their enthalpy values, and the resulting enthalpy intervals are used to calculate the heat exchanger area in Equation (5.4).

For certain systems, it may also be desirable to use different cost correlations across different temperature ranges. For example, some cost correlations are only valid for certain stream phases, such as those for a recuperator or boiler. In addition, if the system contains process streams with fluids, pressures, or temperatures that require heat exchangers with specialized construction, it may be beneficial to use multiple multistream heat exchangers so that the more complex construction is not needed for the entire heat exchange system.

To automatically classify process streams between the high and low temperature

exchangers, we have developed a new nonsmooth method to neglect streams below or above an enthalpy bound. Mathematically, all streams are included in both heat exchanger area calculations. However, the enthalpy values Q^k are adjusted so that enthalpy intervals above or below the bound do not contribute to the calculated area. The procedure for calculating the initial enthalpy intervals is very similar to the one presented by Watson et al. The only modification we made to this part of the calculation was to add the cutoff temperature T^* to the list of hot stream temperatures, T^k. As a result, when the enthalpy intervals are determined using Equations (2.7) and (2.8), a boundary point is calculated at (Q^*, T^*, t^*). Alternatively, in a general problem, Q^* or t^* could be specified instead of T^* and used to calculate the remaining values. If the heat exchanger area is being determined, β^* is also included in this set.

Once the enthalpy-temperature sets are computed and sorted, the heat exchanger areas or UA values are given by Equations (2.9) and (5.4), respectively. However, we modify the calculations for ΔQ^k or $\Delta\beta^k$ according to

$$(\Delta Q^k)_{\text{high}} = \max\{Q^{k+1}, Q^*\} - \max\{Q^k, Q^*\}, \tag{5.6}$$

$$(\Delta Q^k)_{\text{low}} = \min\{Q^{k+1}, Q^*\} - \min\{Q^k, Q^*\}, \tag{5.7}$$

$$(\Delta \beta^k)_{\text{high}} = \max\{\beta^{k+1}, \beta^*\} - \max\{\beta^k, \beta^*\}, \tag{5.8}$$

$$(\Delta \beta^k)_{\text{low}} = \min\{\beta^{k+1}, \beta^*\} - \min\{\beta^k, \beta^*\}. \tag{5.9}$$

Here high and low denote the high- or low-temperature heat exchangers, respectively.

In principle, this sorting procedure can also be performed by adjusting the stream temperatures before determining enthalpy intervals, i.e.,

$$T_{\text{high}} = \max\{T^k, T^*\} \qquad t_{\text{high}} = \max\{t^k, t^*\} \tag{5.10}$$

$$T_{\text{low}} = \min\{T^k, T^*\} \qquad t_{\text{low}} = \min\{t^k, t^*\} \tag{5.11}$$

However, because this method generates repeated temperatures, there will be points with a large number of potential selection functions which makes generalized deriva-

tive calculations more expensive.

When using these methods in an optimization formulation, we make one additional modification to ensure the objective function is defined at all points. If the solver reaches an infeasible point where the composite curves overlap, ΔT^k_{LM} may be undefined. Therefore, we define:

$$\Delta T^k := \max\{T^k - t^k, \Delta T_{\min}\}. \tag{5.12}$$

Because the heat exchanger area, and thus the heat exchanger cost, decreases as ΔT^k increases, setting ΔT^k to $\Delta T_{\min}$ when the system is infeasible helps increase $T^k - t^k$ and find a feasible point.

To our knowledge, this method is the first presented to estimate the cost of heat integration systems without needing to determine the full network design. Other targeting approaches have only been used to calculate utility and operating costs, and superstructures are required to assess equipment needs. With our approach, we are able to screen and optimize power generation systems by their capital costs while retaining the efficiency of the targeting method. By dividing the heat exchanger into multiple temperature regions, we also improve the accuracy of our approach, and in principle, this technique can be used to continue to divide it into as many MHEXs as are necessary to fully describe its behavior.

5.3 Case Studies

5.3.1 Cycle Selection and Models

For the following case studies, we chose to optimize a set of two power cycles to improve cogeneration for two different chemical processes. These power cycles consist of a steam Rankine cycle and a supercritical CO_2 (sCO_2) Brayton cycle. We selected these two cycles because they can cover the temperature ranges of the process waste heat. Because the fluid in a Brayton cycle remains the same phase throughout the power cycle, it can operate at high temperatures relative to Rankine cycles. However,

because a compressor is required instead of a pump, the efficiency of a simple Brayton cycle is lower than a Rankine cycle. Using a Rankine cycle at lower temperatures can therefore improve the overall efficiency of the combined cycle system while still better-utilizing high-temperature waste heat. This Rankine-Brayton cycle combination is used to improve efficiency in traditional combined-cycle power plants [53],[79] and has also been applied to alternative energy sources such as nuclear [100] and thermal solar [28], [75]. Our work extends these approaches by uniquely considering a variable temperature heat source and allowing it to be paritioned between the Brayton and Rankine cycles instead of just using the Rankine system as a bottoming cycle.

For the Rankine cycle, we chose water as a working fluid because it can be cooled at ambient temperatures. sCO_2 is a popular choice of working fluid for closed Brayton cycles because it has a higher specific heat capacity than other choices such as helium used in nuclear power plants or air in the open Brayton cycles in combined-cycle power plants or jet engines. While sCO_2 cycles have not yet been used on an industrial scale, they are widely studied [65, 78, 90, 98, 17] and have been implemented in several pilot plants up to 50 MW [25, 4, 66] and a small commercial facility [46]. Although the sCO_2 Brayton cycle is a promising case study for our method, it is important to note that the immaturity of the sCO_2 Brayton technology means that the capital costs we estimate for this cycle are likely higher than they will be in the future.

To optimize this Rankine-Brayton power generation system, we implemented models for each power cycle. The most significant portions of these models were the property models used to describe the specific enthalpies and entropies of the working fluids.

For water, we implemented the IAPWS R7-97 steam property model [85]. We utilized the expressions for specific enthalpy and entropy as functions of temperature and pressure, as well as the expression for specific enthalpy as a function of specific entropy and pressure and the expression for temperature as a function of specific enthalpy and pressure. We implemented these expressions for both Regions 1 and 2 to capture both the liquid and vapor properties in the temperature ranges of a typical steam Rankine cycle. We also included the Region 4 equation for the two-

phase temperature as a function of pressure.

In combination with these IAPWS property equations, we also developed a nonsmooth method that automatically selects the correct phase of the working fluid for a given pressure and specific entropy. This approach determines the quality, x at a point (s, P) using the equation

$$0 = \text{mid}\{x, x - \frac{s - s_l}{s_v - s_l}, x - 1\}, \tag{5.13}$$

where the nonsmooth mid function selects the middle value of its three arguments. Here, $s_l(P)$ and $s_v(P)$ are the water liquid and vapor entropies, respectively, at pressure P on the two-phase boundary. If (s, P) is in the liquid region, the entropy fraction is negative, so the mid function will select $x = 0$. If (s, P) is in the vapor region, the entropy fraction is greater than one, so the mid function will select $x - 1 = 0$. If (s, P) is in the two-phase region, the entropy fraction is between zero and one, and therefore, the quality is equal to this fraction.

Once Equation (5.13) is solved implicitly for the quality, this value can be used to determine the enthalpy at (s, P) using the equation

$$h(s, P) = x h_{R2}(P, s_{R2}) + (1 - x) h_{R1}(P, s_{R1}), \tag{5.14}$$

where $s_{R2} := \max\{s, s_v\}$ and $s_{R1} := \min\{s, s_l\}$.

While we use this approach in our model to convert between enthalpy and entropy values at a given pressure, the theory can be extended to conversions between other properties with different state variables specified. Our approach of automatically determining the water phase has the advantage of not constraining the problem by needing to assume the phases in certain regions of the power cycle. Even when two phases are not allowed in the turbine, this approach is useful in considering outlet conditions for which the isentropic enthalpies are in the two-phase region. It can also be used to constrain the phase within the turbine or pump.

Additionally, because this method is nonsmooth, we can find LD-derivatives for the arguments of Equation (5.13) using the implicit function theorem from Khan

and Barton [12, 55]. Therefore, we can use this approach inside of an optimization formulation with the arguments of the nonsmooth functions as decision variables; whereas, this flexibility is not possible to achieve using alternative methods like if/else statements.

To model the properties of sCO_2, we use the Lee-Kessler equation of state [59]. Lee-Kessler is a useful property model for non-ideal gasses and has been demonstrated to be one of the most accurate methods for describing the behavior of sCO_2 [95]. The Lee-Kessler property model solves the Lee-Kessler equation to find the compressibility factor of an ideal fluid and a reference fluid at a given temperature and pressure. These compressibility factors are combined using fluid-specific acentric factors to find the compressibility factor for the fluid of interest. This compressibility factor can then be used to calculate enthalpy and entropy departures. For this work, we used acentric factors of $\omega_r = 0.3978$ and $\omega_{CO_2} = 0.239$. To calculate temperature as a function of pressure and enthalpy or pressure and entropy, we implicitly solve the departure functions for temperature. The calculated temperature can then be used to convert between enthalpy and entropy values.

We incorporated these property models into process models for basic Rankine and Brayton power cycles. Figure 5-2 shows a diagram of one of these power cycles. For these models, we treat the turbine inlet and outlet pressures and the turbine and compressor or pump inlet temperatures as decision variables. We assume both the heating and cooling units are isobaric, which fixes the pressures for the cycle. Then, we model the turbine and compressor or pump by assuming fixed isentropic efficiencies, η_s as model parameters, which we set to $\eta_s = 0.80$. These models give the work input or output for each unit as well as the outlet temperatures. The resulting equations are

$$h^{\text{out}}_{\text{turbine}} = \eta_s(h_s - h^{\text{in}}) + h^{\text{in}}, \tag{5.15}$$

$$h^{\text{out}}_{\text{comp/pump}} = \frac{1}{\eta_s}(h_s - h^{\text{in}}) + h^{\text{in}}, \tag{5.16}$$

$$W^{\text{out}} = \dot{m}(h^{\text{in}} - h^{\text{out}}), \tag{5.17}$$

where $h_s(s, P^{\text{out}})$ and $s(P^{\text{in}}, T^{\text{in}})$ are calculated using the property models given above and $\dot{m}$ is the mass flow rate of the working fluid in the cycle.

These process models fully define the power cycles and provide all the information required to calculate our objective functions and the hot and cold composite curves for the cycles. In our formulation, we chose to embed these calculations within the objective or constraint evaluations to reduce the search space for optimization.

To obtain the composite curve data, we calculate the enthalpies at temperatures along the heating and cooling units. We then calculate the heat capacity flow rates in each temperature region by assuming a linear dependence between enthalpy and temperature. Each region is then treated as a separate hot or cold stream in our formulation. For the Brayton cycle heating, we selected 4 evenly spaced temperature intervals and for the Brayton cycle cooling, 2 intervals. For the Rankine cycle heating, we used 3 intervals partitioned at the phase boundaries. In general, any number or spacing of temperature intervals can be selected to improve the accuracy of the linearization. Because the heat rejected by the Rankine cycle is not high enough temperature to be reused and we assume the Rankine cycle cooling can be accomplished by ambient cooling water, we do not need to include the hot streams from this unit in our composite curves.

5.3.2 Cost Calculations

For the following case studies, we optimize the power system design for two objective functions: maximum power output and minimum system cost. To minimize the system cost, we use a version of the levelized cost of electricity defined by

$$LCOE = \frac{\sum_{l \in L} \mathcal{C}_l(Z_l, T_l, P_l)}{W^{\text{out}}}, \tag{5.18}$$

where $\mathcal{C}_l$ are correlations used to estimate the capital costs of each of the $|L|$ major components in the power system that are functions of their size factors Z_l and, for some components, a temperature factor T_l or pressure factor P_l. W^{out} is the total turbine power output for the given power system for the fixed waste heat input. For

the purposes of these calculations, we only consider capital costs and neglect auxiliary costs such as piping and installation. If desired, these costs can be easily added using additional multiplicative factors. The cost correlations are taken from literature data. The steam turbine and water pump costs are calculated from basic cost correlations [96], while the correlations for the sCO2 turbine and compressor are specialized functions for sCO_2 power generation developed and baselined by researchers at Sandia National Laboratory [94]. We have adjusted all cost correlations to 2020 dollars using the Chemical Engineering Plant Cost Index.

These correlations take the following forms:

$$\mathcal{C}_l(Z_l) = \mathcal{C}_{0,l} f_l \left(\frac{Z_l}{Z_{0,l}} \right)^n. \tag{5.19}$$

For the steam turbine, $f_{\text{steam}} = 1$, and for the pump and Brayton cycle components,

$$f_{\text{pump}}(P_l) = \left(\frac{P_l}{1 \text{ MPa}} \right)^a, \tag{5.20}$$

$$f_{\text{Brayton}}(T_l) = 1 + a \max\{0, T_l - T_c\} + b(\max\{0, T_l - T_c\})^2, \tag{5.21}$$

where $T_c = 550°\text{C}$. For the Brayton cycle components, we have reexpressed these temperature factors using nonsmooth functions instead of the conditionals in the original work so that we can obtain generalized derivative information for the objective function. The constants for the turbine, pump, and compressor correlations are given in Table 5.1.

For the Brayton-Rankine power generation system presented above, the available heat exchanger correlations are limited by the relative immaturity of sCO_2 Brayton cycle technology. The costing data provided by Sandia National Laboratory includes targeted correlations for sCO_2 heaters, coolers, and recuperators. These correlations are valuable for assessing the costs of this specialized equipment. However, using these expressions to cost the entire heat exchanger system will likely overestimate its cost both because equipment for high-temperature sCO_2 processing is more complex than what is necessary for the other process streams and because these costs are

Table 5.1: Constants for the capital cost correlations used in this work. Outputs are in millions of 2020 USD.
* includes 1.6 factor for high pressure steam turbine
** size factor is (pump head)(mass flow rate)
*** includes 2.4 factor for nickel alloy construction, selected to reduce corrosion from low-temperature sCO_2 streams

Component	Size factor units	$\mathcal{C}_{0,l}$	$Z_{0,l}$	n	a	b
Rankine turbine	kW	1.45*	3000	0.46	-	-
Rankine pump	m kg/s**	6.1×10^{-5}	1	0.75	0.3553	-
Brayton turbine	MW	0.1826	1	0.5561	0	1.106×10^{-4}
Brayton compressor	MW	1.23	1	0.3992	0	0
Low-temp heat exchangers	m^2	0.2156***	100	0.71	-	-
High-temp recuperator	W	4.945×10^{-5}	1	0.7544	0.02141	0

likely higher than they will be in the future. Therefore, we use our new approach for costing heat exchangers to divide the network into two temperature regions. We chose to use the sCO_2 recuperator correlation to cost a high-temperature multistream heat exchanger and a more standard shell and tube heat exchanger correlation to cost a second lower-temperature heat exchanger. These correlations are given in Table 5.1. The prefactor for the low-temperature exchanger is $f_{\text{lt}} = 1$, and the correlation for the high-temperature recuperator takes the form in Equation (5.21). We used 450 °C as a temperature cut off because it is at the high end of what can be handled by the nickel construction of the low-temperature exchanger.

Because the Rankine cycle cooling is not included in the heat integration constraints, we separately calculate the area and cost of the condenser. We assume a constant temperature heat sink at 20 °C and use Equation (5.4) to estimate the exchanger area. Then we calculate the exchanger cost using the same low-temperature correlation as for the heat integration network.

5.3.3 Sulfuric Acid Cogeneration

In our first case study, we optimized the design of a Brayton-Rankine power system for the heat output of a sulfuric acid production plant. Because the sulfuric acid production process is highly exothermic, it is common for plants to recover the waste heat for power production [8]. However, current systems use single steam Rankine cycles that cannot take full advantage of the high temperatures reached during sulfuric acid production. Since sulfuric acid is a widely produced commodity chemical, improving sulfuric acid cogeneration by utilizing this high-temperature heat has the potential to result in significant power generation worldwide.

We solved the optimization problem given by Equation (5.1) for a variety of different objective functions to understand the potential improvements from a combined-cycle design and the specifications required to acheive them. We optimized these objectives over the cycle sizes, the two free temperatures and pressures in each cycle, and the minimum feasible temperature for heat transfer so that $\boldsymbol{x} = [\dot{m}_{\text{Brayton}}, t_{2,\text{Brayton}}, T_{4,\text{Brayton}}, P_{2,\text{Brayton}}, P_{3,\text{Brayton}}, \dot{m}_{\text{Rankine}}, t_{2,\text{Rankine}}, T_{4,\text{Rankine}}, P_{2,\text{Rankine}}, P_{3,\text{Rankine}}, \Delta T_{\text{min}}]$.

Table 5.2: Waste heat streams for the sulfuric acid production process.
* Heat transfer coefficients are typical values for high pressure gas streams [47].

Hot stream	T_i^{in} (°C)	T_i^{out} (°C)	F (MW/K)	U* (W/m^2 K)
Burner outlet	464	207	0.130	190
Converter 1 outlet	495	447	0.133	190
Converter 2 outlet	584	427	0.136	190
Converter 3 outlet	1003	394	0.139	190

Table 5.3: Parameters used in IPOPT.

hessian_approximation	'limited-memory'
limited_memory_max_history	Number of decision variables
mu_strategy	'adaptive'
tol	1×10^{-4}
constr_viol_tol	1×10^{-6}
recalc_y_feas_tol	10

We also considered a fixed sulfuric acid waste heat input. The hot stream data for this input are given in Table 5.2. These values are derived from process data for a wet production process with a 16 kg/s sulfur feed.

We solved these optimization problems using the solver IPOPT as described in the Nonsmooth Optimization Section. Table 5.3 gives the solver parameters used. Most of these parameters are adopted from Watson et al. [93]. Unlike Watson et al., we did not change the *bound_push* and *bound_frac* tolerances from their default values because empirically, we found that convergence improved when the initial guess was not a feasible point.

We also specified upper and lower bounds for each of the decision variables in the optimization problem, which are given in Table 5.4. The pressure and temperature bounds are typical ranges for sCO_2 and steam cycles. While most of these bounds are flexible assuming they are within the equipment specifications, several are important for maintaining the feasibility of the system. Pressures in the Brayton system must be greater than 7.4 MPa so the CO_2 remains supercritical. In addition, the temperatures in the Rankine cycle must remain a feasible temperature difference above the available cooling sink. We also use the pressure and temperature bounds to ensure

Table 5.4: Bounds for decision variables used in cogeneration optimization.

Variable	Units	Lower bound	Upper bound
$\dot{m}_{\text{Brayton}}$	kg/s	0	1000
$P_{2,\text{Brayton}}$	MPa	18	30
$P_{3,\text{Brayton}}$	MPa	7.6	15
$t_{2,\text{Brayton}}$	°C	400	980
$T_{4,\text{Brayton}}$	°C	90	200
$\dot{m}_{\text{Rankine}}$	kg/s	0	1000
$P_{2,\text{Rankine}}$	MPa	2	20
$P_{3,\text{Rankine}}$	MPa	0.1	1
$t_{2,\text{Rankine}}$	°C	400	600
$T_{4,\text{Rankine}}$	°C	25	75
ΔT_{min}	K	20	200

the turbine inlet pressures are greater than their outlet and the turbine outlet temperatures are greater than the pump or compressor inlet temperatures. Alternatively, these conditions can be enforced through additional inequality constraints.

When optimizing over this space, we used a variety of initial guesses. Due to the differences in parameters across objectives, we could not achieve convergence in all scenarios with the same initial guess. With an appropriate choice of initial guess, we converged to a local minimum in 30 to 80 iterations. We observed that if the number of iterations exceeded these values, the solver was unlikely to converge. In these cases, we saw the solution path continuously oscillate around the local minimum but never reach the specified absolute tolerances.

To achieve convergence, we can either modify the initial guess or increase the absolute tolerance. For the results given below, we chose to keep the tolerances in Table 5.3. However, we noticed that increasing the absolute tolerance does not typically change the design parameters that the solver converges to, and thus, this strategy may be useful to quickly understand the types of designs that optimize the current objective.

Using these constraints, we first maximized the power output for the given waste

Table 5.5: Cogeneration optimization results for sulfuric acid production.

Variable	Units	Minimum Cost Rankine Cycle	Minimum Integrated Cost	Maximum Power	Maximum Power with SA heating
$\dot{m}_{\text{Brayton}}$	kg/s	0	124.4	112.6	112.6
$P_{2,\text{Brayton}}$	MPa	-	30.00	30.00	30.0
$P_{3,\text{Brayton}}$	MPa	-	7.60	7.60	7.60
$t_{2,\text{Brayton}}$	°C	-	559.6	972.2	972.1
$T_{4,\text{Brayton}}$	°C	-	90.0	90.0	101.5
$\dot{m}_{\text{Rankine}}$	kg/s	47.0	45.7	40.1	34.1
$P_{2,\text{Rankine}}$	MPa	5.18	3.90	11.93	11.96
$P_{3,\text{Rankine}}$	MPa	0.10	0.10	0.10	0.10
$t_{2,\text{Rankine}}$	°C	596.4	600.0	600.0	600.0
$T_{4,\text{Rankine}}$	°C	73.4	75.0	65.7	101.5
ΔT_{min}	K	164.8	20	20	20
W^{out}	MW	38.5	41.8	54.2	47.3
$LCOE$	\$/W	0.520	0.656	1.478	1.695

heat input:

$$W_{\text{tot}}^{\text{out}} = W_{\text{turbine,Rankine}} + W_{\text{turbine,Brayton}} + W_{\text{pump,Rankine}} + W_{\text{compressor,Brayton}}. \quad (5.22)$$

Results from solving this optimization problem are given in Table 5.5. When maximizing the power output of the sulfuric acid cogeneration system, we were not able to find an initial guess that allowed the equality formulation in (5.2) to converge in under 500 iterations. However, by using the inequality constraints, we converged to a local minimum in under 50 iterations.

Maximizing the power output for the system results in a significant increase in power output of 40.8% compared to the minimum-cost Rankine cycle. To improve the total heat recovery, this design maximizes the high temperature and pressure drop accross the Brayton cycle.

Given this potential for improved power output, we next mimimized the combined-cycle LCOE to understand if the capital costs of these designs are competitive with single-cycle approaches. For this problem, we used Equation (5.18) as our objective

function where

$$\mathcal{C} = \mathcal{C}_{\text{turbine,Rankine}} + \mathcal{C}_{\text{turbine,Brayton}} + \mathcal{C}_{\text{pump,Rankine}} + \mathcal{C}_{\text{compressor,Brayton}} + \mathcal{C}_{\text{condenser,Rankine}} + \mathcal{C}_{\text{HEX,high}} + \mathcal{C}_{\text{HEX,low}}. \tag{5.23}$$

Because the system with the minimum $LCOE$ consisted of only a Rankine cycle, we also minimized $LCOE$ for an integrated system to provide insight on the parameters that reduce costs for sCO_2 Brayton cycles. This optimal integrated system contains a Brayton cycle because the size of the Rankine cycle is reduced to achieve a pinch point, and a Brayton cycle is required to recover the remaining waste heat. Because optimal $LCOE$ is independent of optimal heat recovery, the choice to analyze the integrated system is an arbitrary approach to producing a two-cycle design. Alternatively, the cycle flow rates could be constrained to ensure both are present.

To minimize the $LCOE$ of an integrated system, it is necessary to use the equality formulation to constrain $\Delta T_{\text{min}} = 20$ K and enforce the presence of a pinch point. However, unlike optimizing the power output, Formulation (5.2) converges for a variety of initial guesses. To minimize the integrated $LCOE$, we also chose to remove the minimum cold stream inlet temperature from the set of candidate pinch points, P. Because all the power cycle temperatures are decision variables, if this Rankine cycle temperature is included, the minimum hot and cold stream temperatures can be selected so they are separated by ΔT_{min}. This solution would result in an artificial pinch point where composite curves only approach at their minimum temperatures and could include a solution with only a Rankine cycle.

The results for both the Rankine and integrated minimum-LCOE designs are included in Table 5.5. In the minimum-LCOE combined-cycle design, the Brayton cycle temperatures do not approach the temperatures of the sulfuric acid waste heat because minimizing the costs of an integrated system reduces the costs over the maximum-power design by lowering the maximum Brayton cycle temperature. Table 5.6 shows the difference in the cost of the cycle components between this system and the maximum power system as a percentage of the total system cost. We see that the Brayton

Table 5.6: Comparison of component costs for sulfuric acid cogeneration.

Component	Maximum Power		Minimum *LCOE*	
	Capital Cost (M$)	Percent of Total	Capital Cost (M$)	Percent of Total
Brayton Turbine	23.925	29.9	0.969	3.5
Brayton Compressor	3.398	4.3	3.5364	12.9
Rankine Turbine	9.712	12.1	9.299	33.9
Rankine Pump	0.481	0.6	0.154	0.6
Rankine Condenser	1.094	1.4	1.073	3.9
High temp MHEX	34.635	43.3	8.3867	30.6
Low temp MHEX	6.775	8.5	3.980	14.5

turbine is a significant portion of the total cost in the maximum-power system, and that reductions in the turbine cost result most in the difference in the costs between the two cycles. Because the cost of the sCO_2 turbine is temperature dependent for an inlet temperature over 550 °C, reducing the Brayton cycle temperatures decreases its capital cost.

In addition, we also have found another local minimum in the integrated cycle *LCOE* at $\boldsymbol{x} = [157.0, 18.33, 15, 400, 90, 46.2, 5.99, 0.10, 600, 75, 20]$ with a maximum Brayton cycle temperature at its lower bound. This result suggests that further decreasing the Brayton cycle temperatures continues to lower its *LCOE* because the cost of the high-temperature heat exchanger network decreases. Given the high cost of the sCO_2 -specific equipment, these capital cost improvements outweigh the reduction in power output.

With these changes, the combined-cycle cost approaches the optimal Rankine cost. However, the reductions in power output from the maximum-power system result in improvements of only 8.6% over the Rankine-only cycle. The pinch plots in Figure 5-3 shows the decrease in Brayton temperature and the corresponding reduction in overall heat recovery for the minimum-LCOE integrated design.

Because sCO_2 cycles are a new technology that is primarily in the pilot stage, there is still potential for the costs of the sCO_2 components to decrease significantly. For the cost of the maximum-power system to reach the same *LCOE* of the Rankine-

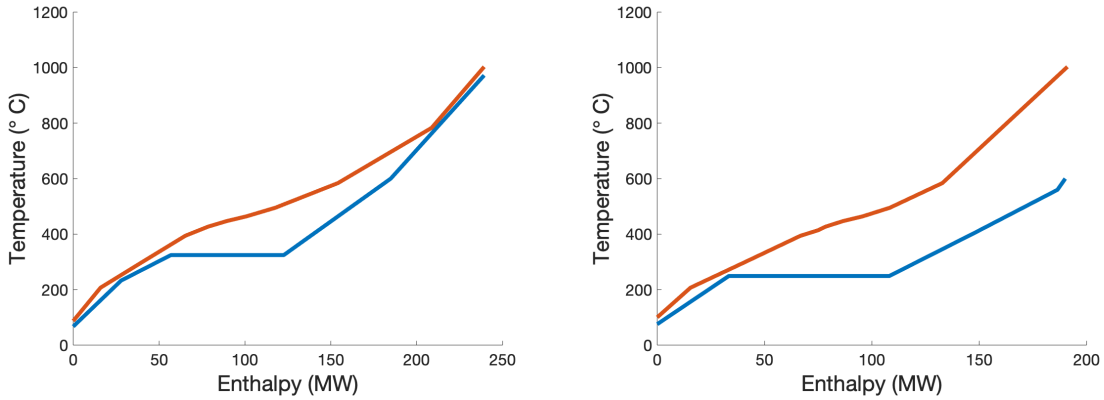

Figure 5-3: Composite curves for maximum-power (left) and minimum integrated LCOE (right) combined-cycle systems for sulfuric cogneration. The hot and cold composite curves are shown in red and blue, respectively. The lower maximum cold-stream temperature for the minimum-LCOE design decreases the total heat recovery as shown by the decrease in the magnitude of the x-axis.

only cycle, the overall cost of the sCO_2 -specific components needs to decrease by 87.7%.

Although the capital investment for the maximum-power system is higher, there still may be economic benefits from increased power production. Thus, we also estimate the difference in net present value (NPV) over time between the Rankine and combined-cycle systems. For these calculations, we multiply the capital costs from our $LCOE$ by an additional factor of 1.25 to account for installation, piping, and wiring costs [42]. We also assume yearly operating and maintenance costs of 2% of the capital costs of the turbines, compressors, and pumps, and 4% of the heat exchangers [42]. We choose an installation period of two years and divide the capital and installation costs evenly between them. Then, for a AAA corporate bond interest rate of $i = 0.03$, the NPV of the system at year n is given by:

$$NPV = \sum_{t=0}^{n} \frac{R_t}{(1+i)^t}, \tag{5.24}$$

where R_t is the cash flow over year t.

We first calculated the NPV assuming the electricity produced can be sold at the average US electricity price of about 0.10 \$/kWh [87]. The results from this

calculation are shown in Figure 5-4. Although the costs for both combined cycles are initially higher than that of the Rankine cycle, the profits exceed those of the Rankine cycle after 6 years for the minimum-LCOE combined system and 12 years for the maximum power system. And at 15 years after beginning construction, the NPV of the maximum power system begins to exceed that of the minimum-LCOE design.

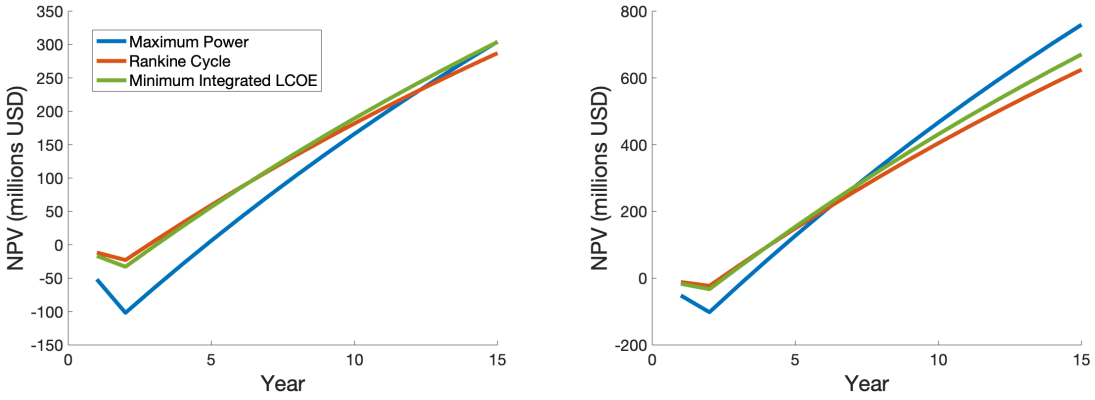

Figure 5-4: Plots of the NPV of the sulfuric acid cogeneration designs, assuming electricity prices of 0.10 $/kWh (left) and 0.20 $/kWh (right).

Since energy prices can vary widely by region, the benefits of a combined-cycle system may be even more pronounced in regions with expensive or variable power sources. For instance, the average electricity price in Europe is more than double the average for the United States [35]. Thus, we compared the NPV of these designs for an electricity price of 0.20 $/kWh. These results are also included in Figure 5-4. Now, the minimum-LCOE NPV exceeds the Rankine cycle NPV at only 4 years. The maximum power NPV becomes larger than the Rankine system and the minimum-LCOE design at 6 and 7 years, respectively. By the 15-year mark, the combined-cycle NPVs exceed the Rankine system by 7 and 20%, respectively.

There is potential to increase the NPV for a given project duration even further by calculating the maximum NPV designs using our optimization approach. Thus, we used Formulation (5.2) to maximize NPV in Equation (5.24) for a variety of project durations and an electricity price of 0.20 $/kWh. These results are given in Table 5.7. Figure 5-5 compares the optimal NPV for each project duration to the NPV of

minimum-capital cost Rankine and maximum-power combined cycle designs.

As expected, the optimal-NPV designs result in improvements over the other designs that do not account for the project duration. In addition, for each project length we considered, the optimal-NPV designs are all combined-cycle systems. The NPV improvements for these combined-cycle designs exceed at least 10% over the minimum-capital cost design even for project durations of only 5 years. These results demonstrate that although combined-cycle designs required larger initial investments, they improve the project outcome even for short-duration projects.

Figure 5-5 illustrates how the optimal NPV values transition between the NPV of the Rankine-only design at the start of operation and the maximum-power NPV for long project durations. The design parameters in Table 5.7 also transition between those of a minimum-LCOE and a maximum-power design. In particular, the temperature of the Brayton turbine inlet increases as the project length increases and the benefits of improved electricity output outweight the increase in turbine cost. As a result, we also see the improvements in the NPV over the Rankine-only designs increase as the project duration increases and the revenue from the electricity production further dominates over the capital costs. We see that for a project duration of over 15-years, our combined-cycle approach results in substainal increases in profit exceeding 23%.

We also used our method of analysis to assess the tradeoffs between using waste heat sources for power production versus heating process cold streams. In some sulfuric acid production processes, waste heat from the SO_2 conversion process is used to provide heat to the recycled sulfuric acid stream. Data for this cold stream is given in Table 5.8. Including this data in the set of cold streams C, we repeated the design process above to find the parameters that maximize the power output when there is process heating. The results from this optimization are included in Table 5.5.

To compare the NPV for this design, we introduce an external hot utility with a cost of 100 \$/kW/year [20] to the systems without internal heating. The results from this calculation are included in Figure 5-6. They show that the total capital cost of the system with process heating is nearly as high as the capital costs of the

Table 5.7: Maximum NPV results for SA production.

Variable	Units	Project Length		
		5 years	10 years	15 years
$\dot{m}_{\text{Brayton}}$	kg/s	120.0	117.9	115.0
$P_{2,\text{Brayton}}$	MPa	30.00	30.00	30.00
$P_{3,\text{Brayton}}$	MPa	9.16	9.36	9.01
$t_{2,\text{Brayton}}$	°C	684.6	843.2	895.0
$T_{4,\text{Brayton}}$	°C	90.0	90.0	90.0
$\dot{m}_{\text{Rankine}}$	kg/s	42.7	41.5	41.1
$P_{2,\text{Rankine}}$	MPa	11.26	12.73	12.84
$P_{3,\text{Rankine}}$	MPa	0.10	0.10	0.10
$t_{2,\text{Rankine}}$	°C	600.0	600.0	600.0
$T_{4,\text{Rankine}}$	°C	75.0	75.0	75.0
ΔT_{min}	K	20.6	20.0	20.0
NPV	M$	167.3	486.3	768.6
Improvment over Rankine-only	%	11.9	20.2	23.0

Table 5.8: Cold stream data for the sulfuric acid production process.

Cold stream	t_j^{out} (°C)	t_j^{in} (°C)	F (MW/K)	U (W/m^2 K)
Burner outlet	390	204	0.118	190

system with external heating. These costs are comparable because the additional heat exchanger costs for internal heating negate the cost decreases from a smaller power generation system. Thus, it is not worth the decrease in revenue from using waste heat for heating instead of power generation. These results suggest that for intra-process heat integration to be competitive with heat recovery for just electricity production, the system with process heating must significantly decrease the capital costs of the design.

5.3.4 Cement Cogeneration

The next case study optimizes the design of the Brayton-Rankine power system for heat recovery from a cement production plant. Because cement production is very energy and heat intensive, it is a good candidate for power cogeneration, and cogen-

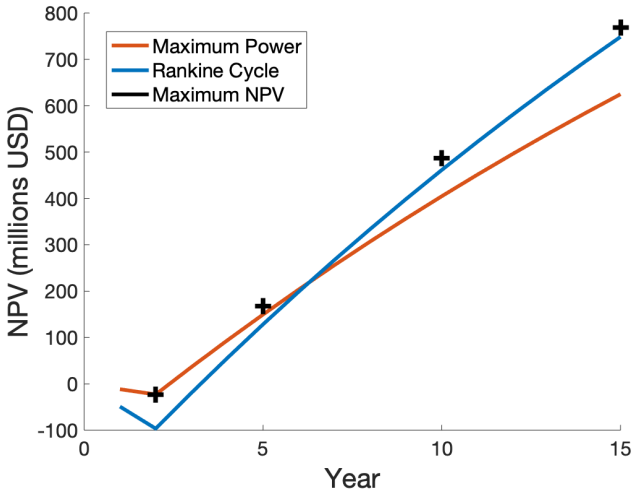

Figure 5-5: Plot comparing the NPV of the sulfuric acid cogeneration designs to the optimal values, assuming an electricity price of 0.20 $/kWh.

eration systems have been implemented for a number of cement plants, primarily in Asia [3]. As for sulfuric cogeneration systems, these current heat recovery systems for cement production use steam Rankine cycles that only capture low temperature heat from the kiln preheaters and the clinker cooler exhaust. However, the raw material in this process must reach temperatures of over 1000 °C for clinker conversion. As a result, waste heat recovery from cement production has been suggested as an application for sCO_2 Brayton cycles to utilitze this high-quality heat [96].

We consider the waste heat streams in Table 5.9, given in Boldyryev et al. [15] for a plant with a 57 t/h production rate. As for the sulfuric acid case study, we optimized the Brayton-Rankine system for this heat source to both maximize the power output and minimize the $LCOE$. Once again, the minimum-LCOE design consists of only the Rankine cycle, so we also minimized the LCOE for an integrated system with $\Delta T_{\min} = 20$ K. For these optimizations, we used the solver parameters included in Table 5.3 and the bounds in Table 5.4, although we increased the upper bound for $T_{2,\text{Brayton}}$ to 1430 K. As before, we use the inequality Formulation (5.3) to maximize power and the equality constraints in Formulation (5.2) to minimize the integrated $LCOE$, and we see similar convergence behavior. The resulting design parameters for each system are given in Table 5.10 and a comparison of the capital costs of the

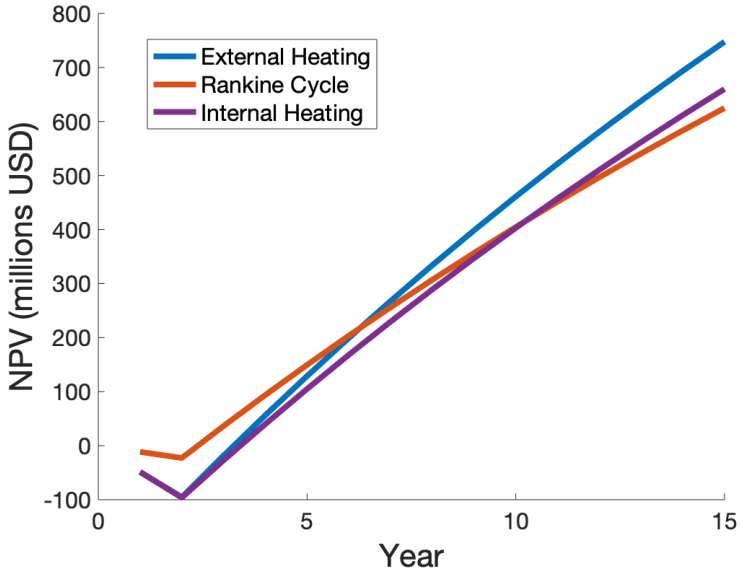

Figure 5-6: Plot comparing the NPV of the sulfuric acid cogeneration designs with internal and external process heat sources assuming electricity prices of 0.20 $/kWh.

components are in Table 5.11. The pinch plots for the two integrated designs are shown in Figure 5-7.

Overall, these results show similar behavior to those in the sulfuric acid case study. The high costs of the sCO_2 Brayton cycle components prevent the combined-cycle capital costs from being competitive with the Rankine-only system. In particular, the cost of the high-temperature sCO_2 turbine dominates the maximum-power system, and the minimum-LCOE design reduces this cost by significantly decreasing the

Table 5.9: Waste heat streams for the cement production process from Boldyryev et al. [15].
* Heat transfer coefficent for the cement clinker is taken from Cheng et al. [23]

Hot stream	T_i^{in} (°C)	T_i^{out} (°C)	F (kW/K)	U (W/m^2 K)
Gases to raw mill	370	105	13.35	190
Hot gases from kiln	860	380	40.97	190
Gasses to cooling tower	370	175	11.68	190
Gases to coal mill	370	90	0.73	190
Clinker after kiln	1450	60	15.00	73*
Hot air to cement grinding	270	105	8.86	190

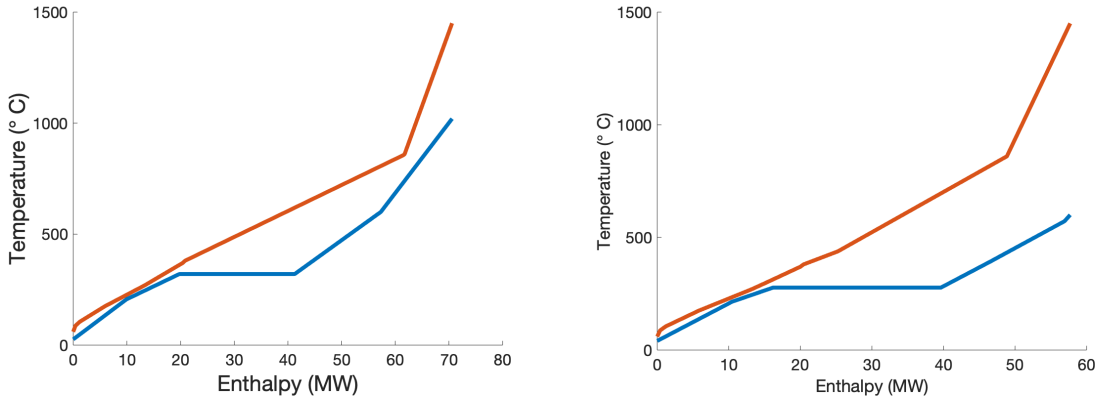

Figure 5-7: Composite curves for maximum-power (left) and minimum integrated LCOE (right) combined-cycle systems for cement cogneration. The hot and cold composite curves are shown in red and blue, respectively.

maximum heat intake temperature for the power system. As a result, even though the minimum-LCOE integrated design approaches the LCOE for the Rankine system, the power improvements are small.

Although the maximum-power system improves power output over the Rankine cycle by 14.7%, these improvements are less significant than for sulfuric acid cogeneration. This difference is likely due to the relatively lower heat loads that are released at high temperatures during cement production. Because a high proportion of the cement production waste heat is at lower temperatures, there is less heat available to reuse between cycles, and the benefits from a large Brayton cycle decrease.

Even for a system with high temperature waste heat, there may not be power improvements from the addition of a Brayton cycle. For example, in some cement production systems, it is also possible to include a lower-temperature combined waste stream with the residual hot gasses [15]. However, with the addition of this stream, it is no longer feasible to include a Brayton cycle. The Rankine cycle necessary to capture the low-temperature heat is now large enough that it requires the entire waste heat source.

We also repeated the NPV calculations for the cement cogeneration designs. The results assuming both a 0.10 $/kWh and 0.20 $/kWh price of electricity are shown in Figure 5-8. Because the power improvements are lower for cement cogeneration, for

Table 5.10: Cogeneration optimization results for cement production.

Variable	Units	Rankine Only	Maximum Power	Minimum Integrated Cost
$\dot{m}_{\text{Brayton}}$	kg/s	0	24.4	23.2
$P_{2,\text{Brayton}}$	MPa	-	25.2	30.00
$P_{3,\text{Brayton}}$	MPa	-	8.00	8.70
$t_{2,\text{Brayton}}$	°C	-	1020	572.0
$T_{4,\text{Brayton}}$	°C	-	90.0	90.0
$\dot{m}_{\text{Rankine}}$	kg/s	15.3	13.1	14.3
$P_{2,\text{Rankine}}$	MPa	6.24	11.30	6.12
$P_{3,\text{Rankine}}$	MPa	0.10	0.10	0.10
$t_{2,\text{Rankine}}$	°C	600.0	600.0	600.0
$T_{4,\text{Rankine}}$	°C	75.0	25.0	40.0
ΔT_{min}	K	69.1	20	20
W^{out}	MW	12.9	14.8	13.1
$LCOE$	\$/W	0.828	1.823	1.073

Table 5.11: Comparison of component costs for cement cogeneration.

Component	Maximum Power		Minimum $LCOE$	
	Capital Cost (M\$)	Percent of Total	Capital Cost (M\$)	Percent of Total
Brayton Turbine	11.685	43.4	0.381	2.7
Brayton Compressor	5.567	20.6	5.612	39.8
Rankine Turbine	1.682	6.2	1.714	12.2
Rankine Pump	0.196	0.7	0.106	0.8
Rankine Condenser	0.552	2.1	0.552	3.7
High temp MHEX	4.152	15.4	2.935	20.8
Low temp MHEX	3.132	11.6	2.827	20.1

a 0.10 $/kWh electricity price, the NPV of the combined cycle designs do not surpass the stream Rankine system in a 15-year period. For 0.20 $/kWh, the NPV of the maximum power design now exceeds the other systems after 9 years. However, at 15 years, the percent improvement over the Rankine cycle is still lower than the sulfuric acid combined-cycle system at 5%.

By optimizing the NPV for an electricity price of 0.20 $/kWh, we can increase the improvements to 6.6% for a 15-year project and we can reach improvements of 5% for a shorter 10-year project. The results for these optimizations are given in Table 5.12, and Figure 5-9 compares the optimal NPV for each project duration to the NPV of the minimum-capital cost Rankine and maximum-power combined-cycle designs.

As for sulfuric acid cogeneration, the improvement in NPV increases as the project length increases. Specifically, the temperature of the Brayton turbine inlet increases to increase the power output as the benefits of improved electricity output outweight the increase in turbine cost. However, because the improvements in power output from a combined cycle are smaller for cement cogeneration, our results show that the combined-cycle system is not optimal for project durations under 10 years. For a 5-year project, a Rankine-only design still optimizes the NPV. This outcome highlights the importance of considering project duration when selecting a system design and suggest that the project must reach a certain duration threshold before combined-cycle designs become the optimal choice.

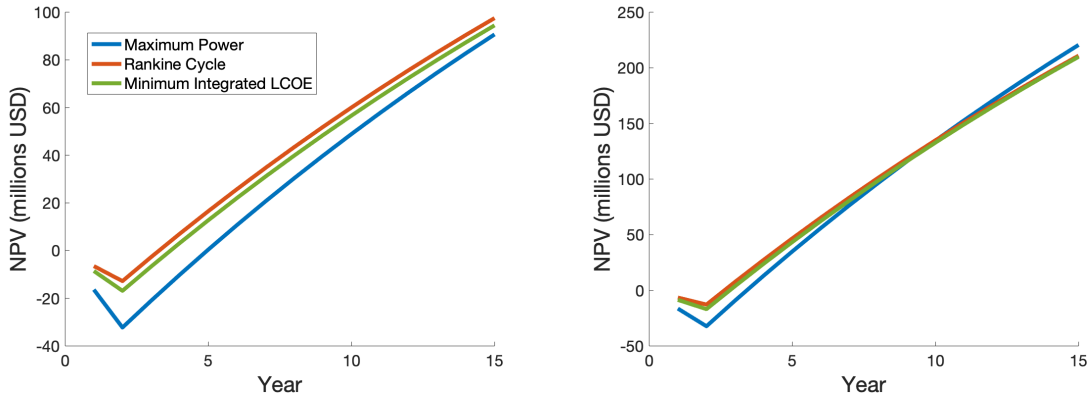

Figure 5-8: Plots of the NPV of the cement cogeneration designs, assuming electricity prices of 0.10 $/kWh (left) and 0.20 $/kWh (right).

Table 5.12: Maximum NPV results for cement production.

Variable	Units	Project Length (years)		
		5	10	15
$\dot{m}_{\text{Brayton}}$	kg/s	0	12.1	11.9
$P_{2,\text{Brayton}}$	MPa	-	30.00	30.00
$P_{3,\text{Brayton}}$	MPa	-	7. 85	7.60
$t_{2,\text{Brayton}}$	°C	-	737.2	810.2
$T_{4,\text{Brayton}}$	°C	-	90.0	90.0
$\dot{m}_{\text{Rankine}}$	kg/s	14.8	14.5	14.5
$P_{2,\text{Rankine}}$	MPa	12.6	12.73	12.87
$P_{3,\text{Rankine}}$	MPa	0.10	0.10	0.10
$t_{2,\text{Rankine}}$	°C	600.0	600.0	600.0
$T_{4,\text{Rankine}}$	°C	75.0	75.0	75.0
$\Delta T_{\min}$	K	62.8	20	20
NPV	M$	48.3	136.7	212.9
Improvment over Rankine	%	2.9	5.2	6.6

5.4 Discussion

This work presents two novel methods that apply approaches in heat integration to real systems. Our methods are uniquely able to:

1. Optimize the design of power systems for variable-temperature heat sources by considering all potential methods for heat recovery, including transfer to any power cycle, heat cascading between power cycles, and intra-cycle recuperation,

2. Estimate the cost of heat integration networks whose equipment requirements vary by temperature without needing to determine the full network design.

In addition to being the only methods in the literature designed to solve these problems, our approaches also use nonsmooth equations to improve scaling so the resulting optimization formulations remain a tractable size for large systems.

We applied these new methods to design combined Brayton-Rankine cogeneration systems for two different waste heat sources. In both cases, we saw a significant increase in power production through the addition of the high-temperature Brayton cycle. However, we found that the current costs of the specialized sCO_2 components

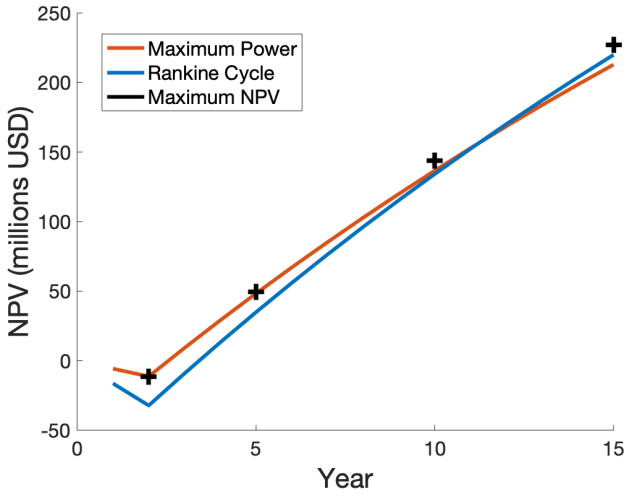

Figure 5-9: Plot comparing the NPV of the cement cogeneration designs to the optimal values, assuming an electricity price of 0.20 $/kWh.

required for the combined-cycle system make the $LCOE$ of these systems not competitive with a single Rankine cycle design. Nevertheless, we also show that in regions with higher energy costs, high-power combined-cycle systems can improve long-term profits by over 20%.

Comparing our optimal designs for the two different waste heat sources, we see that adding a high-temperature cycle is more beneficial when the portion of the waste heat at these temperatures is larger. If too large a portion of the waste heat is at low temperatures, it may not even be feasible to design a fully integrated system with the additional Brayton cycle. However, if most of the waste heat is high-quality, incorporating multiple power cycles can result in significant cost and energy savings.

We also use our methods to determine how best to allocate waste heat sources between heating process cold streams and producing electricity. We show that for the heating requirements of our sulfuric acid cogeneration case study, the additional heat exchanger costs are too large to justify decreasing the power output of the cycle design. These results show that for intra-process heat integration to be competitive with heat recovery for just electricity production, the system with heat integration must significantly decrease the captial costs of the design.

Although, we focused our case studies on analyzing the potential of using simple

Brayton cycles for high-temperature heat recovery, our approach is generalizable to any type of power cycle. Our approach automatically considers recuperation within the cycle, but we can extend our process models to describe other complex cycle designs including recompression or stream splitting [65].

We can also incorporate additional power cycles with different working fluids. We particularly see potential for our approach to be used to design cogeneration systems with organic Rankine cycles. Organic Rankine cycles have been widely proposed as bottoming cycles for heat recovery because they can reach lower temperatures than steam Rankine cycles [64]. However, no other approach has optimized their design for low-temperature heat recovery from variable temperature sources.

We are particularly interested in using organic Rankine cycles in cogeneration designs for recovering waste heat from Haber-Bosch ammonia production processes. Ammonia is the second most produced industrial chemical, and Haber-Bosch, the primary production method, accounts for over 1.5% of the world's fossil fuel use [22]. As a result, these processes offer significant potential for waste heat recovery. However, the waste heat temperatures are lower than those in our case studies, making it impossible to achieve a fully integrated system with the addition of a Brayton cycle. As a result, an organic Rankine cycle combined with a steam Rankine cycle and/or a sCO_2 Brayton cycle may be a promising approach for maximizing heat recovery from this process.

Overall, we believe that the flexibility of our approach allows for the design of cogeneration systems for a wide variety processes whose waste heat is not currently recovered.

The primary challenge for this approach is the current limitations in nonsmooth optimization methods. While we were able to obtain local minima using the LD-derivative approach for each system we considered, at times, achieving convergence required careful choices of initial guess. In addition, we used a local optimization approach, which means that there may be better solutions than those we found. Bongartz and Mitsos [16] show that power cycle design problems are particularly prone to having multiple suboptimal local minima, and in practice, we also encountered these

for our system.

We suggest that future work focus on applying deterministic global optimization methods to solve the nonsmooth optimization formulations. One approach could be to adopt the method of Khan et al. [56] who develop and apply differentiable McCormick relaxations to solve nonsmooth optimization problems using continuous branch and bound. This approach can take advantage of existing branch and bound algorithms and converges to a global solution. To compute upper bounds in this approach, we could quickly find feasible points using nonsmooth equation-solving algorithms or local optimization with large absolute but small constraint tolerances. We think that this global optimization approach can improve the robustness of our cogeneration design method and make it even easier to design for a wide range of heat sources and power cycles.

Chapter 6

Conclusions

This thesis presents three contributions to the field of process integration. These contributions use nonsmooth functions to develop methods for solving process integration problems that are scalable, flexible, and efficient.

First, we extend a previous nonsmooth approach for heat integration to develop a generalized integration operator that can integrate any resource with a single limiting quality. This operator uniquely

- Only requires two equations per integrated resource, regardless of the number of sources and sinks in the system,
- Uses new methods in nonsmooth equation-solving to easily determine resource targets or any process variables, including qualities that require sorting,
- Can be combined with process models and other operators to simultaneously integrate multiple resources,
- Automatically identify and solve threshold problems where the source or sink utility is zero and a pinch point may be infeasible.

Thus, we have formulated a readily adaptable approach that significantly reduces problem complexity and can provide computationally practical solutions to a wide variety of new integration problems to improve resource use and sustainability in chemical processes.

Our next contibution was to adapt our generalized integration operator so that it can address more complex cases in which mass or water integration is limited by multiple components. The multicomponent operator can be solved give a target fresh solvent flow rate that is a lower bound on the minimum attainable flow rate for the system and incorporates concentration scaling techniques to account for different mass transfer relations within the operating units and to increase the tightness of the lower bound.

Like the general integration operator, our multicomponent approach

- Retains only two equations regardless of the size and complexity of the system, which now includes both the number of solvent streams, the number of components present, and the mass transfer assumptions in the problem,
- Can be solved for any process variables, including component concentrations that are arguments of the nonsmooth scalings.

Finally, we develop methods to apply these nonsmooth integration approaches to the design of variable-temperature cogeneration systems. Our methods are uniquely able to:

1. Optimize the design of power systems for variable-temperature heat sources by considering all potential methods for heat recovery,
2. Estimate the cost of heat integration networks whose equipment requirements vary by temperature without needing to determine the full network design,
3. Remain tractable for large systems with numbers of constraints that either remain the same or scale linearly with the number of process streams or substreams.

Each of these projects provide a tool to address a key type of integration problem, and together, they increase the applicability of computationally efficient process integration methods to a wide range of chemical processes. We demonstrate the application of these approaches using a variety of case studies. These applications include

carbon-constrained energy planning, hydrogen conservation networks, simultaneous mass and water integration, and water recovery from petroleum refining with multiple contaminants. In addition, we designed improved cogeneration systems for sulfuric acid and cement production processes hat can increase power production by over 40% and long-term profits by over 20%. The results from these examples show the flexibility and scalability of our approaches and the breadth of improvements they can provide to both established systems and new designs.

Therefore, we believe that process integration can be a key tool in transitioning to a sustainable chemical industry with a decreased environmental impact. Developing tools, like the nonsmooth integration operators in this thesis, that can handle more complex types of integration and larger systems will increase the number of available opportunities for resource recovery.

We recommend that future work with these methods focus on making them more robust and accessible to design engineers. These steps could include

1. Packaging and distributing code for the general integration operator: Because the general integration operator is widely applicable and uses well-established methods for solving nonsmooth equations, it is a good candidate to distribute and reduce the barrier for implementing and applying nonsmooth approaches.

2. Implementing deterministic global optimization methods to solve nonsmooth optimization formulations: We believe applying the methods discussed in Chapter 5 will make it easier to perform simultaneous optimization and integration using our nonsmooth approaches by being robust to different initial guess and ensuring the best possible solution.

3. Continuing to extend nonsmooth methods to more complex integration types: While the approaches in this thesis cover a wide array of integration problems, there are still a few key areas that are out of the scope of this work. We suggest beginning with multicomponent water integration to ensure our nonsmooth methods are applicable to real processes in which flow rates vary within operating units.

As these nonsmooth methods are implemented and improved, they can be extended to more problems across all fields of engineering. By compactly describing properties and phenomena that vary by physical regime, nonsmooth equations can significantly reduce the complexity and improve the efficiency of modeling and optimization approaches. This thesis demonstrates this potential for nonsmooth approaches to improve process and system design and to increase the scope of cost savings, waste reduction, and other benefits by solving problems on a scale that was previously impossible.

Bibliography

[1] Antigone. Software package last accessed Feb. 2022 at. URL `swmath.org/software/9241`.

[2] Gams. Software package last accessed Feb. 2022 at. URL `gams.com`.

[3] Waste heat recovery for the cement sector: Market and supplier analysis. Technical report, International Finance Corporation and Industrial Productivity, June 2014.

[4] R. Allam, S. Martin, B. Forrest, J. Fetvedt, X. Lu, D. Freed, G. W. Brown, T. Sasaki, M. Itoh, and J. Manning. Demonstration of the Allam cycle: An update on the development status of a high efficiency supercritical carbon dioxide power process employing full carbon capture. *Energy Procedia*, 114:5948–5966, 2017.

[5] A. Alva-Argaez, A. Vallianatos, and A. Kokossis. A multi-contaminant transhipment model for mass exchange networks and wastewater minimisation problems. *Comput. Chem. Eng.*, 23:1439–1453, 1999.

[6] A. Alva-Argaez, A. C. Kokossis, and R. Smith. A conceptual decomposition of MINLP models for the design of water-using systems. *Int. J. Environ. Pollut.*, 29(1/2/3):177–205, 2007.

[7] J. J. Alves and G. P. Towler. Analysis of refinery hydrogen distribution systems. *Ind. Eng. Chem. Res.*, 41:5759–5769, 2002.

[8] N. G. Ashar and K. R. Golwalkar. *A Practical Guide to the Manufacture of Sulfuric Acid, Oleums, and Sulfonating Agents*. Springer, 2013.

[9] Miguel J. Bagajewicz, Margiori Rivas, and Mariano J. Savelski. A robust method to obtain optimal and sub-optimal design and retrofit solutions of water utilization systems with multiple contaminants in process plants. *Comput. Chem. Eng.*, 24:1461–1466, 2000.

[10] A. Bagirov, L. Jin, N. Karmitsa, A. Al Nuaimat, and N. Sultanova. Subgradient method for nonconvex nonsmooth optimization. *J. Optim. Theory Appl.*, 157: 416–435, 2013.

[11] A. Bagirov, N. Karmitsa, and M. Mäkelä. *Introduction to Nonsmooth Optimization*. Springer, 2014.

[12] P. I. Barton, K. A. Khan, P. Stechlinski, and H. A. J. Watson. Computationally relevant generalized derivatives: theory, evaluation, and applications. *Optim. Methods Softw.*, 33:1030–1072, 2018.

[13] Norbert Bendo, Endre Rev, and Zsolt Fonyo. The use of nonlinear programming to optimal water allocation. *Chem. Eng. Comm.*, 178:67–101, 2000.

[14] M. Boix, L. Montastruc, C. Azzaro-Pantel, and S. Domenech. Optimization methods applied to the design of eco-industrial parks: a literature review. *Journal of Cleaner Production*, 87:303–317, 2015.

[15] S. Boldyryev, H. Mikulcic, G. Krajacic, and N. Duic. Waste heat utilisation of Croatian cement industry accounting total site demands. *Comput. Aided Chem. Eng.*, 38:2223–2228, 2016.

[16] D. Bongartz and A. Mitsos. Deterministic global optimization of process flowsheets in a reduced space using McCormick relaxations. *J. Glob. Optim.*, 69: 761–796, 2017.

[17] K. Brun, P. Friedman, and R. Dennis, editors. *Fundamentals and Applications of Supercritical Carbon Dioxide (sCO2) Based Power Cycles*. Woodhead Publishing Series in Energy. Woodhead Publishing, 2017.

[18] Kai Cao, Xiao Feng, and Hang Ma. Pinch multi-agent genetic algorithm for optimizing water-using networks. *Comput. Chem. Eng.*, 31:1565–1575, 2007.

[19] P. A. C. Castillo and V. Mahalec. Inventory pinch algorithm for gasoline blend planning. *AIChE J.*, 59(10):3748–3766, 2013.

[20] J. Cerda, V. G. Cafaro, and D. C. Cafaro. Novel mathematical approaches for the structural synthesis of heat exchanger networks. *Ind. Eng. Chem. Res.*, 61 (1):464–486, 2022.

[21] Chuei-Tin Chang and Bao-Hong Li. Improved optimization strategies for generating practical water-usage and -treatment network structure. *Ind. Eng. Chem. Res.*, 44:3607–3618, 2005.

[22] I. I. Cheema and U. Krewer. Operating envelope of Haber-Bosch process design for power-to-ammonia. *RCS Adv.*, 8:34926–34936, 2018.

[23] Z. Cheng, Z. Guo, Z. Tan, J. Yang, and Q. Wang. Waste heat recovery from high-temperature solid granular materials: Energy challenges and opportunities. *Renew. Sust. Energ. Rev.*, 116:109428, 2019.

[24] H. H. Chin, P. S. Varbanov, P. Y. Liew, and J. J. Klemes. Pinch-based targeting methodology for multi-contaminant material recyle/reuse. *Chem. Eng. Sci.*, 230:1–22, 2020.

[25] T. Conboy, S. Wright, J. Pash, D. Fleming, G. Rochau, and R. Fuller. Performance characteristics of an operating supercritical CO2 Brayton cycle. *J. Eng. Gas Turbines Power*, 134(11):111703, 2012.

[26] V. R. Dhole, N. Ramchandani, R.A. Tainsh, and M. Wasilewski. Make your process water pay for itself. *Chem. Eng.*, 103(1):100–103, 1996.

[27] S. J. Doyle and R. Smith. Targeting water reuse with multiple contaminants. *Trans IChemE*, 75(B3):181–189, 1997.

[28] M. T. Dunham and W. Lipinski. Thermodynamic analyses of single Brayton and combined Brayton–Rankine cycles for distributed solar thermal power generation. *J. Sol. Energy Eng.*, 135(3):031001–8, 2013.

[29] M. A. Duran and I. E. Grossmann. Simultaneous optimization and heat integration of chemical processes. *AIChE J.*, 32(1):123–138, 1986.

[30] M. M. El-Halwagi. *Sustainable Design Through Process Integration.* Elsevier, 2012.

[31] M. M. El-Halwagi and V. Manousiouthakis. Synthesis of mass exchange networks. *AIChE J.*, 35(8):1233–1244, 1989.

[32] M. M. El-Halwagi and V. Manousiouthakis. Automatic synthesis of mass-exchange networks with single-component targets. *Chem. Eng. Sci.*, 45(9): 2813–2831, 1990.

[33] M. M. El-Halwagi, F. Gabriel, and D. Harrell. Rigorous graphical targeting for resource conservation via material recycle/reuse networks. *Ind. Eng. Chem. Res.*, 42(19):4319–4328, 2003.

[34] Amelia Elson, Rick Tidball, and Anne Hampson. Waste heat to power market assessment. Technical report, ICF International, March 2015.

[35] Eurostat. Electricity price statistics. Webpage, October 2021.

[36] F. Facchinei, A. Fischer, and M. Herrich. An LP-Newton method: nonsmooth equations, KKT systems, and nonisolated solutions. *Math. Program.*, 146:1–36, 2014.

[37] A. Fischer, M. Herrich, A. F. Izmailov, and M. V. Solodov. A globally convergent LP-Newton method. *SIAM J. Optim.*, 26(4):2012–2033, 2016.

[38] D. C. Y. Foo. Flowrate targeting for threshold problems and plant-wide integration for water network synthesis. *J. Environ. Manage.*, 88:2, 2008.

[39] D. C. Y. Foo. State-of-the-art review of pinch analysis techniques for water network synthesis. *Ind. Eng. Chem. Res.*, 48:5125–5159, 2009.

[40] D. C. Y. Foo. *Process Integration for Resource Conservation*. Taylor & Francis Group, 2013.

[41] K. C. Furman and N. V. Sahinidis. A critical review and annotated bibloigoraphy for heat exchnger network synthesis in the 20th century. *Ind. Eng. Chem. Res.*, 41:2335–2370, 2002.

[42] M. R. Gomaa, R. J. Mustafa, M. Al-Dhaifallah, and H. Rezk. A low-grade heat organic Rankine cycle driven by hybrid solar collectors and a waste heat recovery system. *Energy Reports*, 6:3425–3445, 2020.

[43] I. E. Grossmann and R. W. H. Sargent. Optimum design of heat exchanger networks. *Comput. Chem. Eng.*, 2:1–7, 1978.

[44] I. E. Grossmann, J. A. Caballero, and H. Yeomans. Mathematical programming approaches to the synthesis of chemical process systems. *Korean J. Chem. Eng.*, 16(4):407–426, 1999.

[45] I.E. Grossmann, H. Yeomans, and Z. Kravanja. A rigorous disjunctive optimization model for simultaneous flowsheet optimization and heat integration. *Comput. Chem. Eng.*, 22:S157–S164, 1998.

[46] T. J. Held. Initial test results of a megawatt-class supercritical CO2 heat engine. In *The 4th International Symposium - Supercritical CO2 Power Cycles*, Pittsburgh, Pennsylvania, USA, September 2014.

[47] G. F Hewitt and S. J. Pugh. Approximate design and costing methods for heat exchangers. *Heat Transf. Eng.*, 28(6):76–86, 2007.

[48] E. C. Hohman. Optimum networks for heat exchange. *Ph.D. Thesis, University of Southern California*, 1971.

[49] K. Holiastos and V. Manousiouthakis. Minimum hot/cold/electric utility cost for heat exchange networks. *Comput. Chem. Eng.*, 26:3–16, 2002.

[50] Jacek Jezowski. Review of water network design methods with literature annotations. *Ind. Eng. Chem. Res.*, 49:4475–4516, 2010.

[51] N. Karmitsa, A. Bagirov, and M. Mäkelä. Comparing different nonsmooth minization methods and software. *Optim. Methods Softw.*, 27(1):131–153, 2012.

[52] V. Kazantzi and M. M. El-Halwagi. Targeting material reuse via property integration. *Chem. Eng. Prog.*, 101:28–37, 2005.

[53] A. Khaliq and S. C. Kaushik. Second-law based thermodynamic analysis of Brayton/Rankine combined power cycle with reheat. *Applied Energy*, 78(2): 179–197, 2004.

[54] K. A. Khan and P. I. Barton. A vector forward mode of automatic differentiation for generalized derivative evaluation. *Optim. Methods Softw.*, 30(6):1185–1212, 2015.

[55] K. A. Khan and P. I. Barton. Generalized derivatives for hybrid systems. *IEEE Trans. Automat. Contr.*, 62(7):3193–3208, 2017.

[56] K. A. Khan, H. A. J. Watson, and P. I. Barton. Differentiable McCormick relaxations. *J. Glob. Optim.*, 67:687–729, 2017.

[57] C. S. Khor, B. Chachuat, and N. Shah. Optimization of water network synthesis for single-site and continuous processes: Milestones, challenges, and future directions. *Ind. Eng. Chem. Res.*, 53:10257–10275, 2014.

[58] V Lavric, P Iancu, and V. Plesu. Genetic algorithm optimisation of water consumption and wastewater network topology. *J. Clean. Prod.*, 13(15):1405–1415, 2005.

[59] B. K. Lee and M. G. Kesler. A generalized thermodynamic correlation based on three-parameter corresponding states. *AIChE J.*, 21(3):510–527, 1975.

[60] B. H. Li and C. T. Chang. A simple and efficient initialization strategy for optimizing water-using network designs. *Ind. Eng. Chem. Res.*, 46(25):8781–8786, 2007.

[61] B. Linnhoff, D. R. Mason, and I. Wardle. Understanding heat exchanger networks. *Comput. Chem. Eng.*, 3:295–302, 1979.

[62] Z. Y. Liu, Z. J. Zhang, L. N. Hu, and Z. L. Wu. Wastewater minimisation using a heuristic procedure. *Int. J. Chem. React. Eng.*, 2:A25, 2004.

[63] Y. Luo and X. Uan. Global optimization for the synthesis of integrated water systems with particle swarm optimization algorithm. *Chin. J. Chem. Eng.*, 16 (1):11–15, 2008.

[64] A. Mahmoudi, M. Fazli, and M. R. Morad. A recent review of waste heat recovery by organic Rankine cycle. *Appl. Therm. Eng.*, 143:660–675, 2018.

[65] M. Marchionni, G. Bianchi, and S. A. Tassou. Techno-economic assessment of joule-brayton cycle architectures for heat to power conversion from high-grade heat sources using CO2 in the supercritical state. *Energy*, 148:1140–1152, 2018.

[66] J. Marion, M. Kutin, A. McClung, J. Mortzheim, and R. Ames. The STEP 10 MWe sCO2 pilot plant demonstration. In *Proceedings of ASME Turbo Expo*, page 91917, Phoenix, Arizona, USA, June 2019.

[67] S. M. Munir, Z. A. Manan, and S. R. W. Alwi. Holistic carbon planning for industrial parks: a waste-to-resources process integration approach. *J. Clean. Prod.*, 33:74–85, 2012.

[68] M. A. Navarro-Amoros, J. A. Caballero, R. Ruiz-Femenia, and I. E. Grossmann. An alternative disjunctive optimization model for heat integration with variable temperatures. *Comput. Chem. Eng.*, 56:12–26, 2013.

[69] R. D. Neidinger. Introduction to automatic differentiation and MATLAB object-oriented programming. *SIAM Review*, 52(3):545–563, 2010.

[70] C. J. Nielsen and P. I. Barton. Design of variable-temperature cogeneration systems. *In Preparation*, .

[71] C. J. Nielsen and P. I. Barton. A nonsmooth operator for multicomponent mass integration. *In Preparation*, .

[72] C. J. Nielsen and P. I. Barton. 110th anniversary: A generalized nonsmooth operator for process integration. *Ind. Eng. Chem. Res.*, 59:253–264, 2020.

[73] S. A. Papoulias and I. E. Grossmann. A structural optimization approach in process synthesis - II: Heat recovery networks. *Comput. Chem. Eng.*, 7(6): 707–721, 1983.

[74] D. Prakotpol and T. Srinophakun. GAPinch, genetic algorithm toolbox for water pinch technology. *Chem. Eng. Process.*, 43(2):203–217, 2004.

[75] J. Sachdeva and O. Singh. Thermodynamic analysis of solar powered triple combined Brayton, Rankine and organic Rankine cycle for carbon free power. *Renewable Energy*, 139:765–780, 2019.

[76] Mariano J. Savelski and Miguel J. Bagajewicz. On the necessary conditions of optimality of water utilization systems in process plants with multiple contaminants. *Chem. Eng. Sci.*, 58(23-24):5349–5362, 2003.

[77] S. Scholtes. *Introduction to Piecewise Differentiable Equations*. Springer, 2012.

[78] M. E. Siddiqui, A. A. Taimoor, and K. H. Almitani. Energy and exergy analysis of the S-CO2 Brayton cycle coupled with bottoming cycles. *Processes*, 6(153): 1–17, 2018.

[79] O. K. Singh and S. C. Kaushik. Thermoeconomic evaluation and optimization of a Brayton–Rankine–Kalina combined triple power cycle. *Energy Convers. Manag.*, 71:32–42, 2013.

[80] R. Smith. *Chemical process design and integration*. John Wiley & Sons, Ltd, 2005.

[81] N. Takama, T. Kuriyama, K. Shiroko, and T. Umeda. Optimal water allocation in a petroleum refinery. *Comput. Chem. Eng.*, 4(4):251–258, 1980.

[82] R. R. Tan and D. C. Y. Foo. Pinch analysis approach to carbon-constrained energy sector. *Energy*, pages 1422–1429, 2007.

[83] J. P. Teles, P. M. Castro, and A. Q. Navais. LP-based strategies for the optimal design of industrial water networks with multiple contaminants. *Chem. Eng. Sci.*, 63(2):376–394, 2008.

[84] J. P. Teles, P. M. Castro, and A. Q. Navais. MILP-based initialization strateiges for the optimal design of water-using networks. *Chem. Eng. Sci.*, 64(17):3736–3752, 2009.

[85] The International Association for the Properties of Water and Steam. Revised release on the IAPWS industrial formulation 1997 for the thermodynamic properties of water and steam, 2007.

[86] M. J. Tsai and CT Chang. Water usage and treatment network design using genetic algorithms. *Ind. Eng. Chem. Res.*, 40(22):4874–4888, 2001.

[87] U.S. EIA. State electricity profiles: Data for 2020. Webpage, November 2021.

[88] M. Vikse, H. A. J. Watson, P. I. Barton, and T. Gundersen. Nonsmooth formulation for handling unclassified process streams in the optimization of work and heat exchange networks. *Ind. Eng. Chem. Res.*, 58:9526–9539, 2019.

[89] K. Walczyk and J. Jezowski. A single stage approach for designing water networks with multiple contaminants. *Comput.-Aided Chem. Eng.*, 25:719–725, 2008.

[90] X. Wang, Y. Yang, Y. Zheng, and Y. Dai. Exergy and exergoeconomic analyses of a supercritical CO2 cycle for a cogeneration application. *Energy*, 119:971–982, 2017.

[91] Y. P. Wang and R. Smith. Wastewater minimisation. *Chem. Eng. Sci.*, 49(7): 981–1006, 1994.

[92] H. A. J. Watson, K. A. Khan, and P. I. Barton. Multistream heat exchanger modeling and design. *AIChE J.*, 61(10):3390–3403, 2015.

[93] H. A. J. Watson, M. Vikse, T. Gundersen, and P. I. Barton. Optimization of single mixed-refrigerant natural gas liquefaction processes described by nondifferentiable models. *Energy*, 150:860–876, 2018.

[94] N. T. Weiland, B. W. Lance, and S. R. Pidaparti. sCO2 power cycle component cost correlations from DOE data spanning multiple scales and applications. In *Proceedings of ASME Turbo Expo*, pages GT2019–90493, 2019.

[95] C. W. White and N. T. Weiland. Evaluation of property methods for modeling direct-supercritical CO2 power cycles. *J. Eng. Gas Turbines Power*, 140: 011701–1–9, 2018.

[96] D. R. Woods. *Rules of Thumb in Engineering Practice*. Wiley-VCH, 2007.

[97] T. F. Yee, I. E. Grossmann, and Z. Kravanja. Simultaneous optimization models for heat integration- I. Area and engery targeting and modeling of multi-stream exchangers. *Comput. Chem. Eng.*, 14(10):1151–1164, 1990.

[98] Y. Zhang, H. Li, W. Han, W. Bai, Y. Yang, M. Yoa, and Y. Wang. Improved design of supercritical CO2 Brayton cycle for coal-fired power plant. *Energy*, 155:1–14, 2018.

[99] T. K. Zhelev and J. L. Ntlhakana. Energy-environment closed loop through oxygen pinch. *Comput. Chem. Eng.*, pages S79–S83, 1999.

[100] B. Zohuri, P. J. McDaniel, and C. R. R. De Oliveira. Advanced nuclear open air-Brayton cycles for highly efficient power conversion. *Nucl.*, 192(1):48–60, 2017.